Earthquake-induced rotational ground motion observed by optical rotational sensors

Andreino Simonelli

München 2018

Earthquake-induced rotational ground motion observed by optical rotational sensors

Andreino Simonelli

Dissertation zur Erlangung des Doktorgrades
an der Fakultät für Geowissenschaften
der Ludwig–Maximilians–Universität
München

Vorgelegt von
Andreino Simonelli
Aus
Pietrasanta

München, 2018

Erstgutachter: Prof. Dr. Heiner Igel
Zweitgutachter: Dr. Isidoro Ferrante
Tag der Fertigstellung: 20/02/2018
Tag der mündlichen Prüfung: 18/7/2018

Contents

Introduction **1**

Introduction **1**

0.1 Basic theory 3

0.1.1 Rotations by Love waves 5

0.1.2 Rotations by Rayleigh waves 5

0.2 Why measuring rotations in seismology ? 9

0.3 How to measure rotations ? 11

0.4 Literature review of earthquakes observations by optical gyroscopes 15

0.4.1 The first observations in New Zealand 15

0.4.2 The "Grossring" in Wettzell-Germany 17

0.4.3 The Ring laser Gyroscopes in Italy 18

0.4.4 Open questions 20

1 First deep underground observation of rotational signals from an earthquake at teleseismic distance using a large ring laser gyroscope **23**

1.1 Introduction 25

1.2 Instrumental apparatus 26

1.3 Method 28

1.4 First results 30

1.5 Conclusions 32

2 Deep underground rotation measurements: Gingerino ring laser gyroscope in gran sasso 35

2.1 Introduction 37

2.2 GINGERino working principle and experimental setup 39

2.3 Data acquisition 43

2.4 Sensitivity of the apparatus 44

2.5 Backscattering analysis 45

2.6 Seismological observations 47

2.6.1 Background noise analysis 49

2.7 Conclusions 52

3 Rotational motions from the 2016, Central Italy seismic sequence, as observed by an underground ring laser gyroscope 55

3.1 Introduction 57

3.2 Geological and Structural Framework 59

3.3 The experimental setup 59

3.4 Data analysis 61

3.4.1 Source Magnitude 65

3.4.2 Back Azimuth estimation 66

3.4.3 Phase velocity estimation 72

3.5 Conclusions 75

4 6-Component Ground Motion Observations of Local Earthquakes: The 2016 Central Italy Sequence 79

4.1 Introduction 80

4.2 Geological framework 83
4.3 Observations and processing 84
4.3.1 Zero lag correlation check on the rotational data 87
4.3.2 BAZ determination 89
4.3.3 Phase velocity measurements 90
4.4 Discussion and conclusions 92

Conclusions **99**

Appendices **105**

List of Figures

1 Rayleigh component (acceleration and rotation rate) of the Alaska MW 7.8 23/01/2018 Earthquake recorded at the ROMY station 8

2 Scheme of the Sagnac principle 12

1.1 Map of the LNGS underground laboratories 27

1.2 The GINGERino RLG 28

1.3 The NANOMETRICS Trillium 240 s (left) and Guralp CMG 3T360s (right) and the Lippmann 2-K tilt meter (on top), the red arrow shows the North direction 29

1.4 (top) Ground rotation and transverse acceleration time histories (black and red lines, respectively), time zero is at 12:40:00 UTC. (bottom) ZLCC between the above traces. 31

1.5 Map of correlation versus rotation of transverse acceleration 32

1.6 Superposition of trace-by trace normalized narrow band filtered signals (rotation in blue and transverse acceleration in black respectively), for every dominant period we report the estimated phase velocity 33

2.1 Top: the granite frame of GINGERino, just after its installation in the LNGS tunnel. Bottom: completed setup inside the isolation chamber. . . . 41

2.2 Optical setup. Three optical signals are continuously acquired: the combined beams intensity (Sagnac interferogram) S and the two monobeam intensities I_1 and I_2. The G signal is the intensity of the plasma fluorescence, filtered around the laser line. It is acquired as a monitor of the laser excitation level. IBS: Intensity Beam Splitter, PMT: Photo Multiplier Tube, LF: Line Filter (633 nm), TA:Transimpedance amplifier, FC=Fiber Coupler, CL: Collimating Lens. 42

2.3 Angular velocity linear spectral density of GINGERino calculated a dataset of 3600 s from 11-06-2016 at 00:00. Power spectral density is estimated from the raw data interferogram. 45

2.4 Black: raw data. Red: backscattering corrected data. 46

2.5 Relative Allan deviation for the Sagnac frequency after backscattering subtraction. Straight line represents the calculated shot noise limit. 47

2.6 Mid Atlantic ridge earthquake, June 17, 2015, 12:51 p.m., MWC 7. Top: seismograms for the transverse acceleration (black) and vertical rotation (red). Center: the zero lag correlation coefficient between rotation and transverse acceleration. Bottom: apparent phase velocity of the surface waves. Phase velocities are computed for the seismograms parts where the correlation between rotation and translation is larger than 0.6. 48

2.7 Rykyu Islands earthquake, November 13, 2015, 08:51 p.m., MWC 6.8. Plot legend is the same as in Fig.2.6. 49

2.8 Probabilistic power spectral densities for the three components of ground acceleration as recorded by the seismometer. Vertical scale is relative to $1\,\mathrm{m^2 s^{-4} Hz^{-1}}$. For each frequency bin, the maps illustrate the probability of observing a given spectral power, according to the color scale at the right. . 50

2.9 Principal polarization direction of the background noise over the $50 - 200$ s period range. Results from the two seismometers are coherent within a 5 degrees tolerance, indicating ground oscillations aligned along the tunnel's direction. This suggests a main control of the underground cavity in the generation of seismic noise at very long periods. 51

3.1 The GINGERino RLG and the seismometer Trillium 240 in the central box. The arrows indicates the observables that are object of this study, i.e. vertical rotation rate in red (from the RLG) and transverse acceleration in black (after processing the seismometer data) and the direction of the wavefield $\hat{k}$. In this figure the vector $\hat{k}$ is pointing to the North. It corresponds for example to the direction of a propagating shear wave causing a transverse acceleration in the $\ddot{u}_T$ direction. 61

3.2 The map shows the epicenters locations and the focal mechanism of the 10 strongest events. Red triangle denotes the Gingerino seismic station. The top figure in the inset shows a map of the underground laboratories, while the bottom one shows the Gingerino RLG. 63

3.3 The recorded event waveforms, in red the vertical rotation rate, in black the transverse acceleration. The time window is 45-seconds long. Individual rotation and translation traces are normalized to their respective peak value. 64

3.4 Peak angular displacement for the recorded events vs. epicentral distance, the continuous lines represents the local magnitude scale that we fit to the data 67

3.5 The back azimuth analysis in different frequency bands for the Visso M 5.9 mainshock, In this plot the red color denotes the correlation in red and anticorrelation in blue (see the colorbar). On top of the figure the superposition of rotation rate (red) and transverse acceleration (black). . . 68

3.6 The Visso M 5.9 mainshock; histogram for the distribution of maximum correlation values in the Love waves time windows and in the 2 seconds to 5 seconds of period range. The solid red line represent the KDE estimation of the distribution. For this event the theoretical BAZ is 324° 69

3.7 Theoretical and observed BAZ for all the events listed in Table 4.1 70

3.8 Misfit distribution and the relative gaussian KDE modeling in solid red line 71

3.9 The amplitude spectral densities calculated with the multitaper method, in black the transverse acceleration and in red the vertical rotation rate. From left to right the three seismic phases that we analyzed, in blue the noise level of the RLG 73

3.10 The Visso MW 5.9 mainshock. Superposition of vertical rotation rate (red) and transverse acceleration (black) and determination of phase velocities as a function of central frequency of the half octave bandpass filter. The phase velocity values are measured by taking the ratio of the envelopes of the band passed seismogram 76

3.11 The result of the phase velocity estimation method applied to P-coda, S-coda and Love waves time windows 77

4.1 The experimental setup: (top left) the BlueSeis3C; (top right) the seismometer Trillium 120c, (bottom left) the LCG-demonstrator; Bottom right the Guralp CMG-5 82

4.2 Event 1. Broadband ground acceleration after numerical instrumental response correction and numerical differentiation in black; rotation rate (red) measured of the ML 3.8 earthquake of the 12 Nov 2016 at 12:34:11 85

4.3 Event 2. Broadband ground acceleration after numerical instrumental response correction and numerical differentiation in black; rotation rate (red) measured after the ML 3.7 earthquake of the 12 Nov 2016 at 12:59:18 . . . 86

4.4 The ZLCC check between the rotational components recorded by LCG demonstrator in black and BlueSeis3A for the event number one of Tab. 4.1, the data are band-pass filtered in the interval [5-10] Hz 87

4.5 The ZLCC check between the rotational components recorded by LCG demonstrator in black and BlueSeis3A for the event number two of Tab. 4.1 88

4.6 Amplitude spectra calculated for the S phase window of the recoded events. 89

4.7 The BAZ estimation and the distribution of the maximum vales of WTC vs angle for event 1 estimated after step-rotation of horizontal seismometer traces and correlation with vertical rotation rate (Lg waves). The red trace represents the vertical rotation rate and the black trace the transverse acceleration. The black continuous line is the theoretical BAZ: 101.5° . . . 93

4.8 The BAZ estimation and the distribution of the maximum vales of WTC vs angle for event 2 estimated after step-rotation of horizontal seismometer traces and correlation with vertical rotation rate (Lg). The red trace represents the vertical rotation rate and the black trace the transverse acceleration. The black continuous line is the theoretical BAZ: 102° 94

4.9 The BAZ estimation and the distribution of the maximum vales of WTC vs angle for event 1 estimated after step-rotation of horizontal rotation rate traces and correlation with vertical acceleration (Rg waves). The red trace represents the transverse rotation rate and the black trace the vertical acceleration. The black continuous line is the theoretical BAZ: 101.5° 95

4.10 The BAZ estimation and the distribution of the maximum vales of WTC vs angle for event 2 estimated after step-rotation of horizontal rotation rate traces and correlation with vertical acceleration (Rg waves). The red trace represents the transverse rotation rate and the black trace the vertical acceleration. The black continuous line is the theoretical BAZ: 102° 96

4.11 Scatter plot of the couple of sets $\{\Omega_Z, a_T\}$ in Black (Lg waves) and $\{\Omega_T, a_Z\}$ in Red (Rg waves); on the left panel the event number one, on the right panel the event number two. 97

12 Wavelet decomposition BAZ analysis fot the MW9.0 Tohoku-Oki earthquake recorded at the Wettzell station 110

13 The phase velocity estimation method applied to to Tohoku-Oki earthquake as recorded by the Wettzell station, in this case we measure the Love waves phase velocity and SH 111

List of Tables

3.1 List of earthquakes analyzed in this study. 62

4.1 The recorded events 84

4.2 The results of the ODR on the events band pass filtered in the [5-10] Hz interval; we report the estimated phase velocity for Lg and Rg waves, the Error on the linear fit of equations 4.1 as the sum of orthogonal distances and the maximum values of zero lag correlation coefficient estimated my means of sliding one second long window 92

Acronyms list

4C	Four components
6C	Six components
ASD	Amplitude spectral density
BAZ	Back azimuth
CCW	Counter clock-wise
CMT	Centroid moment tensor
CW	Clock-wise
FIR	Finite impulse response
FOG	Fiber optic gyroscope
GINGER	Gyroscopes in general relativity
GPS	Global positioning system
IERS	International Earth Rotation and Reference Systems Service
INFN	Istituto Nazionale di Fisica Nucleare
INGV	Istituto Nazionale di Geofisica e Vulcanologia
KDE	Kernel density estimation
LASER	Light amplification by stimulated emission of radiation
LNGS	Laboratori Nazionali del Gran Sasso
LOD	Length of the day
NHNM	New high noise model
NLNM	New low noise model
ODR	Ortogonal distance regression
PMT	Photomultiplier
PPS	Pulse per second
PREM	Preliminary earth model
PZT	Piezo electric actuator
RLG	Ring laser gyroscope
ROMY	Rotational Motions in Seismology
SNR	Signal-to-noise ratio
VLBI	Very long baseline interferometer
WTC	Wavelet coherence
ZLCC	Zero-lag correlation coefficients
ZLWC	Zero-lag wavelet coherence

Summary

Summary

During the transit of seismic waves the earth and the ground is not only translating but it also rotates. Traditionally seismologists could only measure translations along three cardinal axes but earthquakes also generates tilt motions which rotate the ground. This fact was predicted by the linear elasticity theory but it took more than thirty years of technological progress in the instrumentation to achieve the sensitivity needed to record this tiny but extremely important ground motion. The most reliable instruments to capture rotational motions are optical gyroscopes. The large ring lasers (RLG) provide top sensitivity and are able to detect any M7+ earthquake. The new portable fiber optic gyroscopes (FOG) specifically designed for seismology, at the expense of a lower sensitivity, provide the great advantage of portability, which is a mandatory requirement for in-field measurements. We have, since at least ten years, consistent four components (three translations and one vertical rotation rate) observations from the G-ring in Wettzell, Germany. These observations permitted to establish the importance of colocated rotational and translational measurements for the study of earthquakes and ocean generated noise. Still at the beginning of this Ph.D. project there was need of confirming and expanding the observations to different sites, possibly in a different structural context and exploring higher amplitude signals and closer epicentral distances with a large RLG. Broadband six component (6C) measurements from a portable rotational sensor of local earthquakes were missing too. These open questions are faced in this work whose chapters are constituted by scientific publications in chronological order. From 2015 I contributed to the experimental activity, construction and data analysis of a new RLG located in gran Sasso underground laboratories named Gingerino. The first three chapters regard the measurements of the Gingerino RLG instrument inside the Gran Sasso, in a deep underground environment. In the first chapter I report the detection and the analysis of the first underground rotational signals from a tele-seismic event. The characterization of the instrument as well as an

analysis of the noise of the installation site can be found in chapter two. The analysis of the data from the 2016 central Italy seismic sequence is presented in chapter three. In this chapter we report a large dataset of events that a are studied with new methods based on the wavelet decomposition of the signals. The last chapter shows the results of the first field campaign with 6C observations (three rotational and three translational degrees of freedom) during the aftershocks of the MW 6.1 Norcia earthquake of 2016. This configuration can be alternative to a seismometer array; this is an undeniable logistic advantage for future applications in extreme environments as well as in planetary seismology. By the time of writing this abstract we have three large ring laser gyroscope operative in the world: G-wettzell, Gingerino and the new ROMY, a four components RLG that allows the reconstruction of the ground rotation vector with a record sensitivity. We expect then very soon advances in this research field thanks to the recent developments in instrumentation and processing techniques, some of them are already present in this work.

Introduction

Rotational seismology is the field of study devoted to the investigation of all aspects of rotational motions induced by any kind of seismic signal e.g. earthquakes, explosions and environmental noise. It plays an important role in a wide range of disciplines. These vary from various branches of seismology to earthquake engineering and seismic exploration.
The impact on seismology itself is expected to be large and involving many aspects like seismic tomography [Bernauer et al., 2012, Wassermann et al., 2016]; point and finite source inversion [Donner et al., 2016, Donner et al., 2017]; volcano source inversion [van Driel et al., 2015], scattering phenomena constraints, wavefield reconstruction, tilt-translation coupling.
The results of modern seismology are primarily based on observations of translational ground motions and strain. However, since at least two centuries, it was possible to proof theoretically the existence of three components of rotational ground motions around three orthogonal axes. The lack of an adequate broadband instrument delayed their observation until today. This thesis deals with two aspects of rotational seismology, the first is the instrumental aspect, the second one is about the observation and the interpretation of colocated measurements of ground rotation and translation. The introduction to this work guides the reader trough an historical overview of the developments in instrumentation and outlines fundamental works on the observation of rotational ground motion. Like in many other fields of science theory can predict some aspects of nature that can only be proven experimentally by suitable instruments. This can happen years decades or centuries after the prediction of a particular phenomenon; a great recent example is the detection of gravitational waves ([Phy, 2016]). In a similar way also the existence of ground rotations was predicted by linear elasticity theory but the technological limits of the instrumentation hindered their detection for several decades.
The technological deficit include, in chronological order:

- the sensitivity of the rotational sensors.

- the number of rotational components that could be recorded at the same time.

- the portability in order to permit an in-field deployment of rotational sensors.

Two fundamental questions arise: why measuring rotations in seismology and how ?

0.1 Basic theory

Here the basic theoretical background of seismic rotations is described. We use therefore classical elasticity approximation where the symmetry of stress and strain tensors is assumed. We also remark that, as pointed out by [Lee et al., 2009], some near field measurements report observations of rotational motions that are one or two orders of magnitude larger than what expected from linear elasticity. In addition some theoretical works suggests that in granular materials or in cracked continua, the asymmetries in the stress and strain tensors can cause rotations others than those predicted by linear elasticity [Pujol, 2009, Teisseyre, 2012].
Following [Cochard et al., 2006a] and [Aki and Richards, 2002], in the framework of linear elasticity and the infinitesimal deformation assumption, the displacement of a point in $\mathbf{x}$ is related to that of a neighboring point $\mathbf{x} + \delta\mathbf{x}$ by

$$\begin{aligned} \mathbf{u}(\mathbf{x} + \delta\mathbf{x}) &= \mathbf{u}(\mathbf{x}) + \mathbf{G}\delta\mathbf{x} \\ &= \mathbf{u}(\mathbf{x}) + \boldsymbol{\varepsilon}\delta\mathbf{x} + \boldsymbol{\Theta}\delta\mathbf{x} \\ &= \mathbf{u}(\mathbf{x}) + \boldsymbol{\varepsilon}\delta\mathbf{x} + \boldsymbol{\theta} \times \delta\mathbf{x} \end{aligned} \tag{1}$$

where the second-order strain $\boldsymbol{\varepsilon}$ and rotation $\boldsymbol{\Theta}$ tensors are the symmetric and antisymmetric parts of the displacement gradient $\mathbf{G}$ and $\boldsymbol{\theta}$ represents the rotation vector, the angle

of rigid rotation generated by the seismic perturbation.

$$\boldsymbol{\theta} = \frac{1}{2}\nabla \times \mathbf{u}(\mathbf{x}) = \frac{1}{2}\begin{pmatrix} \frac{\partial u_z}{\partial y} - \frac{\partial u_y}{\partial z} \\ \frac{\partial u_x}{\partial z} - \frac{\partial u_z}{\partial x} \\ \frac{\partial u_y}{\partial x} - \frac{\partial u_x}{\partial y} \end{pmatrix}. \tag{2}$$

In other words if we want to characterize the change in the elastic medium around $\mathbf{x}$ we must measure three components of translation, six components of strain and three components of rotation. Let's recall Hooke's law

$$\sigma_{ij} = \lambda\delta_{ij}\sum_{k=1}^{3}\varepsilon_{kk} + 2\mu\varepsilon_{ij} \tag{3}$$

here σ_{ij} and ε_{ij} are generic components of stress and strain tensors, $\sum_{k=1}^{3}\varepsilon_{kk} = \nabla \cdot \mathbf{u}$, λ, μ, are the Lame' constants and δ_{ij} is the Kroneker delta. Let's suppose the free surface on the xy plane and assume the zero traction boundary condition, a direct application of eq. 3 in a homogeneous, isotropic medium on the free surface gives us

$$\frac{\partial u_x}{\partial z} = -\frac{\partial u_z}{\partial x}; \quad \frac{\partial u_y}{\partial z} = -\frac{\partial u_z}{\partial y}; \quad \frac{\partial u_z}{\partial z} = -\frac{\lambda}{\lambda + 2\mu}\left(\frac{\partial u_x}{\partial x} + \frac{\partial u_y}{\partial y}\right). \tag{4}$$

from eq. 2 and 4 we can derive

$$\theta_x = \frac{\partial u_z}{\partial y}; \quad \theta_y = \frac{\partial u_z}{\partial x}; \tag{5}$$

and

$$\theta_z = \frac{1}{2}\left(\frac{\partial u_y}{\partial x} - \frac{\partial u_x}{\partial y}\right). \tag{6}$$

these are the expressions for rotation angles respect to displacement gradient elements. In order to start from the simplest condition, we treat now the case of plane wave propagation

and the zero traction boundary condition i.e. at the free surface.

0.1.1 Rotations by Love waves

Love-waves are horizontally polarized surface waves, at constant velocity (which is not the case of Love waves in a multilayered medium), the displacement for a wave propagating along the X-axis can be expressed by

$$\boldsymbol{u}(x, y, z, t) = (0, u_y(t - x/c_L), 0) \tag{7}$$

with c_L being the horizontal phase velocity. Love-waves induce rotations around the Z-axis that can be expressed using eq. 2 and 4 by

$$\theta_z = \frac{1}{2}\frac{\partial \dot{u}_y}{\partial x} = -\frac{\dot{u}_y(t - x/c_L)}{2c_L} \tag{8}$$

and in rotation rate

$$\Omega_z = \frac{\partial \theta_z}{\partial t} = -\frac{\ddot{u}_y(t - x/c_L)}{2c_L} \tag{9}$$

The transverse acceleration and rotation rate about Z-axis are in phase and scaled by a factor $-1/2c_L$. A ring-laser installed horizontally to the ground free surface is in principle sensitive only to rotations about vertical axis, that means, only to Love and S waves that are horizontally polarized i.e. SH waves.

0.1.2 Rotations by Rayleigh waves

Rayleigh waves are surface waves characterized by a retrograde elliptic particle motion that takes place in the vertical plane containing the propagation direction. This kind of waves can be recorded both on the vertical and longitudinal component of a seismometer. For a half space Poisson solid we can express the displacement caused by a Rayleigh wave

propagating along the x-axis at zero depth by [Lay and Wallace, 1995]

$$\begin{aligned} u_x &= -0.42Ak\sin(\omega t - kx) \\ u_z &= 0.62Ak\cos(\omega t - kx) \end{aligned} \tag{10}$$

Where A is the incident P-wave scalar potential for a plane wave characterized by the frequency ω and the wavenumber k. In velocity and acceleration we have:

$$\begin{aligned} \dot{u}_x &= -0.42Ak\omega\cos(\omega t - kx) \\ \dot{u}_z &= -0.62Ak\omega\sin(\omega t - kx) \end{aligned} \tag{11}$$

$$\begin{aligned} \ddot{u}_x &= +0.42Ak\omega^2\sin(\omega t - kx) \\ \ddot{u}_z &= -0.62Ak\omega^2\cos(\omega t - kx) \end{aligned} \tag{12}$$

If we use eq. 2 we can obtain the rotation angle around y axis

$$\theta_y = -0.62Ak^2\sin(\omega t - kx) \tag{13}$$

and the rotation rate by differentiating:

$$\Omega_y = \dot{\theta}_y = -0.62Ak^2\omega\cos(\omega t - kx) \tag{14}$$

Considering the observables $\{\dot{u}_x, \ddot{u}_x\}$ and $\{\theta_y, \Omega_y\}$, we calculate the ratios

$$\frac{\ddot{u}_x}{\Omega_y} = -\frac{0.42}{0.62}\frac{\omega}{k}\frac{\sin(\omega t - kx)}{\cos(\omega t - kx)} \tag{15}$$

$$\frac{\ddot{u}_x}{\theta_y} = -\frac{0.42}{0.62}\frac{\omega^2}{k} = -0.677\left(\frac{\omega}{k}\right)\omega = -0.677c_R\omega \tag{16}$$

$$\frac{\dot{u}_x}{\Omega_y} = 0.677/k \tag{17}$$

where $\frac{\omega}{k} = c_R$ by definition is the phase velocity of the Rayleigh wave. From eq.15 we see that the acceleration in x-direction and the rotation rate in y-direction are shifted by $\pi/2$ and scaled by the Rayleigh waves phase velocity. Eq.16 shows that x-acceleration is in phase with y-rotation angle and scaled by frequency and phase velocity. The eq.17 says that the x-velocity and y-rotation rate are in phase and scaled by the wavenumber. Finally, comparing the z-acceleration to the y-rotation rate we get

$$\frac{\ddot{u}_z}{\Omega_y} = \frac{\omega}{k} = c_R \tag{18}$$

i.e. the two observables are in phase and scaled by the phase velocity of the Rayleigh wave c_R. The previous derivation is valid for an homogeneous half space where a solution to the wave equation exists and propagates along the free surface and the ground motion at one station can be described by the equations above. [Marano and Fah, 2014] showed that if we account also for the ellipticity in the description of the ground motion, still in the comparison of eq. 18 this term cancels out, so in the end if we compare the vertical acceleration to the transverse rotation rate (tilt) we get rid of the ellipticity unknown and we can still estimate the phase velocity for a single Rayleigh wave. We know from observations that Rayleigh waves exhibit a dispersive behavior that is clear in the seismograms, specially in the vertical component of a seismometer, where mainly Rayleigh surface waves should be observed. This is evident for example from the data recorded by the ROMY ring laser after the 23-01-2018 Alaska MW 7.8 earthquake. In the Fig. 1 in fact we can clearly see how, also for the rotational part of the wave-field the period decreases with time after the Rayleigh waves onset. We know that this behavior is generally driven by the increase in Vp and Vs velocities with depth in the earth, as well as the presence of multi layered

structures. The Rayleigh waves in multilayered media were studied e.g. by [Haskell, 1953] with the important result of being then able to calculate synthetic phase velocity dispersion curves for Rayleigh waves. In rotational seismology the dispersion curves are experimentally derived assuming plane wave propagation, the principle of superposition and a bandpass approach that allows us to estimate via amplitude ratios in different bands the relation $C = C(f)$ for Rayleigh and Love waves. The difference that occurs between Love and Rayleigh waves is that for Love waves their existence implies automatically the dispersivity. This is not the case for Rayleigh waves where the dispersivity is due to the change in elastic properties of the medium with depth.

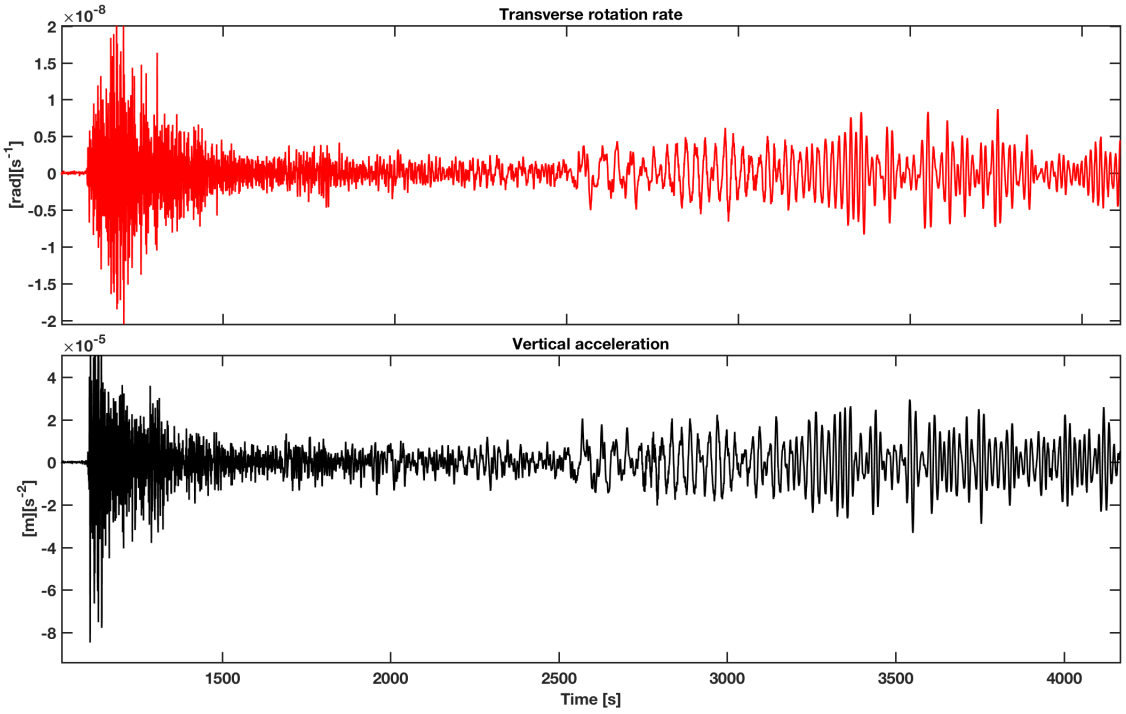

Figure 1: Rayleigh component (acceleration and rotation rate) of the Alaska MW 7.8 23/01/2018 Earthquake recorded at the ROMY station

0.2 Why measuring rotations in seismology ?

Seismology is a science based on the observation of ground motions. With suitable instruments seismologist follow the motion of a particle placed at the position $\mathbf{x} = (z, y, z)$ at the time t_0 in a defined reference frame. When the ground moves, this particle is dislocated, at time t, in the position defined by the coordinates $\mathbf{u} + \mathbf{x} = (u + x, v + y, w + z)$. The quantity defined by $\mathbf{u} = \mathbf{u}(\mathbf{x}, t)$ is what we want to measure i.e. the ground displacement. The previous is known as Lagrangian formulation and it is the approach that we use when we perform measures of the ground motion. In fact what we do is to attach to that ideal particle e.g. a seismometer or other instruments. In seismology two types of measures are routinely implemented, translations and strain. The observation of translations is based on the inertial seismometer. The observation of the displacement of two nearby points on the Earth is called strain, observed by strain meters based on optical or mechanical principles. Then, as [Aki and Richards, 2002] states at pag. 598

> "In principle a third type of measurement is needed in seismology and geodesy, namely rotation"

In earlier times there were attempts to measure and investigate the rotational ground motions. [Ferrari, 2006] reports a first attempt to measure the so called "vortical motion". P. Filippo Cecchi in 1876 built two models of an electrical seismograph with sliding smoked paper, dedicated to record three-component translational motions and also the rotational movements from earthquakes. That experiment did not show any evidence of ground rotations. Nevertheless there were examples of obelisks and monuments rotated after strong earthquakes. This was suggesting probably a much larger amplitude for rotations. However [Lee et al., 2011] show that those effects could be caused by only simple linear accelerations. [Schlueter, 1903] provides a more quantitative intuition of the utility of

measuring horizontal tilt (rotation) and vertical acceleration:

> *Nun knüpfen sich hieran interessante Folgerungen. Würde man im Stande sein, an einer Stelle der Erdoberfläche für die langen Wellen zu gleicher Zeit die Neigung und die Vertikalekomponente der Bewegung zu messen, so würde dadurch offenbar die Wellenlänge und mit Hinzuziehung der Schwingungsperiode auch die Fortpflanzungsgeschwindigkeit der über die Erdoberfläche dahingehenden Neigungswelle bestimmt sein. ...So würde man also eine Methode haben, um die wichtige Konstante der Fortpflanzungsgeschwindigkeit an jedem beliebigen Ort der Erdoberfläche unabhngig von Beobachtungen an anderen Orten zu bestimmen.*

The translation of this passage is:

> Now interesting conclusions follow. If one was able to measure the inclination (tilt) and the vertical component of the motion at the same time at a point on the surface of the Earth for the long waves, the wave length and the propagation velocity of the inclination would be determined by the oscillation period, thus we would have a method of determining the important constant of the propagation velocity at any place on the Earth's surface, independently of observations at other places.

In this fragment the author anticipates the importance and the potential of point-like colocated measurements based on observations of vertical accelerations and horizontal tilts (rotations). Note that also an important seismologist like [Richter, 1958] reasoned that the rotations were not only negligible by theory but also that their non-existence was already confirmed experimentally. Years later this claim was confirmed to be false.

0.3 How to measure rotations ?

Proven that ground rotations exist it is time to understand how to measure those tiny ground movements. Let's start with a wish list for the sensor.

- The first requirement is to have a very high sensitivity (better than $10^{-9} rad/s$ for periods longer than one second) associated with a complete decoupling from ground translations. Given an amplitude in acceleration from a tele seismic event of $10^{-7} m/s^2$ a simple scaling of a factor 10^3 i.e. a reasonable phase velocity for periods longer than one second gives rotation rates of the order $10^{-10} rad/s$

- Secondary three components of ground rotation must be measured with the same high sensitivity.

- Seismology is an experimental science, where field applications play a major role, the last wish is to have a portable broadband rotational motion sensor, that measures all three components of rotational motions with high sensitivity.

[Aki and Richards, 1980] proposed the use of a suspending mass at its center of mass, coupled to the ground with a spring and a dashpot as a rotational sensor. This approach never produced good results. Another idea is the use of a mechanical gyroscope and exploit the angular moment conservation principle to detect rotations. Also this approach has two problems: first, the sensitivity depends on the mechanical machining quality of the parts. Second, the measurement principle is based on moving masses that are intrinsically sensitive to inertial forces an so coupled to linear accelerations. The decoupling from inertial forces is achieved by using massless particles i.e. photons circulating clockwise and anti-clockwise in a closed loop interferometer. Let's give now some definitions. An active circular interferometer is called Ring Laser Gyroscope (RLG). It is the most sensitive rotational sensor nowadays and in general is not deployable in field campaigns. A passive

circular interferometer is a Fiber optic Gyroscope (FOG), it is less sensitive than the state of the art RLGs but much lighter and field deployable. The basic operating principle of a ring laser is the Sagnac effect. This was discussed by [Sagnac, 1913] when he considered the use of a ring interferometer as a rotation sensor. The Sagnac effect can be easily understood by considering an ideal circular interferometer of radius R, shown in Fig. 2. The light enters the interferometer at point A and is divided by a beam splitter into two counter propagating beams. If the interferometer does not rotate, the light beams recombine in A after a time $t = 2\pi R/c$, where c is the speed of light in the active medium. When the system is rotating at an angular velocity Ω, around an axis perpendicular to the plane of the interferometer, the two beams recombine at different times. The travel times for the

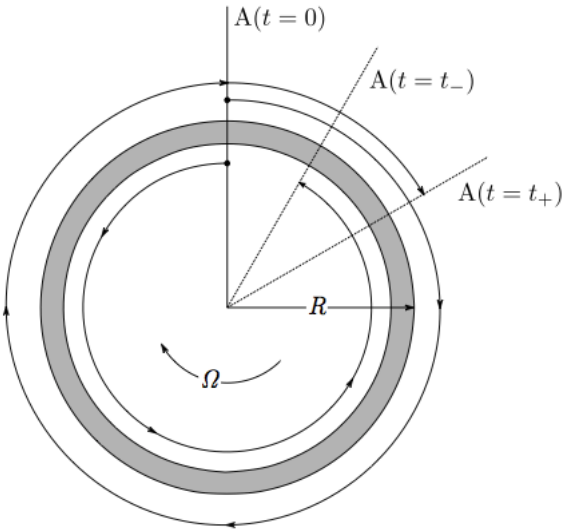

Figure 2: Scheme of the Sagnac principle

CW and CCW beams are

$$t_{\pm} = \frac{2\pi R}{c}\left(1 \mp \frac{R\Omega}{c}\right)^{-1} \tag{19}$$

using the approximation of $R\Omega << c$

$$\Delta t = \frac{4\pi R^2 \Omega}{c^2 - (R\Omega)^2} \approx \frac{4\pi R^2 \Omega}{c^2} \tag{20}$$

. The last approximation is largely valid for reasonable values of R and Ω.

The optical path difference can be written as

$$\Delta L = c\Delta t = \frac{4\pi R^2 \Omega}{c} \tag{21}$$

this equation can be generalized in the case of a general loop path as

$$\Delta L = 4\frac{\vec{\Omega} \cdot \vec{A}}{c} \tag{22}$$

where $\vec{A}$ is the area vector. Due to the presence of the c factor in the denominator, the value of ΔL for the range of rotations we are interested in becomes much smaller than the wavelength of the visible light. This difficulty is overcome in two ways: for fiber optic gyroscopes (FOG) the length of the path is maximized using very long optical fibers (order of 10^3 m). This makes the phase difference detectable in an easier way. Another way is to translate a typically difficult phase difference measure to a frequency difference measure. This is achieved by constructing an active ring laser. An extended closed ring cavity is filled with an active medium, which in our case consists of a gas mixture of Helium and Neon. This mixture is able to amplify light by stimulated emission radiation (LASER).

A resonant cavity can amplify the light only if in the length of the cavity L there is a whole number of wavelengths λ. In a ring cavity we have two electromagnetic waves (light) traveling in opposite directions. In this configuration, an optical path difference for the two circulating beams translates into an optical frequency difference. The optical

frequencies of the two beams are

$$\omega_{\pm} = \frac{2\pi N c}{L_{\pm}} \tag{23}$$

with N an integer value that indexes the longitudinal cavity mode and $L_{\pm}$ the lengths of the cavity as seen by the two beams. The frequency difference for two beams lasing in the same longitudinal mode is therefore proportional to the rotation rate of the optical cavity and can be written:

$$\Delta f = (f_+ - f_-) = Nc\left(\frac{1}{L_+} - \frac{1}{L_-}\right) = 2\pi N c \frac{\Delta L}{L^2} \tag{24}$$

Applying eq. 22 and eq. 23 we obtain

$$f = 4\frac{\vec{A}\cdot\vec{\Omega}}{L\lambda} \tag{25}$$

which is the equation that finally connects the Sagnac frequency to rotation rate for a RLG. In brief, the Sagnac principle can be exploited for seismology in two forms depending on its experimental implementation:

- In an active interferometer (RLG): the difference in travel time of the counter-propagating light is translated in a frequency difference detection problem, this is experimentally easier but involves bulky and heavy structures for the instrument frame. We have higher sensitivity (the highest among gyroscopes) but no transportability.

- In a fiber-optic gyroscope i.e. a passive Sagnac interferometer, the primary measure is the phase difference between the optical path length of two counter propagating laser beams, which is proportional to the externally applied rotation rate. Usually a phase difference measurement is more difficult and requires more complex electronics but also permits a lighter and compact and consequently transportable implementation

at the price of a lower sensitivity compared to (RLG)

0.4 Literature review of earthquakes observations by optical gyroscopes

The first RLGs did not allow to measure the ground rotations with the necessary sensitivity in the frequency range suitable for seismology. Until today the observations by RLGs were limited only to a single component of rotation rate, depending on the instrument orientation. Recently, the largest RLG system in the world called ROMY `romy-erc.eu`, a specific project devoted to measure the entire ground rotation vector has been concluded and is starting to acquire data. This RLG system has a tetrahedral geometry to record 4 components of rotations (3+1 redundant component). The ROMY project represent the state of the art in application of RLG technology to seismology.

0.4.1 The first observations in New Zealand

The first work to report seismological observations of rotations around a vertical axis parallel to the gravity vector is in [Stedman et al., 1995]. The instrument is a RLG named "Canterbury Ring Laser" known also as C1, the effective area is 0.75 m^2 and the shape of the optical cavity is a square. The sensitivity of the instrument is sufficient to detect four earthquakes ranging from MW 6.3 to MW 5; These events occurred in June 1994 during the Arthur Pass-Coleridge seismic sequence. The epicenters of the events were located approximately at 110 km from the RLG. In their paper, the authors report a long recording of ten hours showing a visual correspondence of the RLG rotational data with a seismic colocated station data named MQZ.

After the experimental evidence of ground rotations, [Takeo and Ito, 1997] raised the ques-

tion, what can be learned from rotational motions excited by earthquakes? For the authors the first answer to this question is: "we will have more accurate data for arrival times of SH waves, because the rotational component around the vertical axis is sensitive to SH waves although not to P-SV waves". The authors then treat important aspects about the seismic sources mechanisms. In this thesis we will show how it is possible to identify SH arrivals at local distances. Traditionally this is a hard task due to the complexity of the seismograms.

Using data from the same instrument [McLeod et al., 1998] detect an event of ML 5.3 located at 230 km from the seismic station in the Cashmere cavern (NZ). The authors report a peak rotation angle of 5 milliradiants. They also provide a comparison of the waveforms with a colocated seismometer and they analyze the amplitude spectral density of the rotational signal. The authors also discussed the possibility to "estimate the magnitude of the rotation angle at a remote distance" on the basis of the local Richter scale. This is an open question that we will solve in this work. In the conclusions, they discuss the possibility to use the RLG technology for the detection of ground rotation motions, pointing out that despite this instruments are bulky and expensive they have the advantage of an intrinsic construction simplicity and a very important, by principle, insensitivity to ground displacement.

[Pancha et al., 2000] report the first observations of rotational motions induced by earthquakes at tele seismic distances. Meanwhile two new instruments were established. The first one was C-II, a monolithic RLG made of Zerodur, the material with the lowest thermal expansion coefficient. Despite the size of only 1,2m this instrument showed outstanding performances in therms of sensitivity: C-II was installed horizontally and was able to measure rotations around a vertical axis. The second one, G-0 is bigger in size, 4-m of side length. It was constructed solid to a vertical wall, with sensitivity to rotations around a horizontal axis. Both instruments recorded a Mw 7 earthquake generated in New Ireland.

A second tele seismic event from Vanuatu was recorded by the C-II instrument. [Pancha et al., 2000], thanks to the increased sensitivity of the instruments, were able to see the very high correlation between the vertical and horizontal observations of rotations and the relative associated translational observables i.e. the transverse acceleration for the first and the vertical acceleration for the second. This confirms what was expected and predicted from theory for a seismic wave that propagates under the plane wave assumption.

0.4.2 The "Grossring" in Wettzell-Germany

The feasibility of a RLG of the size of 4 m in side was proved by the construction of G-0 and the undeniable benefits of the zerodur monolithic structure was clearly shown by the C-II results. This experience led to the construction of the G-ring in the Geodetic observatory in Wettzell-Germany. Merging together the benefits of the size and of the monolithic Zerodur structure led to an instrument whose performance are outstanding in therms of sensitivity, stability and observation time.

[Igel et al., 2005] shows the first measurements of vertical rotations from an earthquake 8830 km distant from the Wettzell station WET. This paper shows that the RLG technology provides the required resolution for consistent broadband observations of rotational motions induced by very distant earthquakes. For the first time the physical relations that connect the vertical rotation rate to the transverse acceleration is used to obtain a time/seismic phase dependent phase velocity estimation. In the same period a low-cost project for a vertical ring laser installed in Pinon Flat, California was deployed. The so called Geosensor is specifically designed for the observation of earthquakes in an area of high seismological interest (The San Andreas fault) from local to tele seismic distance. The details of this project are reported by [Schreiber et al., 2006b].

A few years later, [Igel et al., 2007] reports the observations and the analysis of 18 earthquakes recorded by the G-Wettzell RLG. The epicenter of the reported events span from

390 km for a ML 5 regional earthquake to 9000 km for the Great Sumatra-Andaman MW 9.0 earthquake. The first step of processing in this paper is aimed to achieve a period dependent magnitude scale for rotations for surface waves. Later in this paper is introduced an estimator for the level of correlation between the observed rotation rates and transverse acceleration, the zero-lag correlation coefficient (ZLCC). The goodness of the correlation is an important validation tool that permits to give a quantitative meaning to concept of "similarity" between the seismic traces. Another important question that is analyzed is the propagation direction determination, i.e. the determination of the incoming wave-field. This aspect will be analyzed in this thesis using a novel wavelet based approach.
The G-Wetzell ring is providing observations since years and the large database that covers nowadays a decade of events recorded is available at `https://rotations-database.geophysik.uni-muenchen.de/`, where also the online processing of the earthquakes is available.

0.4.3 The Ring laser Gyroscopes in Italy

At the "Istituto Nazionale di Fisica Nucleare" of Pisa, Italy a research group developed a large RLG of 1.2 m side length devoted to investigate the role of horizontal tilt noise at the gravitational waves detector site VIRGO in cascina. [Belfi et al., 2012c] reports the recording and the analysis of the MW 9.0 Tohoku-Oki earthquake in a configuration that was sensitive mainly to Rayleigh waves. The rotational contribution given by Rayleigh waves was already observed by [Pancha et al., 2000] from the G-0 ring laser in New Zealand but in the paper of [Belfi et al., 2012c] the more advanced processing permitted an estimation of the Rayleigh waves phase velocity as well as the direction of the incoming wave-field. This confirmed that multi-component observations allow the estimate of wave-field properties (e.g., phase velocities, propagation direction) as [Igel et al., 2007] did for a vertically oriented RLG.

At the same time, the Tohoku-Oki earthquake was detected by the G-Wettzell RLG and, thanks to his higher sensitivity achieved after the 2009 upgrade. [Nader et al., 2012] could observe the toroidal free oscillations of the Earth. This phenomenon is observed also in other large previous events like the MW 8.8 occurred in Chile the 27 Feb 2010 and the MW 8.1 occurred in Samoa the 29 Sept 2009. Later the G-Pisa instrument was moved to the Gran Sasso national laboratories in an underground environment at 1500m depth below the free surface of the Earth inside the gran sasso massif. During the period of operation of G-Pisa in Gran Sasso, no seismological signals were observed. It is assumed that the reason lies in the fact that the surface waves decays at depth proportionally to their wavelength, for this reason the observation of rotational signal underground could be more difficult than on the free surface. The conclusions abut the first experience of G-Pisa in Gran Sasso were that the instrument was too small to be sensitive enough to measure seismological signals.

A second attempt to measure underground rotations was made in 2015 when the construction of the Gingerino RLG started, this is a 3.6 m side square vertically oriented RLG. The commissioning of the instrument to which the author contributed largely in all the experimental aspects finished in May 2015 when the instrument started to record the first data. Finally after few weeks of operations [Simonelli et al., 2016] observed the first earthquake at tele seismic distance. The paper of the author is completely reported in this thesis as Chapter 1. The analysis of the performances and the description of the instrument is given in [Belfi et al., 2017] i.e. Chapter 2, where the author contributed largely to data analysis, figures and manuscript preparation, especially for what concerns the seismological part. In fall 2016 the central sector of Italy was struck by a very intense seismic sequence. During this period we recorded a large dataset of roto-translational measures. The analysis and the interpretation of the results led to the work by [Simonelli et al., 2017b] i.e Chapter 3. In November 2016 during the aftershock activity following the Mw 6.5, of 30 October, a field

experiment was performed. For the first time a couple of FOGs specifically designed for seismological applications were installed near Colfiorito. An LCG-demonstrator from Litef and a BlueSeis3A from iXblue. The last one represent today the state of the art in terms of sensitivity and portability (see [Bernauer et al., 2017]) for rotational measurements. The first analysis of the six components recorded events is reported in chapter 4 i.e. [Simonelli et al., 2017a].

0.4.4 Open questions

These are the open question that will be treated in this thesis.

- In [Igel et al., 2007] the need of observations of colocated translations and rotations at different sites is outlined. We know that from this kind of measurements we can investigate the local velocity structure. For this reason it is important to implement similar stations (portable or permanent) in different sites on the Earth.
- Is it possible to observe rotational motions in an underground laboratory ?
- In the context of an underground experiment, can we still estimate the BAZ (i.e. the source direction) and the phase velocity under the plane wave assumption ?
- Can we measure high amplitude local or regional events with a large RLG ?
- Which is a possible way to process an event data set in order to give a statistical meaning to our measurements ?
- Can we use a 3C rotational sensor in a field experiment and measure local events ?
- What can we get from the processing of 6C ground motion data at local distance ?
- Can we estimate the BAZ of the incoming Rayleigh waves as well as we do for Love waves ?

- From the processing point of view, can we give a time/frequency measure of the correlation between observables and an estimation of the amplitude ratios in the time frequency domain, higlighting then the different apparent (SH, SV) or real phase velocities for different seismic phases ?

To all this questions we will try to provide an answer in the next chapters.

Chapter 1

First deep underground observation of rotational signals from an earthquake at teleseismic distance using a large ring laser gyroscope

Simonelli, A., Belfi, J., Beverini, N., Carelli, G., Virgilio, A. D., Maccioni, E., Luca, G. D., and Saccorotti, G. (2016). First deep underground observation of rotational signals from an earthquake at teleseismic distance using a large ring laser gyroscope. Annals of Geophysics, 59(0).

The contributions as a first author to this paper consist in:

- *The experimental activity involving the instrument construction, tuning of the optical parts, alignment, optimization and final commissioning.*
- *Row data preparation and preprocessing*

- *Coding of the routines used for the analysis of the earthquake*

- *Manuscript preparation*

Abstract

Recent advances in large ring laser gyroscopes (RLG) technologies opened the possibility to observe rotations of the ground with sensitivities up to 10^{-11} rad/sec over the frequency band of seismological interest (0.01-1Hz), thus opening the way to a new geophysical discipline, i.e. rotational seismology. A measure of rotations in seismology is of fundamental interest for (a) the determination of all the six degrees of freedom that characterize a rigid body's motion, and (b) the quantitative estimate of the rotational motions contaminating ground translation measurements obtained from standard seismometers. Within this framework, this paper presents and describes GINGERino, a new large observatory-class RLG located in Gran Sasso underground laboratory (LNGS), one national laboratories of the INFN (Istituto Nazionale di Fisica Nucleare). We also report unprecedented observations and analyses of the roto-translational signals from a tele-seismic event observed in such a deep underground environment.

1.1 Introduction

Ring Laser Gyroscopes (RLG) are the best sensors for capturing the rotational motions associated with the transit of seismic waves, thanks to the optical measurement principle, these instruments are in fact insensitive to translations. The claim for a rotational sensor in geophysics is outlined in a fundamental text about seismology [Aki and Richards, 2002], where the authors state that "... note the utility of measuring rotation near a rupturing fault plane (...), but as of this writing, seismology still awaits a suitable instrument for making such measurements ". The search for such a sensor is of actual interest, as shown by many recent studies [Kaláb et al., 2013, Brokešová and Málek, 2010, Schreiber et al., 2006a]. Nowadays RLGs allowed to achieve important results, spanning from geodesy [Schreiber et al., 2004] to the analysis of earthquakes recorded over a wide range of distances [Pancha

et al., 2000, Simonelli, 2014, Schreiber et al., 2006a]. The size or RLG changes, depending on the scope, from some centimeters to more than four meters. RLGs for navigation are very small and lightweight; they are produced commercially and are widely adopted for either underwater or airborne platforms. Their sensitivity, however, is not sufficient for geophysical applications. Sensitivity and accuracy of RLGs increase with size, thus maximizing dimensions causes a minimization of physical effects that cause the gyro to work out of an ideal linear regime. Scientific results like the solid tides monitoring or a measure of the length of the day (LOD) are only achievable by very large frame RLG. Actually, the G-ring apparatus in Wettzel Germany represents the reference RLG for geodetic and seismological observations. Smaller in size and less expensive is the range of RLG of the class Geosensor, [Schreiber et al., 2006b, Belfi et al., 2012a]. The GINGERino apparatus funded by INFN in the context of a larger project of fundamental physics is intended as a pathfinder instrument to reach the high sensitivity needed to observe general relativity effects; more detail are found at the URL (`https://web2.infn.it/GINGER/index.php/it/` and in [Belfi et al., 2016].

1.2 Instrumental apparatus

The Gingerino is located Inside the Gran Sasso National Laboratory (LNGS) of the INFN (Fig. 3.10). The equipment of geophysical and seismological interest is constituted by the following instruments: The large He:Ne ring laser visible in Fig. 3.1; this is a 3.6 m side square cavity ring laser installed over a granite structure block anchored to the rock of the B knot tunnel of the LNGS. This is our rotation sensor, it is able to detect rotations around the symmetry axis (oriented vertically) with a sensitivity better than 10^{-10} rad/s in the band of interest for global seismology (5 Hz-300s). A Nanometrics Trillium 240s seismometer which is installed at the center of the RLG granite frame Fig. 1.3. This

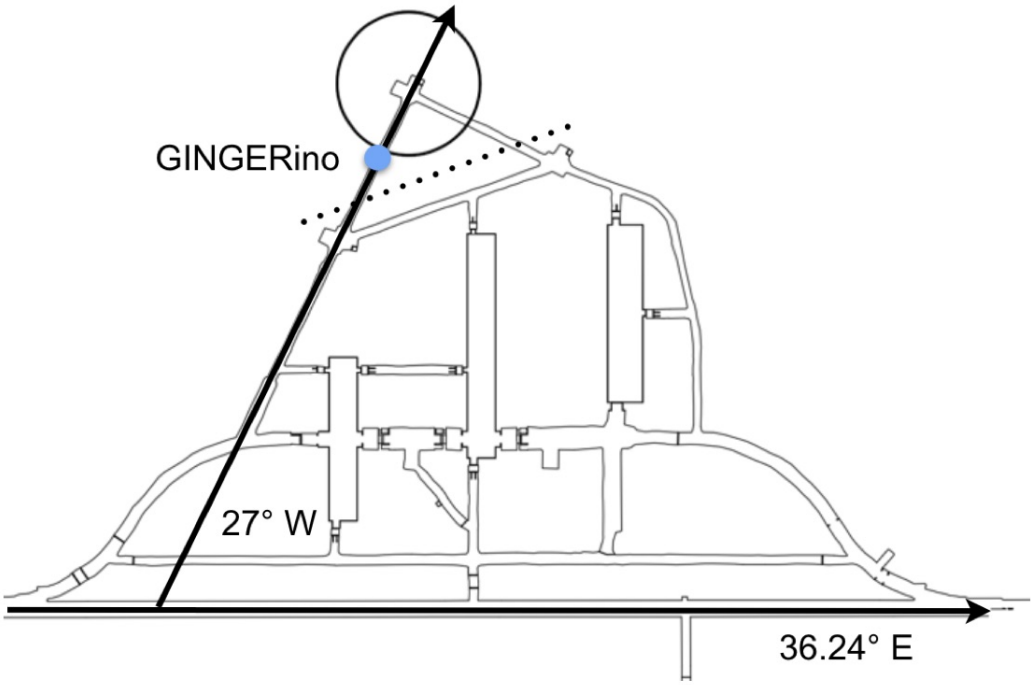

Figure 1.1: Map of the LNGS underground laboratories

instrument is part of the national earthquake monitoring program of the Istituto Nazionale di Geofisica e Vulcanologia (INGV hereinafter), provides the ground translation data to be compared to the RLG rotational data in order to infer the phase velocity measurements during the transit of shear and surface waves from earthquakes at local, regional and tele seismic distances. Further details on this station are at the URL (`http://iside.rm.ingv.it/iside/standard/info_stazione.jsp?page=sta&sta=2571`). A Lippmann 2-K digital tilt-meter with a resolution better then one nrad is placed beside the seismometer in order to monitor the possible slow ground tilt related to either local or wide scale (solid earth tides) effects. A second broadband seismometer, Guralp CMG 3T60s (Fig. 1.3) is placed in the central block for data redundancy.

t

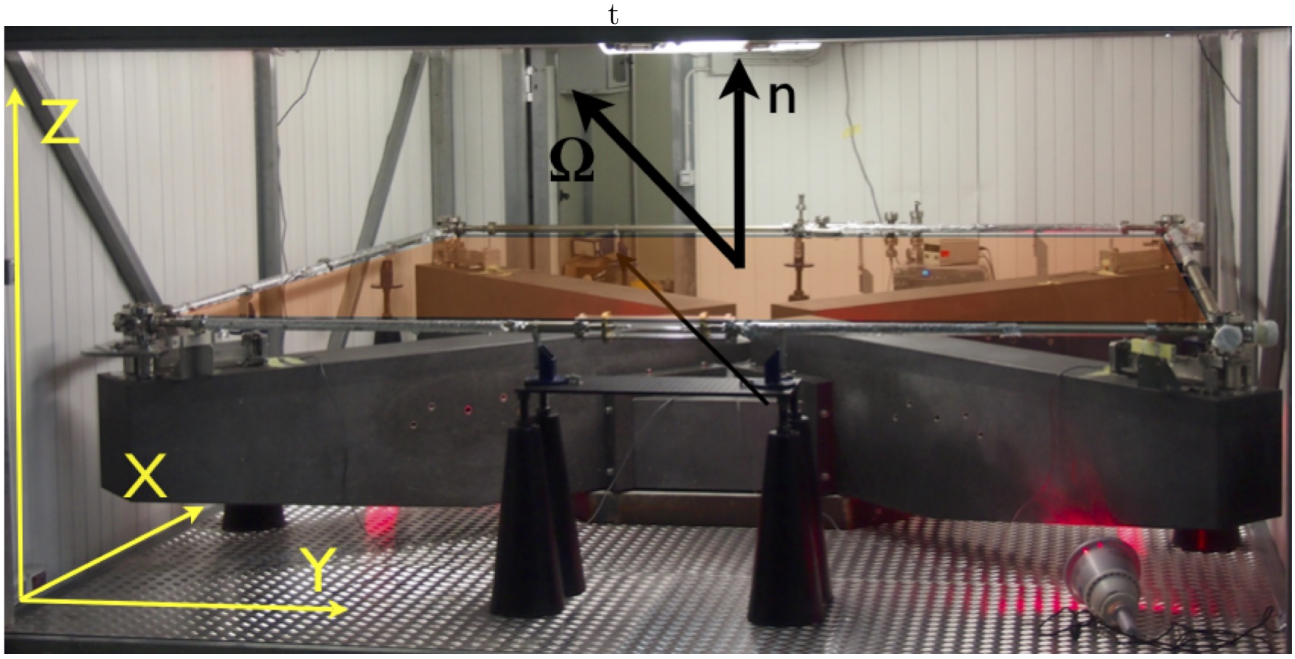

Figure 1.2: The GINGERino RLG

1.3 Method

RLG are based on the Sagnac effect; this effect is caused by a difference in the optical path as seen by two counter propagating laser beams that leads to a difference in the optical frequency between the clockwise and anti-clockwise propagating beams. The two beams are mixed out of the optical cavity in order to reveal the beat of the two slightly different frequencies. The beat frequency f, also called the Sagnac frequency can be related to the rotation rate around the normal vector to the surface outlined by the square optical path (see Fig. 3.1) using the simple following equation:

$$\Omega = \frac{\lambda_{He:Ne}}{L \sin\theta} f \tag{1.1}$$

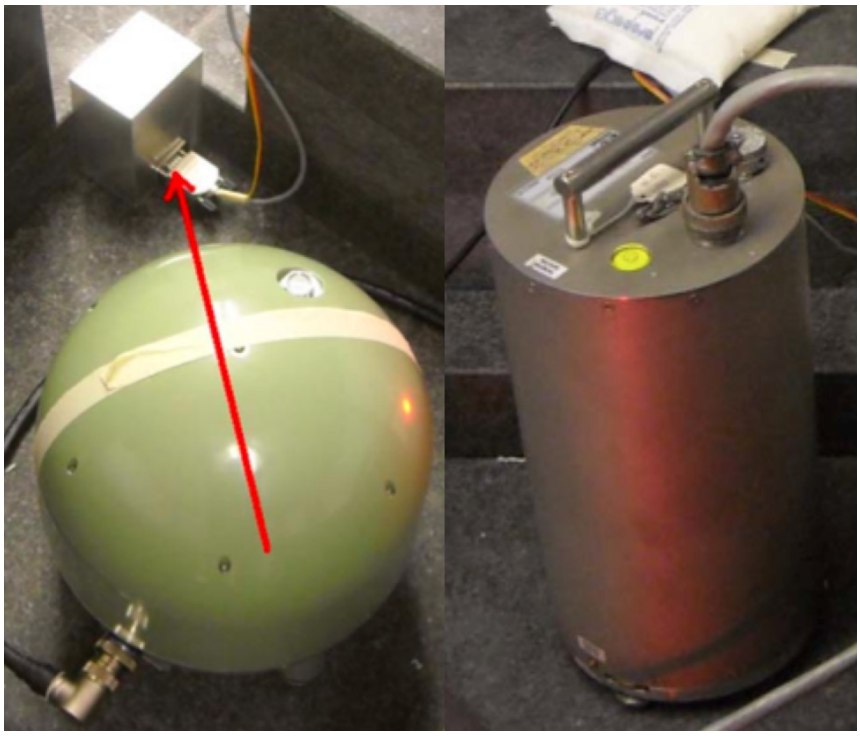

Figure 1.3: The NANOMETRICS Trillium 240 s (left) and Guralp CMG 3T360s (right) and the Lippmann 2-K tilt meter (on top), the red arrow shows the North direction

where $\lambda_{He:Ne}$ is the wavelength of the He:Ne laser (632 nm), L is the square side length and θ is the angle between the versor $\hat{n}$ and $\vec{\Omega}$. We know from theory [Aki and Richards, 2002] that rotations can be retrieved from ground displacement as the curl of the wave-field.

$$\vec{\Omega} = \frac{1}{2}(\nabla \times \vec{u}) \tag{1.2}$$

Referring to our setup (Fig. 3.1) for example, the displacement caused by a Love wave traveling as a plane wave along the x-direction is expressed through the equation:

$$u_y = Ae^{i\omega(x/C_L - t)} \tag{1.3}$$

By applying eq. 3.3 to eq.3.2 we obtain the relationship:

$$\Omega_z = -\frac{\ddot{u}_y}{2c_L} \tag{1.4}$$

which provides a direct estimation of the phase velocity C_L by using only a single-site measurement. From this latter formulation it is also evident that the sensing of ground rotations over the seismic frequency band requires high sensitivity: the phase-velocity scaling implies in fact that ground rotations are two to three orders of magnitude smaller than the associated translational movements. For this purpose a very sensitive and completely decoupled from translations device is required and at present large RLGs are the best candidates.

1.4 First results

An earthquake with magnitude 7 occurred on 17-06-2015 12:51:32 (UTC) with epicenter in the Southern Mid Atlantic Ridge [Sea] has been recorded by our instruments during the longest run of continuous data acquisition from 11/6/15 to 19/6/15. Though the recordings exhibit a poor signal-to-noise-ratio (SNR) their quality is sufficient to perform some analysis of seismological interest. The processing steps have been:

- The N-S and E-W seismometer traces are rotated by a step of 1 deg. over the $\{0, 2\pi\}$ range and for each rotation step, the zero-lag-cross-correlation (ZLCC) between the rotational signal and transverse accelerations is calculated. The maximum is found at a rotation angle of 198 N, the theoretical azimuth derived from epicenter and station coordinates is 202 N. The discrepancy between the observed and theoretical azimuthal values is small, once considering possible seismometer misorientation and deviation of surface wave trajectories from the great circle path as a consequence of

lateral velocity heterogeneities.

- The ZLCC between translational and rotational traces is calculated using a 200-seconds-long window, sliding with 50% overlap. The Love-wave arrival is marked by a clear correlation peak (see Fig.1.4)

- Ground rotations and Transverse accelerations (respectively blue and black lines in Fig. 1.6) are narrow band filtered with a FIR filter with a 1 s large passband region form 1 s to 50 s of Period. In the frequency bands where ZLCC is above a threshold of 0.7, the amplitude ratio between the maxima of the envelopes evaluated via Hilbert transform gives a direct measure of phase velocity for that particular period (see Fig. 1.6).

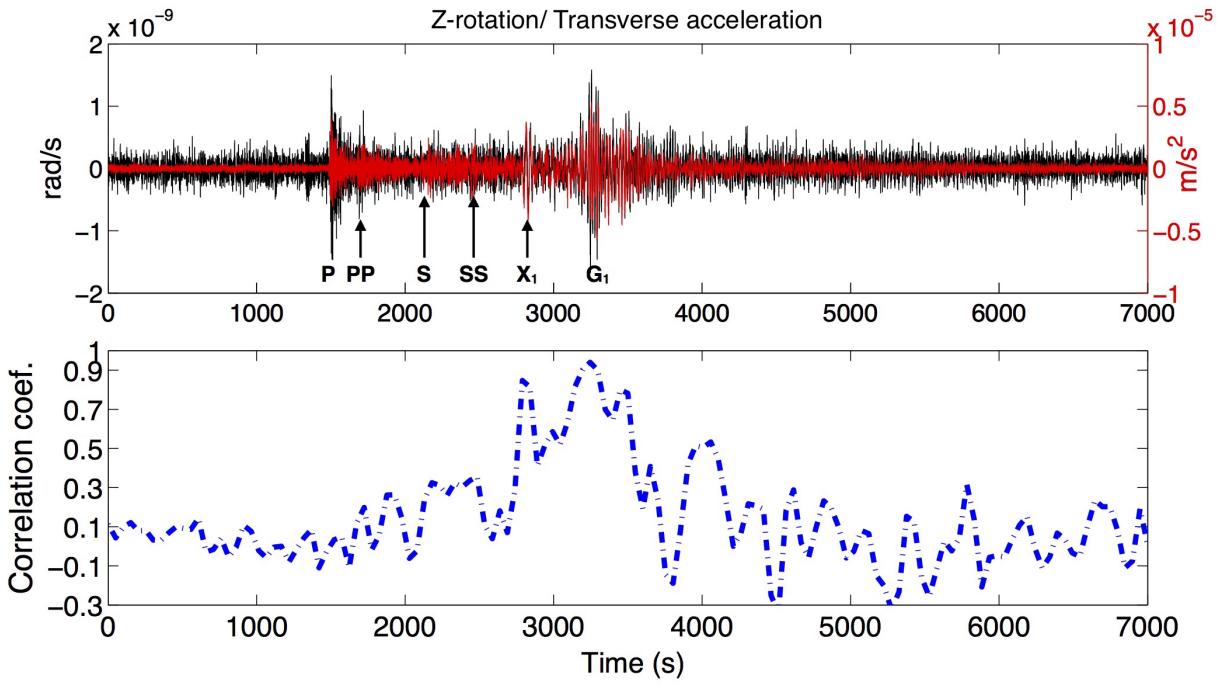

Figure 1.4: (top) Ground rotation and transverse acceleration time histories (black and red lines, respectively), time zero is at 12:40:00 UTC. (bottom) ZLCC between the above traces.

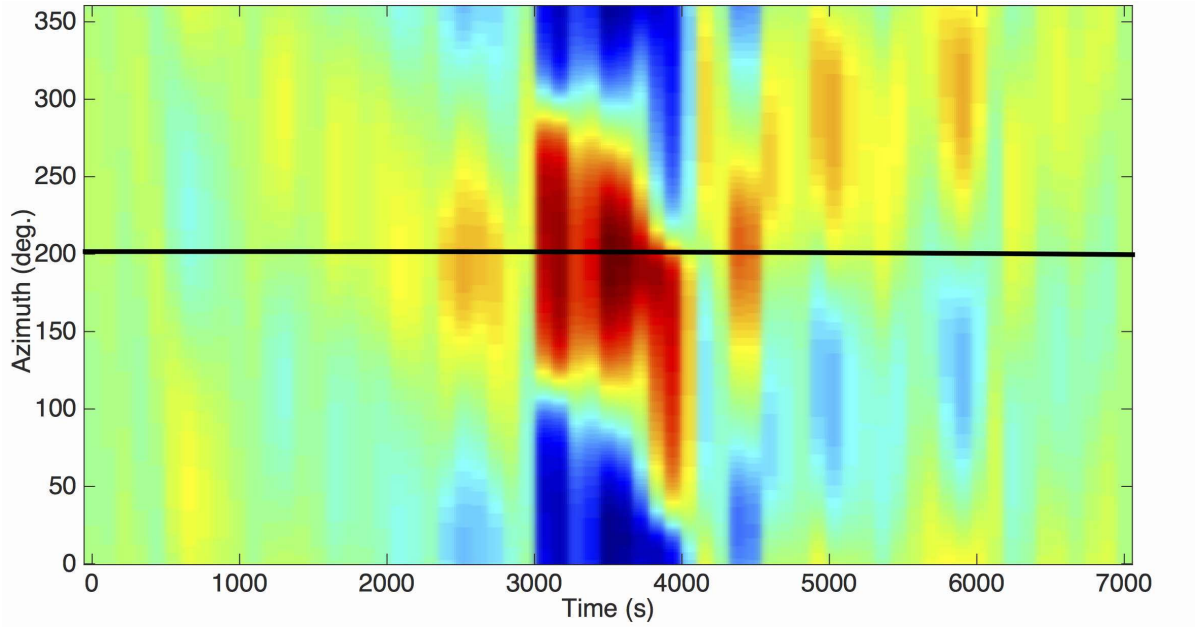

Figure 1.5: Map of correlation versus rotation of transverse acceleration

1.5 Conclusions

Gingerino is a test apparatus, and improvements in sensitivity and stability of the apparatus are foreseen in the near future. At present the RLG is running in a preliminary test mode in order to optimize the experimental parameters that will allow us to let it run continuously together with tilt-meters and seismometers and to increase sensitivity in order to be able to detect the secondary microseism peak that is only a factor five below our noise floor at the 10 seconds period. In a previous study we used a smaller RLG oriented along an horizontal axis and we obtained consistent estimates of ground rotations associated with the transit of Rayleigh waves from the 2011, Mw=9.0 Japan earthquake [Belfi et al., 2012c]. The present availability of a larger and much more sensitive RLG as Gingerino now permits extending the analysis to earthquake signals over a wider magnitude range. The simultaneous measurement of ground translation and rotation of these sources will allow the definition of the dispersion curve of Love waves over a broad frequency range,

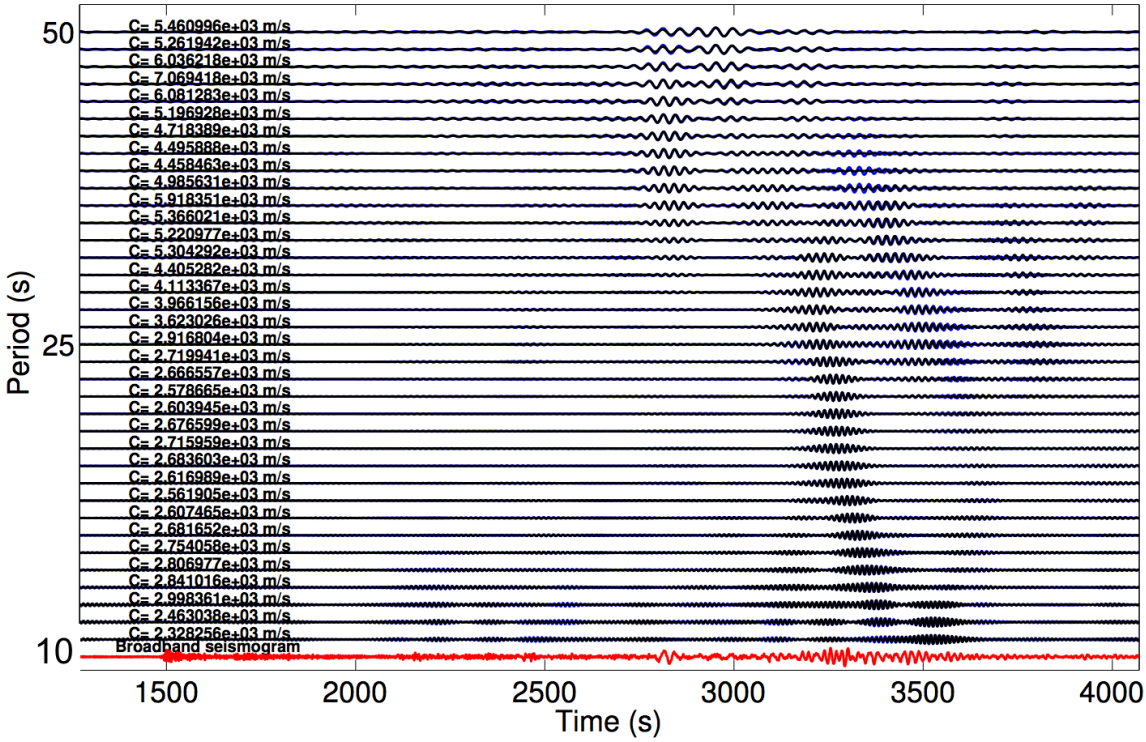

Figure 1.6: Superposition of trace-by trace normalized narrow band filtered signals (rotation in blue and transverse acceleration in black respectively), for every dominant period we report the estimated phase velocity

from which a local shear-wave velocity profile can be inferred with resolutions on the order of 100 m and penetration depths up to several tens of kilometers. To conclude we remark that a seismic station co-located with a RLG has been installed in the underground laboratories of INFN under the Gran Sasso. The Gingerino station is now a good companion of the Wettzel observatory station. For the first time a tele seismic rotational signal has been recorded in an underground environment. The source backazimuth inferred from the directional analysis is in excellent agreement with the theoretical one, suggesting that with a RLG and a seismometer the direction of the incoming wave-field may be estimated accurately. Corresponding to high ZLCC time intervals, we obtained estimates of phase velocities which, though being limited by the low SNR, are consistent with what expected

for Love waves propagating in the PREM Earth's model [Dziewonski and Anderson, 1981] i.e. in the range of 3800 ms^{-1} (at T = 10 s) to 4500 ms^{-1} (at T = 50 s).

Chapter 2

Deep underground rotation measurements: Gingerino ring laser gyroscope in gran sasso

Belfi, J., Beverini, N., Bosi, F., Carelli, G., Cuccato, D., Luca, G. D., Virgilio, A. D., Gebauer, A., Maccioni, E., Ortolan, A., Porzio, A., Saccorotti, G., Simonelli, A., and Terreni, G. (2017). Deep underground rotation measurements: Gingerino ring laser gyroscope in gran sasso. Review of Scientific Instruments, 88(3):034502.

The contributions as a coauthor of this paper consist in:

- *The experimental activity involving the instrument construction, tuning of the optical parts, alignment, optimization and final commissioning.*
- *Row data preparation and preprocessing*
- *Coding of the routines used for the analysis of the earthquakes and of the seismic noise*

- *Preparation of the figures and of the paragraph relative to the seismic interpretation of the data*

Abstract

GINGERino is a large frame laser gyroscope investigating the ground motion in the most inner part of the underground international laboratory of the Gran Sasso, in central Italy. It consists of a square ring laser with a 3.6 m side. Several days of continuous measurements have been collected, with the apparatus running unattended. The power spectral density in the seismic bandwidth is at the level of $10^{-10}(\mathrm{rad/s})/\sqrt{\mathrm{Hz}}$. A maximum resolution of 30 prad/s is obtained with an integration time of few hundred seconds. The ring laser routinely detects seismic rotations induced by both regional earthquakes and teleseisms. A broadband seismic station is installed on the same structure of the gyroscope. First analysis of the correlation between the rotational and the translational signal are presented.

2.1 Introduction

Large Ring Laser Gyroscope (RLG) technology [Schreiber and Wells, 2013a] provides very sensitive inertial rotation measurements. Among the most relevant recent results there are the direct observation of the rotational microseismic noise [Hadziioannou et al., 2012a] up to the detection of very long period geodetic effects on the Earth rotation vector [Schreiber et al., 2011]. The scientific community working on large frame RLGs had a rapid growth in the last decade. After the seminal work started in the '90s at the Canterbury University of Christchurch, (New Zealand) [sit, a], today, other laboratories around the world [Schreiber et al., 2006b, Dunn and Hosman, 2014] both in Europe and US, use RLGs to detect ground rotational motions superimposed on the Earth rotation bias. A dedicated observatory of 3D seismic rotations, named ROMY [sit, b], was started this year in Fürstenfeldbruck (Germany). The state of the art precision, is achieved by the Gross ring G [Schreiber et al., 2009] in Wettzell (Germany), and it is better than some fractions of prad/s, not far from 10^{-14}rad/s, that is the order of magnitude of the General Relativity effects in a

ground based reference frame. The target of the GINGER (Gyroscopes IN GEneral Relativity) proposal is to measure the gravito-magnetic (Lense–Thirring) effect of the rotating Earth, by means of an array of high sensitivity RLGs [Bosi et al., 2011]. Underground locations, far from external disturbances as hydrology, temperature and barometric pressure changes, are essential for this challenging experiments, and LNGS (Laboratori Nazionali del GranSasso, the underground INFN laboratory) may be a suitable one. In order to test the local ground noise, a single axis apparatus called GINGERino, has been installed inside LNGS. This installation is a pilot-prototype for GINGER, and at the same time can provide unique information for geophysics [Simonelli et al., 2016]. In addition, underground installations of large RLGs, free from surface disturbances, could provide useful informations to Geodesy [Nilsson et al., 2012]. Here the goal is to achieve a relative precision of at least 1 ppb in few hours of integration time, in order to integrate the information on Earth's rotation changes provided by the International Earth Rotation System (IERS) that, being based on the collection and elaboration of the observations of Very Large Base Interferometry (VLBI) and GPS systems, does not provide precise subdaily performance. The paper is organized as follows: in section 2.2 we describe the GINGERino optical and mechanical apparatus; section 2.3 is about the data acquisition and transfer; section 2.4 contains the noise characterization and the illustration of the drift removal method based on the backscattering noise identification and subtraction. In section 2.6 we discuss some preliminary results on the seismic properties of the underground site as well as the analysis of the roto-translations induced by two far located earthquake events. Section 2.7 contains the conclusions of this work and the future perspectives of the experiment.

2.2 GINGERino working principle and experimental setup

RLGs measure rotation rate using the Sagnac effect. Oppositely propagating laser beams, generated inside a ring resonator undergo a frequency splitting δf. For a horizontal RLG, located at colatitude θ, the splitting δf induced by the Earth's rotation rate Ω_E, is expressed in function of the cavity area A, perimeter P and laser-wavelength λ:

$$\delta f = \frac{4A\Omega_E}{\lambda P} \cos(\theta + \delta\phi_{NS}) \cos\delta\phi_{EW}, \tag{2.1}$$

where $\delta\phi_{NS}$ and $\delta\phi_{EW}$ are the tilt angles, respectively in the North-South and in the East-West directions. GINGERino is a He-Ne laser operating on the red line at 633 nm. The square optical cavity, 3.6 m in sidelength, is made of four spherical mirrors with 4 m radius of curvature. The plane of the cavity of GINGERino is horizontal, thus the Sagnac frequency bias is provided by the projection of the Earth's rotation vector along the local vertical. At the latitude of LNGS the Sagnac frequency is 280.4 Hz. The whole optical path of the beam inside the cavity is enclosed in a steel vacuum chamber, composed by 4 mirror chambers connected by vacuum pipes. The design is based on the GeoSensor design [Schreiber et al., 2006b, Belfi et al., 2012b, Belfi et al., 2012a], where the alignment can be tuned by means of micrometric tip-tilt systems acting on the mirror chambers orientation. From each corner of the cavity is possible to extract and detect the two counterrotating beams, so that the system has eight optical output beams. While monolithic cavities made of ultra-low expansion materials, like the Gross ring G in Wettzell, have an excellent passive stability, they are not suited to form 3D arrays of very large size. On the other side, heterolithic systems require active stabilization, which is achieved by active control schemes of the cavity geometry, exploiting very accurate optical wavelength references [Di Virgilio

et al., 2014, Santagata et al., 2015]. The present structure of GINGERino does not allow the full implementation of these techniques, and this sets a limit to its present long term stability.

Mirrors dissipative losses set the shot noise limit to the sensitivity of a RLG, while the backscattering characteristics are responsible of the drift induced by the nonlinear coupling between the two counter-propagating laser beams (see ref.[Schreiber and Wells, 2013a]). Dielectric deposition of thin films realized by very accurate ion beam sputtering procedures are typically applied and top quality substrates, with roughness of the order of fractions of angstrom, are necessary. State of the art dielectric mirrors can reach a reflectivity higher than 99.999%, with a total scattering of less than 4 ppm. These mirrors must be manipulated with the maximum care, possibly in clean environment (better than class 100) in order to avoid dust and humidity. A pyrex capillary with internal diameter of 4 mm is installed in the middle of one side and allows to excite the active medium (He-Ne plasma) by means of a radiofrequency capacitive discharge. The capillary diameter forces the laser to operate on single transversal mode (TEM_{00}), while single longitudinal mode operation is obtained by keeping laser excitation near to threshold. Two piezoelectric translator stages can be used to stabilize the optical frequency of the laser against the cavity length variations induced by thermal expansion and mechanical relaxations. This makes it possible to avoid laser mode hops, increasing the device duty cycle up to about 100%. The four mirror chambers are tightly attached to a cross structure made of granite (african black), composed by a central octagonal massive block (3 tons), and four lightened arms each weighting $\approx 800\,\mathrm{kg}$ (see Fig.2.1).

The granite structure is screwed to a reinforced concrete block anchored to the underneath bedrock. The African black granite has been chosen because it can be machined with high precision and has a low thermal expansion coefficient ($6.5 \times 10^{-6}\ /^{\circ}C$). Being the whole set-up coupled to the ground in its central part, ground strain coupling to the

Figure 2.1: Top: the granite frame of GINGERino, just after its installation in the LNGS tunnel. Bottom: completed setup inside the isolation chamber.

cavity shape are minimized. The installation area has a natural temperature of 8 $^{\circ}C$ and a relative humidity close to the dew point all the year round. The whole installation is now protected by a large anechoic box. Infrared lamps are used to increase the temperature inside the box thus reducing the relative humidity from more of 90% down to about $50 - 60\%$. We checked that no oscillations of temperature and humidity on the daily time scale are introduced by this method. Better isolation systems joined to a humidity control systems can be considered in the future. So far, this infrastructure has been running for several months, and has shown that it keeps the GINGERino area at a temperature around

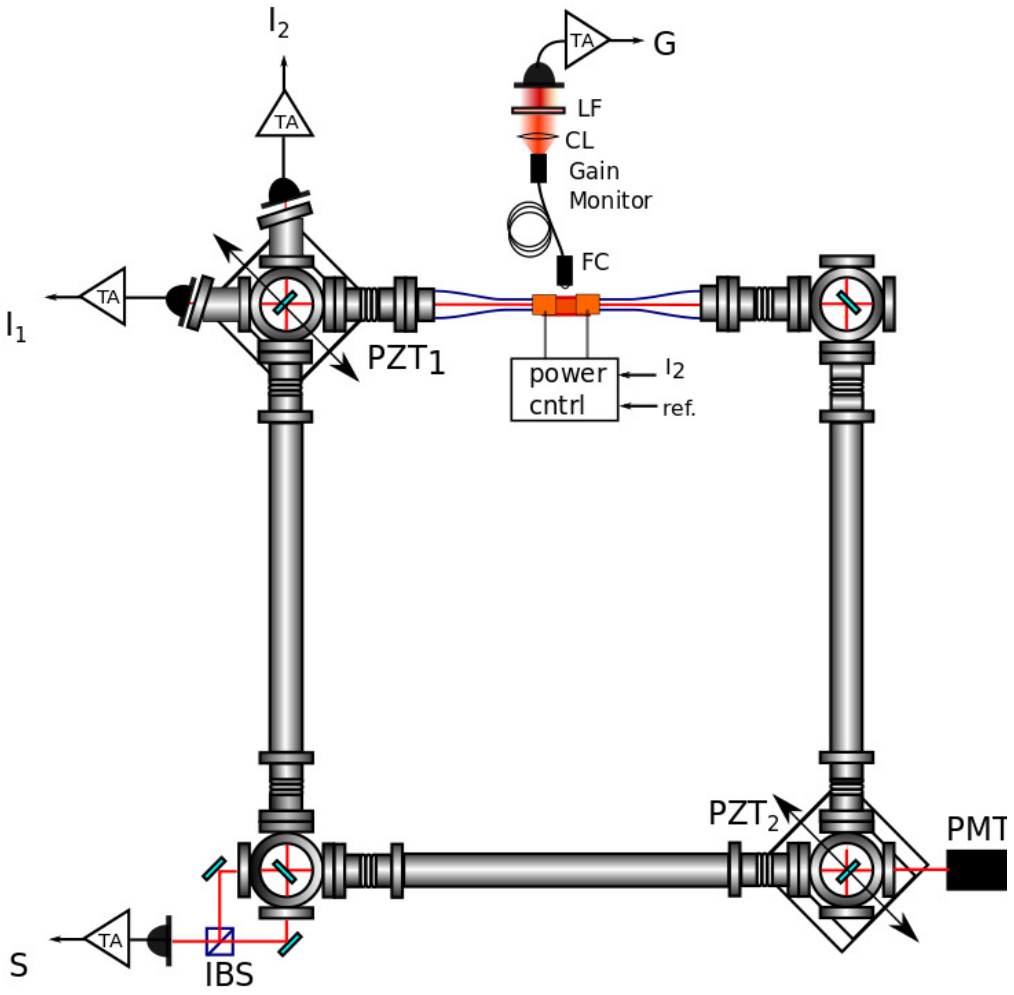

Figure 2.2: Optical setup. Three optical signals are continuously acquired: the combined beams intensity (Sagnac interferogram) S and the two monobeam intensities I_1 and I_2. The G signal is the intensity of the plasma fluorescence, filtered around the laser line. It is acquired as a monitor of the laser excitation level. IBS: Intensity Beam Splitter, PMT: Photo Multiplier Tube, LF: Line Filter (633 nm), TA:Transimpedance amplifier, FC=Fiber Coupler, CL: Collimating Lens.

13 $^{\circ}C$ with a stability better than 0.1°C for several days of operation. On top of the central part of the granite frame we installed additional instruments consisting in: one tiltmeter with nrad resolution (2-K High Resolution Tiltmeter (HRTM), Lipmann) and two high performance seismometers (Trillium 240s and Guralp CMG 3T360s). The combination of different instruments is essential in the interpretation of the data and the characteriza-

tion of the site. In Fig.2.2 is sketched the optical scheme of GINGERino in the present configuration. Three transimpedance amplified silicon photodiodes, with a bandwidth of 4 kHz, are used to detect the Sagnac interference signal at 280.4 Hz and the two single beam intensities. A photomultiplier (PMT), with a bandwidth of 400 MHz, is used for a double purpose: to detect the radiofrequency signals produced by the beating between higher order lasing modes and to occasionally perform ring-down time measurements for estimating the intracavity losses.

2.3 Data acquisition

GINGERino runs unattended, in this way man made disturbances are minimized. We have developed a remote interface with the experiment that allows us to monitor the status of the apparatus and also to drive the mirror positioning PZT actuators sketched in Fig. 2.2. The DAQ system itself is remote-controlled and transfers the data from INFN-LNGS to INFN-Pisa. The DAQ hardware has been selected in order to be transportable; it is based on the PXI-8106 controller by National Instruments. Its main tasks can be listed as follows (referring to Fig. 2.2):

- analog to digital conversion and storage of the Sagnac signal S and the two mono beams signals $I_{1,2}$ with 5 kHz sampling rate;

- analog to digital conversion and storage of environmental signals (temperature, humidity, pressure), laser parameters (plasma fluorescence gain monitor G, average intensities, piezoelectric transducers driving voltage) and tiltmeters, with 1 Hz sampling rate;

- real-time processing of experimental parameters connected to laser gain, backscattering parameters, actuators signals required by active control loops;

- digital to analog generation of the signals driving the laser, necessary for some of the controls of the apparatus.

Acquired data are written in the PXI local hard-disk. Both frequency and time accuracy are important since the former affects the estimation of the Sagnac frequency and the latter introduces errors in the synchronization of the RLG data stream with the data streams of other instruments (mainly seismometers). The PXI receives a GPS-synchronized PPS (pulse per second) signal and is connected to a local NTP server in order to obtain a time stamp with the required precision. The frequency accuracy is obtained by disciplining the 10 MHz clock of the PXI-6653 board to the PPS via the PXI-6682. The error on the time stamp is limited by the uncertainty on the NTP, which is of the order of a few milliseconds. The data written on the PXI hard-disk are copied via FTP into a dedicated directory on a local virtual machine and then copied into the final data storage destination (at INFN Pisa).

2.4 Sensitivity of the apparatus

From a direct estimate of the Sagnac frequency by means of the Hilbert transform of the interferogram, we deduced an instrumental sensitivity limit at the level $100\,\mathrm{prad/sec}/\sqrt{\mathrm{Hz}}$ in the range $(10^{-2} - 1)$Hz. A typical rotational noise spectrum is shown in Fig.2.3. Data refer to 1 hour acquisition on the 11th of June 2016. For this run the cavity ring-down time was $\sim 250\,\mu s$ corresponding to a total loss per round trip of about 190 ppm. As clearly visible, the long term stability of the raw data is limited to 10-20 s, mainly by radiation backscattering on the mirrors. A reduction of the backscattering induced frequency noise can be obtained by identifying and subtracting its contribution from the measurements of the single beam outputs from the cavity. This has been done for the run of June 2016, and it is discussed in the next section.

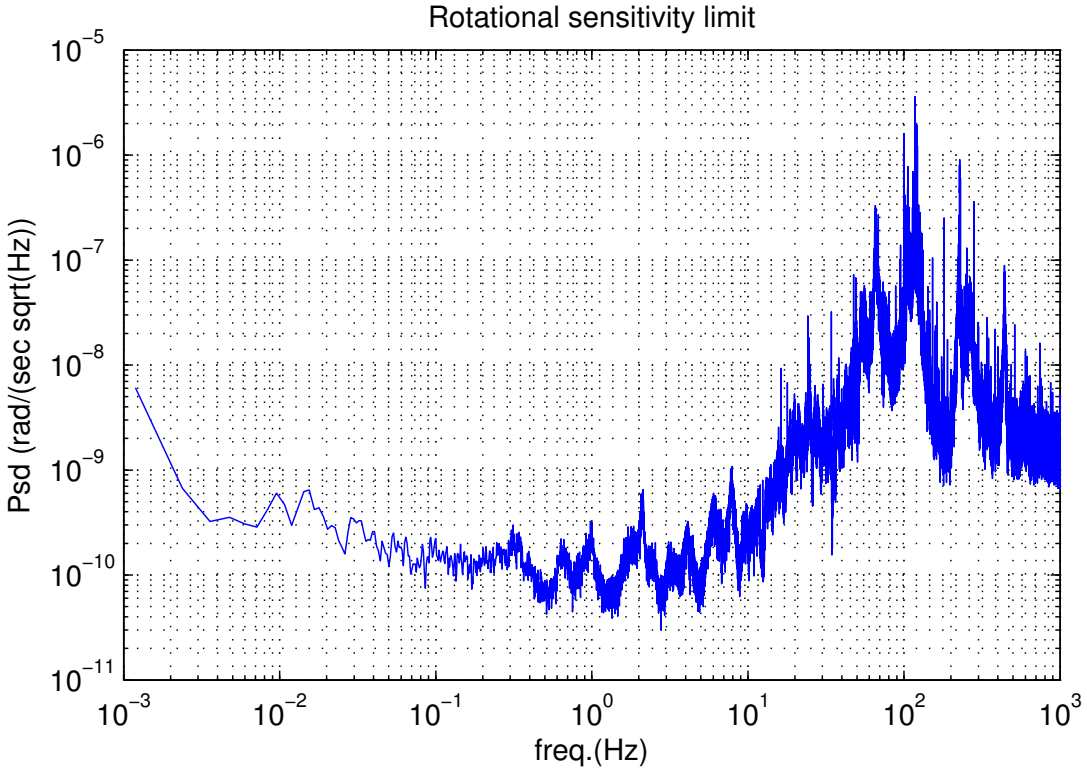

Figure 2.3: Angular velocity linear spectral density of GINGERino calculated a dataset of 3600 s from 11-06-2016 at 00:00. Power spectral density is estimated from the raw data interferogram.

2.5 Backscattering analysis

The strategy for subtracting backscattering noise from ring-laser data has been extensively discussed in [Beghi et al., 2012] and [Cuccato et al., 2014], where we have shown how and why backscattering noise can be efficiently subtracted, by applying an Extended Kalman Filter (see [Cuccato et al., 2014] for details). The time dependence of backscattering contribution can be also estimated using a model which assumes reciprocal ring laser parameters. This approach has been exploited in [Hurst et al., 2014], where the backscattering parameters were estimated by fitting amplitudes and phases of the two monobeam intensities. It has been tested that the two methods give similar results. For this analysis purpose several

service signals are necessary: the two monobeam intensities and the laser gain. Data were processed following the procedure already developed for G-Pisa [Belfi et al., 2012a], tuning the pre-filters to the GINGERino Sagnac frequency, and estimating the laser parameters by averaging over 10 seconds the mono-beams intensities. We firstly extract from the data mono-beam intensities, modulations and phase differences, then we use these quantities to estimate the laser parameters connected to backscattering at a rate of 1 sample every 10 seconds. After the parameter identification, backscattering contribution is calculated. Results for a time series of 12 days are shown in Fig.2.4. The relative Allan deviation of

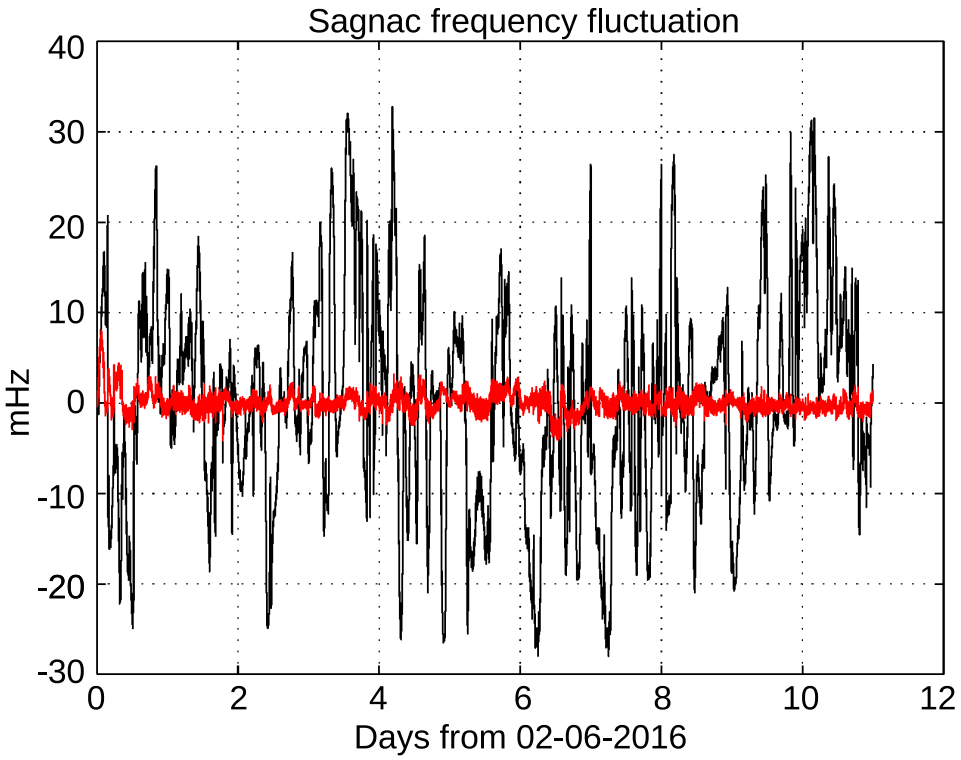

Figure 2.4: Black: raw data. Red: backscattering corrected data.

the backscattering corrected data is shown in Fig.2.5.

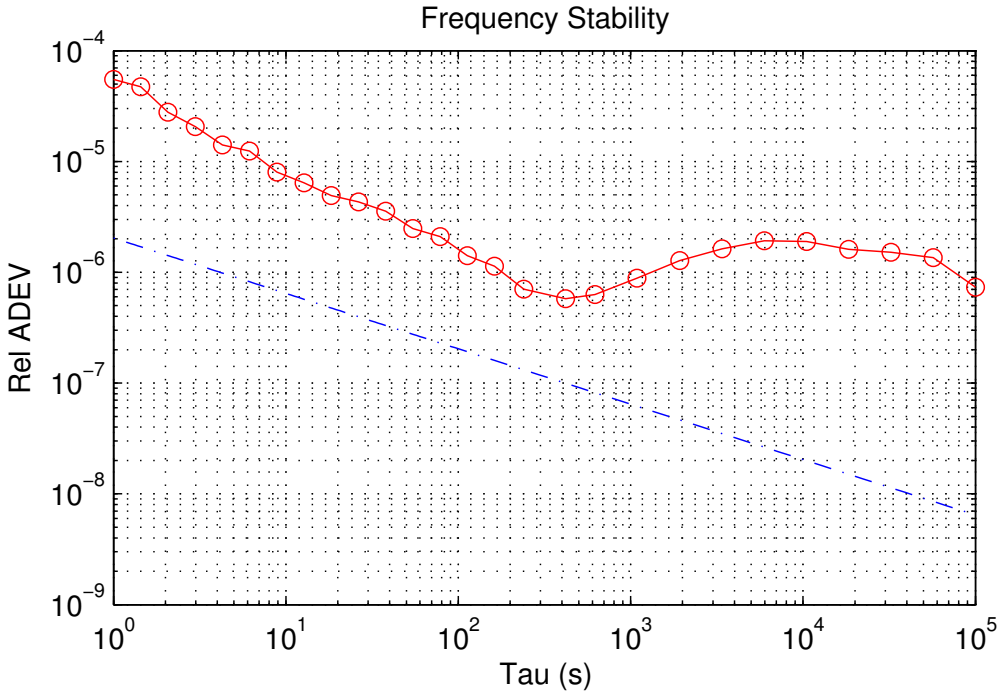

Figure 2.5: Relative Allan deviation for the Sagnac frequency after backscattering subtraction. Straight line represents the calculated shot noise limit.

2.6 Seismological observations

The two independent digitizers for the RLG and the seismometers are synced to the GPS time reference. This allows the direct comparison between rotational and translational signals [Igel et al., 2007]. Two teleseismic events are reported in the following. Results are shown in Fig.2.6 and 2.7. The upper two traces indicate the time history of transverse acceleration and rotation rate as detected by the seismometer and RLG, respectively. The N and E components of the seismometer, after being corrected for the instrumental response, have been rotated in order to construct the transverse component which is analyzed in comparison with the gyroscope signal. We evaluated the Zero-Lag Correlation Coefficient (ZLCC) between transverse acceleration and rotation using a time window of 50 seconds, sliding with 50% overlap.

For Love seismic waves [Cochard et al., 2006b], in the plane wave approximation, the transverse acceleration and the vertical rotation signals are in phase and their ratio is proportional to the phase velocity. Phase velocity measurements contain information about the elastic properties of the ground, and are typically obtained by means of seismometer arrays installations. A system composed by a horizontal RLG and a seismometer provide the same information in a single site installation. An example of this estimate is given in lowest plot of Fig.2.6 and 2.7.

Surface wave phase velocity is calculated in the two cases for the points where the ZLCC is above 0.6.

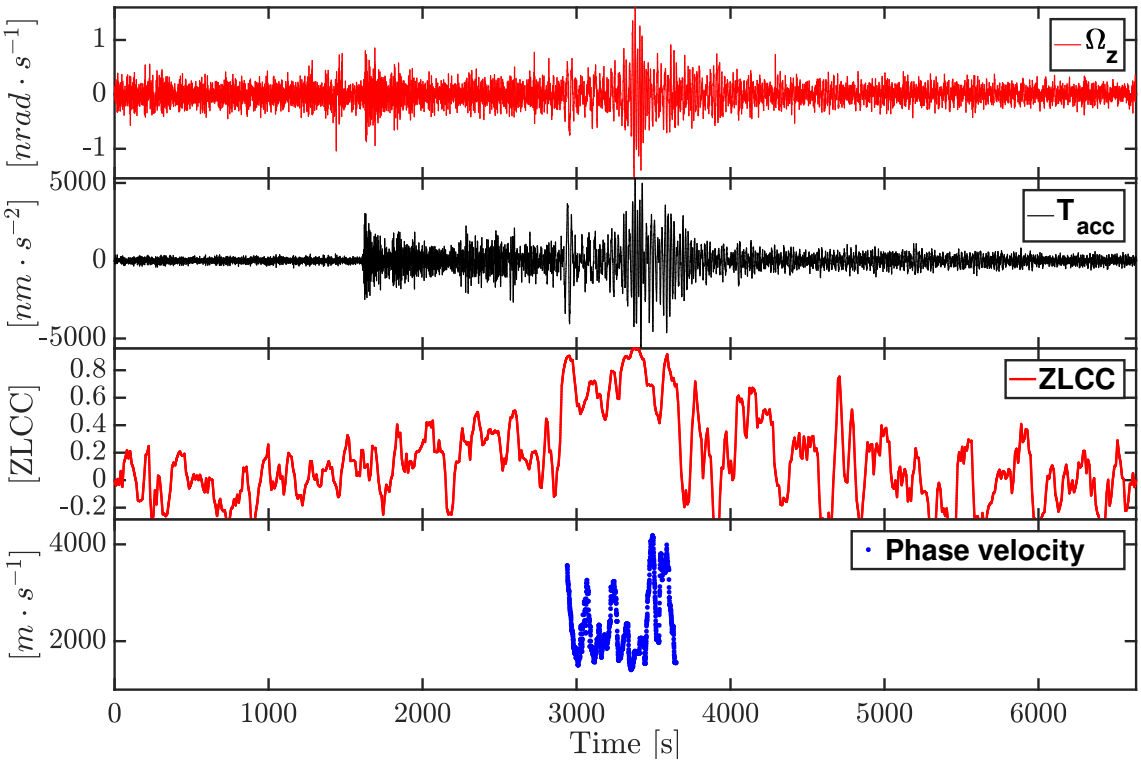

Figure 2.6: Mid Atlantic ridge earthquake, June 17, 2015, 12:51 p.m., MWC 7. Top: seismograms for the transverse acceleration (black) and vertical rotation (red). Center: the zero lag correlation coefficient between rotation and transverse acceleration. Bottom: apparent phase velocity of the surface waves. Phase velocities are computed for the seismograms parts where the correlation between rotation and translation is larger than 0.6.

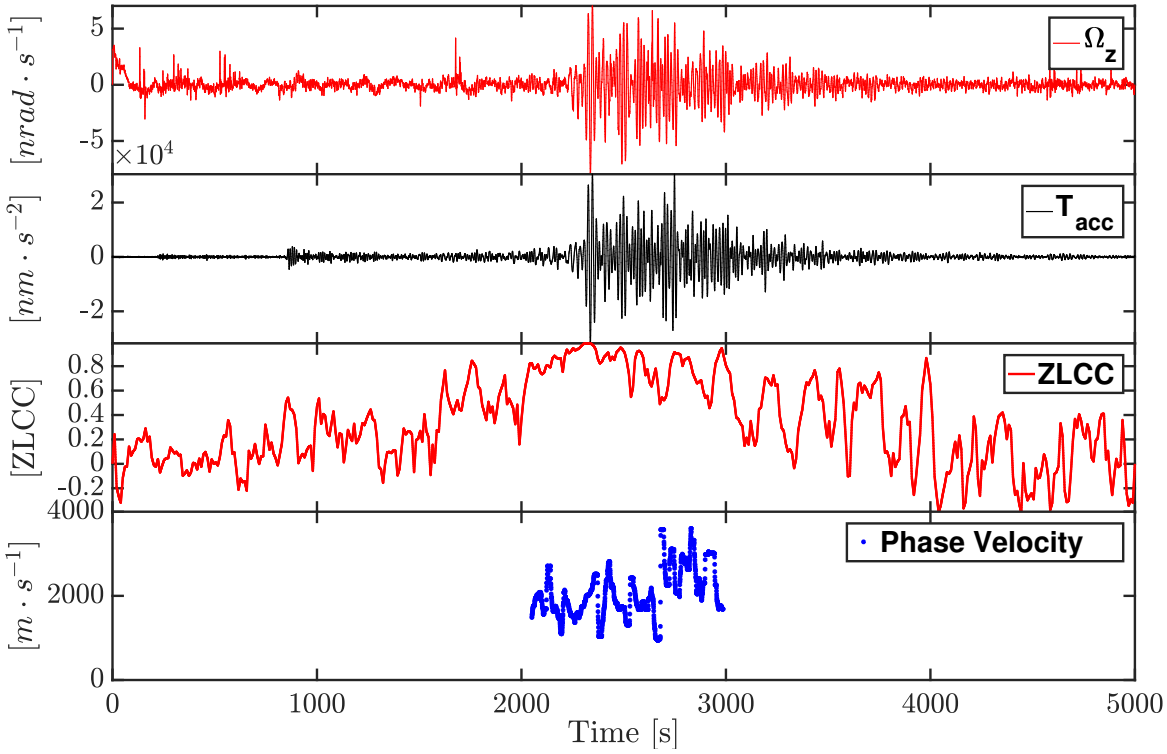

Figure 2.7: Rykyu Islands earthquake, November 13, 2015, 08:51 p.m., MWC 6.8. Plot legend is the same as in Fig.2.6.

2.6.1 Background noise analysis

The characteristics of the background seismic noise at the site are illustrated in Figure 2.8, where the probabilistic power spectral densities (Pround PSD) of the three components of ground acceleration are compared to the High- and Low-Noise Models (NHNM and NLNM, respectively) [Peterson et al., 1993]. The typical spectra are close to the NLNM and shows a very good behavior throughout the spectral region of the primary and secondary microseism (i.e., at periods spanning the 1-10s interval), exhibiting however larger and unwanted noise at low frequency (long periods) for the N and E components. This A deeper analysis consisting in the calculation of the noise polarization over the horizontal plane shows that

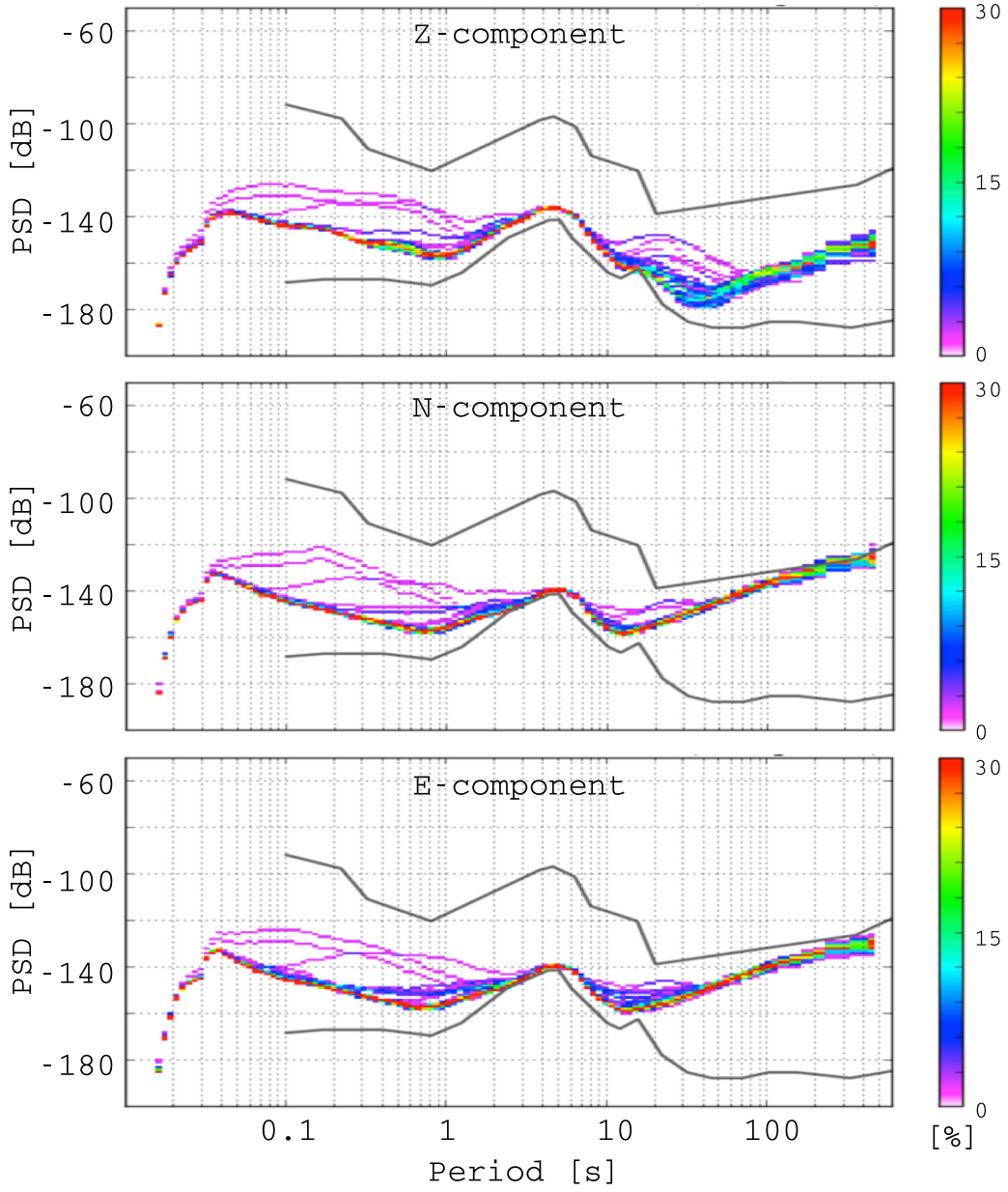

Figure 2.8: Probabilistic power spectral densities for the three components of ground acceleration as recorded by the seismometer. Vertical scale is relative to $1\,\mathrm{m^2 s^{-4} Hz^{-1}}$. For each frequency bin, the maps illustrate the probability of observing a given spectral power, according to the color scale at the right.

the noise polarization is markedly directional and directed along the tunnel (see Fig.2.9). Accordingly to the literature [Beauduin et al., 1996], a possible explanation is that the long-period, high-amplitude noise is induced by the conveyed air motion in the tunnel.

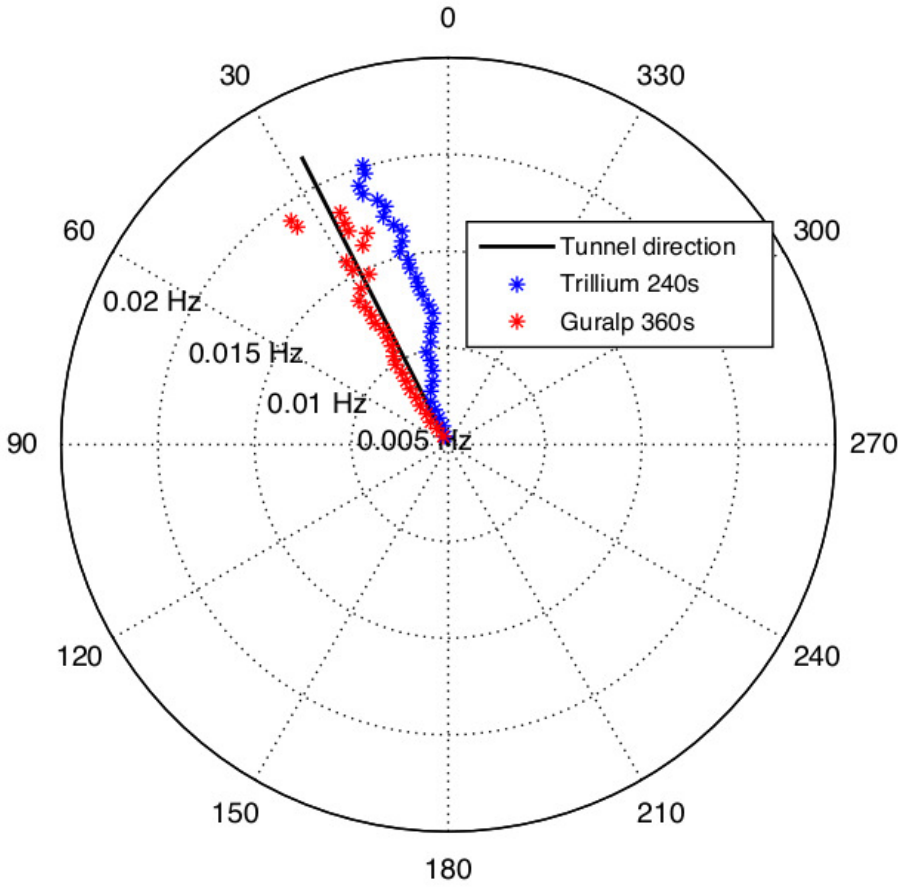

Figure 2.9: Principal polarization direction of the background noise over the $50 - 200$ s period range. Results from the two seismometers are coherent within a 5 degrees tolerance, indicating ground oscillations aligned along the tunnel's direction. This suggests a main control of the underground cavity in the generation of seismic noise at very long periods.

The analysis of the noise polarization is obtained by rotating the horizontal components of the seismometer and then finding the direction of maximum ground acceleration. This appears to be directed as the tunnel, is still not clear by the way if this effect is a direct coupling of the air flow to the instrument or an air flow induced ground motion. In order to clarify this, an high sensitivity 1D hot wire anemometer has been purchased and his installation is planned as a monitoring device for the seismic station. A day-night and week-end/working week dependency of this noise level has been proved by a time frequency analysis of the seismometer data. The anthropic activity in the laboratories in fact involves

also the opening and closing of the doors connecting the underground cavities, this leads to a more unstable and turbulent air flow. We miss a quantitative measure of the air flow but, to have an idea, the feeling of a light wind is always present in the tunnel, this ventilation is needed to expel the radon that is naturally present in the rock. A future plan is to close inside pressure doors the ring laser facility as it is standard for high end seismic observatories. We are non yet convinced that the signal we record is a real ground motion at long periods (>10 s). In any case the mechanism of pressure-to-seismic coupling eventually driven by the ventilation in the tunnel should generate mainly a Rayleigh-like kind of ground motion. In our setup we are sensitive to transverse propagating seismic waves since we record the vertical rotation rate. In general the actual noise level of the Gingerino RLG is higher than the NHNM and unfortunately we do not see the ocean generated noise rotational component. In this sense our roto-traslational measurements are limited by the noise level of the RLG.

2.7 Conclusions

GINGERino has been constructed inside LNGS and performs ground rotation measurements with a very high duty cycle. The system provides Earth rotation rate measurements as well as seismic rotational data thanks to a dedicated architecture for laser remote control, data acquisition and data transfer. The sensitivity curve shows a level around 10^{-10} rad/s compatible with the actual instrument shot noise and ringdown time. During the first runs all the major teleseismic events present in the Global CMT Catalog have been detected. The standard rotation/transverse-acceleration correlation analysis is presented for two different events. Long term stability of raw data is limited by backscattering noise, which can be subtracted in large part via post processing. After correcting the backscattering induced drift a maximum resolution of about 30 prad/s for 500 s of integration time is

obtained. The correlation between the observed instabilities of the gyroscope and the environmental parameters fluctuation (temperature, pressure, humidity, anthropic activities) is under investigation.

Chapter 3

Rotational motions from the 2016, Central Italy seismic sequence, as observed by an underground ring laser gyroscope

Simonelli, A., Igel, H., Wassermann, J., Belfi, J., Virgilio, A., Beverini, N., E.Maccioni, Luca, G. D., and Saccorotti, G. (2017b). Rotational motions from the 2016, central italy seismic sequence, as observed by an underground ring laser gyroscope. Geophysical Journal International, volume 214(1), 705-715, 2018, doi = 10.1093/gji/ggy186.

The contributions as a first author to this paper consist in:

- *The experimental activity involving the instrument construction, tuning of the optical parts, alignment, optimization and final commissioning.*
- *Row data preparation and preprocessing*

- *Coding of the routines used for the analysis of the earthquakes of the sequence*

- *Manuscript preparation*

Abstract

We present the analysis of rotational and translational ground motions from earthquakes recorded during October/November, 2016, in association with the Central Italy seismic-sequence. We use co-located measurements of the vertical ground rotation rate from a large ring laser gyroscope (RLG), and the three components of ground velocity from a broad-band seismometer. Both instruments are positioned in a deep underground environment, within the Gran Sasso National Laboratories (LNGS) of the Istituto Nazionale di Fisica Nucleare (INFN). We collected dozen of events spanning the 3.5-5.9 Magnitude range, and epicentral distances between 30 km and 70 km. This data set constitutes an unprecedented observation of the vertical rotational motions associated with an intense seismic sequence at local distance. Under the plane wave approximation we process the data set in order to get an experimental estimation of the events back azimuth. We compare this results to the theoretical ones. In a second step, after identifying the direction of the incoming wave-field, we extract phase velocity dispersion curves. This analysis is performed on the rotational signals present in the P-coda, S-coda and Lg phase. The number of events recorded permits to provide a statistical error to our measures.
Keywords: ring laser, rotational ground motion, central Italy, phase velocity

3.1 Introduction

On August 24, 2016, at 01:36:32 UTC a Mw=6.0 struck the central sector of the Apennines chain (Italy), (see [Michele et al., 2016]) , causing almost 300 casualties and extensive destruction. During the following two months, both rate and energy of aftershocks decreased progressively. On October 26, 2016, the activity renewed with two energetic events (Mw=5.4 and Mw=5.9) until climaxing, four days later, with a Mw=6.5 shock (see [Chiaraluce et al., 2017]). The colocated observation of ground translations and vertical

rotations permits, with a single station approach, to estimate the back azimuth (hereinafter BAZ) of the incoming wave-field generated by seismic events as well as the phase velocity for surface Love waves and horizontally polarized shear waves. The latter ones can be generated by the P-SH conversion after the onset of the P phase (P-coda) and are present in the S-coda itself. The seismological observations of rotational motions by means of Large Ring Laser Gyroscopes (RLG) (see. [Schreiber and Wells, 2013b]) started from the first pioneering experiments by [Stedman et al., 1995, McLeod et al., 1998, Pancha et al., 2000] in New Zeland. A more quantitative and extensive analysis is performed on the G-Wettzel ring laser data in [Igel et al., 2005, Igel et al., 2007, Cochard et al., 2006a, Simonelli et al., 2016, Belfi et al., 2017] are reported detections and analysis of teleseismic events recorded by the Gingerino RLG inside the LNGS underground laboratories. The vast majority of the previous works are based on teleseismic observations, where, under the plane wave assumption, it is successfully shown the possibility of measuring both the event BAZ and the local phase velocity. The location of the Gingerino RLG and its sensitivity permits to measure earthquakes generated rotations from tele-seismic distances to very local, high amplitude events. As an example, the Campotosto fault system, that generated during this sequence a Mw 5.5 earthquake, is located only 20 km away from the LNGS. Under these conditions, the joint analysis of ground rotation and translations is made challenging due to the higher dominant frequencies of the incoming wavefield and near-field effects. The aim of this paper is to investigate, through the analysis of an unique data set, the performance of co-located rotational and translational sensors toward the wavefield characterization and source location of energetic earthquakes at local distance. On a long term perspective an extensive analysis of many earthquakes having a large span of epicentral distances and BAZ angles will allow us to characterize the local structure of the Gran Sasso region.

3.2 Geological and Structural Framework

Moment tensor solutions (`http://cnt.rm.ingv.it/tdmt`) for the vast majority of significant quakes indicate the activation of extensional faults striking NNW-SSE and dipping 40°-50° to west. Ongoing extension in the area is testified by the analysis of crustal strain and seismicity data ([Bird and Carafa, 2016]), yet the tectonic setting and the landscape of the region are still dominated by the contractional structures of the Neogene-Quaternary Apennines fold-and-thrust belt. The extension in the Apennines is indeed a relatively young process (e.g. [Malinverno and Ryan, 1986]) that proceeds at the relatively slow rate of 2-3mm/yr ([Bird and Carafa, 2016]). Consequently, the currently active structures have not yet fully reshaped the Apennines highs-and-lows of contractional origin with extensional basin-type landforms. It is worth recalling that some of the well-exposed extensional faults, generally bounding an intermountain basin, were created by a pre-orogenic (Mesozoic) or by a synorogenic extensional (Miocene) regime and were shifted to their present location during the Neogene thrusting phase, for instance through a shortcut mechanism (positive inversion tectonics; e.g. [Tavarnelli, 1996, Butler et al., 2006, Scisciani and Calamita, 2009]). The complex framework described above explains why identifying and characterizing seismogenic sources in the Apennines is extremely challenging (see [Di Domenica et al., 2014] for a discussion on this topic).

3.3 The experimental setup

The four components (4-C) seismic station is constituted by the RLG Gingerino and a broadband seismometer Trillium 240 from Nanometrics. The first instrument senses the rotations of the ground around the local vertical axis, while the latter detects ground velocity along three orthogonal axes. GINGERino is an He-Ne Ring Laser Gyroscope

(RLG) operating at a wavelength of 632 nm. The optical cavity is a square of 3.6 m side length and is defined by four spherical mirrors with 4 m radius of curvature. The design of the corners is based on the GeoSensor project (see [Schreiber et al., 2006b]). The alignment can be tuned by means of a micrometric system acting on the mirror chambers orientation. More details on the instrument are described in [Belfi et al., 2017]. Within the active optical cavity two laser beams are circulating in clockwise and anti-clockwise directions. The perimeter represented by the path of the two beams encloses an area A. When an active cavity is rotating around an axis having an orthogonal component with respect to the area A, the optical frequencies of the two laser beams propagating in opposite directions are shifted (with respect to the non-rotating cavity) by a quantity that is proportional to the rotation rate. This is known as Sagnac effect. The detection of this frequency shift is made easier by letting the two beams to interfere out of the optical cavity with an optical system called beam combiner. The raw data from a RLG that is fixed to the Earth ground consist in a sinusoidal interference signal whose mean frequency f is proportional to the earth rotation rate, Ω according to eq. 3.1.

$$f = \frac{\Omega A \sin\theta}{P\lambda_{He:Ne}} \tag{3.1}$$

Here $\lambda_{He:Ne}$ is the wavelength of the He:Ne laser (632 nm), P is the perimeter of the square cavity, A is the enclosed area, θ is the latitude at the experiment site and Ω is the Earth rotation vector. At the latitude of LNGS the Sagnac frequency is 280.4 Hz. During the transit of a transverse polarized seismic wave, the rotation generated is summed to the constant bias given by the Earth rotation (i.e. 7.29 $\mu rad/s$). The Saganc frequency induced by the Earth rotation rate for the Gingerino RLG is 280.4 Hz. This bias sets a reference value to which is possible to compare the peak rotation rates generated by seismic waves in terms of $\delta\Omega = \Omega_{max}/\Omega$. In fact the Earth rotation signal can be treated

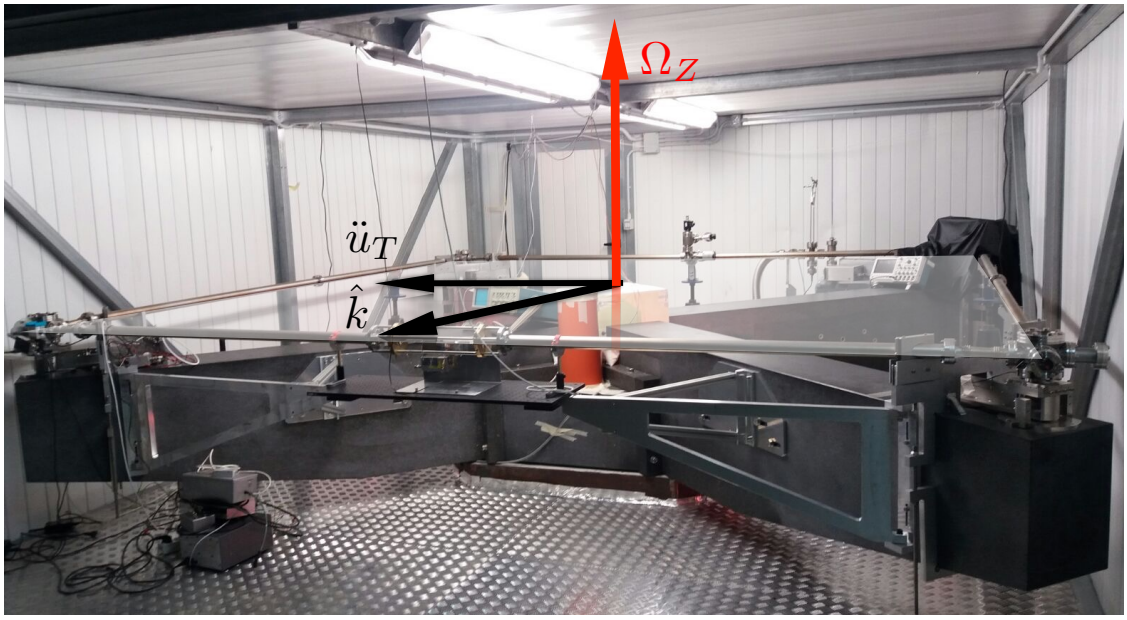

Figure 3.1: The GINGERino RLG and the seismometer Trillium 240 in the central box. The arrows indicates the observables that are object of this study, i.e. vertical rotation rate in red (from the RLG) and transverse acceleration in black (after processing the seismometer data) and the direction of the wavefield $\hat{k}$. In this figure the vector $\hat{k}$ is pointing to the North. It corresponds for example to the direction of a propagating shear wave causing a transverse acceleration in the $\ddot{u}_T$ direction.

as a constant signal on which the rotational motion of earthquake signals are superimposed. The broadband seismometer, installed at the center of the RLG, is part of the national monitoring program of the italian Istituto Nazionale di Geofisica e Vulcanologia (INGV hereinafter), under the station code GIGS.

3.4 Data analysis

Theory ([Aki and Richards, 2002]) predicts that the rotation vector $\vec{\Omega}$ can be obtained from the ground displacement as the curl of the wave-field $\vec{u}$.

$$\vec{\Omega} = \frac{1}{2}(\nabla \times \vec{u}) \tag{3.2}$$

Table 3.1: List of earthquakes analyzed in this study.

Event	Start Time	Lat	Long	Mag	Dist [Km]	BAZ [deg]	Depth [km]	Peak Rot. rate [rad][s]$^{-1}$	Peak Acc. [m][s]$^{-2}$
1	26-Oct-2016 19:18:05	42.909	13.129	5.9	62.3	324.6	7.5	1.74e-05	4.30e-02
2	26-Oct-2016 17:10:35	42.88	13.127	5.4	59.8	322.6	8.7	1.68e-05	2.72e-02
3	01-Nov-2016 07:56:36	42.999	13.158	4.8	69.5	331.0	9.9	7.26e-06	2.51e-02
4	03-Nov-2016 00:35:00	43.029	13.049	4.7	77.0	326.4	8.4	5.65e-06	1.07e-02
5	30-Oct-2016 13:34:54	42.803	13.165	4.5	51.2	319.5	9.2	2.24e-06	3.64e-03
6	30-Oct-2016 12:06:59	42.844	13.078	4.5	59.4	317.2	9.7	5.55e-06	7.88e-03
7	26-Oct-2016 21:41:59	42.861	13.128	4.5	58.1	321.4	9.9	3.88e-06	8.06e-03
8	27-Oct-2016 08:21:45	42.873	13.1	4.3	60.6	320.5	9.4	1.70e-06	3.79e-03
9	31-Oct-2016 07:05:44	42.841	13.129	4.2	56.4	320.1	10.0	2.08e-06	5.02e-03
10	30-Oct-2016 10:19:25	42.815	13.145	4.1	53.3	319.1	10.8	2.45e-06	2.24e-03
11	27-Oct-2016 03:19:26	42.844	13.15	4.0	55.5	321.6	9.2	4.56e-06	8.03e-03
12	16-Oct-2016 09:32:34	42.748	13.176	4.0	46.1	315.4	9.2	3.57e-06	6.03e-03
13	31-Oct-2016 06:17:19	42.771	13.207	3.9	46.3	319.9	9.9	1.07e-06	1.35e-03
14	27-Oct-2016 17:22:22	42.846	13.108	3.9	57.9	319.1	9.0	9.18e-07	4.19e-03
15	08-Oct-2016 18:11:08	42.738	13.185	3.9	44.8	315.1	9.5	1.73e-06	2.97e-03
16	07-Nov-2016 18:56:15	42.888	13.151	3.8	59.4	324.6	8.1	3.23e-06	4.40e-03
17	28-Oct-2016 15:56:58	42.788	13.119	3.8	52.6	315.2	9.8	1.84e-06	3.43e-03
18	26-Oct-2016 19:43:42	42.893	13.069	3.8	63.9	320.1	12.6	1.61e-06	2.44e-03
19	09-Nov-2016 06:13:09	42.661	13.192	3.7	38.8	306.7	10.7	4.18e-06	4.93e-03
20	30-Oct-2016 12:32:56	42.715	13.243	3.7	39.7	317.3	8.2	8.28e-07	7.40e-04
21	30-Oct-2016 11:14:20	42.803	13.19	3.7	49.9	321.3	9.4	1.42e-06	1.90e-03
22	28-Oct-2016 19:56:31	42.866	13.162	3.7	56.9	323.9	13.2	1.51e-06	2.61e-03
23	26-Oct-2016 21:24:51	42.867	13.078	3.7	61.3	318.8	10.3	2.41e-06	3.32e-03
24	06-Nov-2016 18:15:17	42.806	13.185	3.6	50.5	321.2	8.9	7.63e-07	1.32e-03
25	05-Nov-2016 08:17:39	42.699	13.147	3.6	44.3	308.2	11.1	1.29e-06	7.50e-04
26	31-Oct-2016 09:34:16	42.816	13.151	3.6	53.1	319.6	9.2	1.25e-06	1.33e-03
27	30-Oct-2016 23:56:19	42.828	13.09	3.6	57.4	316.7	7.9	1.40e-06	2.20e-03
28	30-Oct-2016 10:26:24	42.836	13.071	3.6	59.1	316.2	10.8	1.21e-06	1.40e-03
29	09-Oct-2016 04:42:42	42.74	13.185	3.6	45.0	315.3	11.8	7.65e-07	1.17e-03
30	02-Nov-2016 06:41:12	42.796	13.167	3.5	50.6	319.1	10.3	6.14e-07	5.42e-04
31	01-Nov-2016 17:59:12	42.806	13.135	3.5	53.1	317.8	10.8	1.75e-06	3.08e-03
32	30-Oct-2016 13:14:16	42.766	13.061	3.5	54.4	309.9	8.7	1.00e-06	1.26e-03
33	28-Oct-2016 23:18:08	42.88	13.094	3.5	61.5	320.6	14.0	1.53e-06	2.01e-03

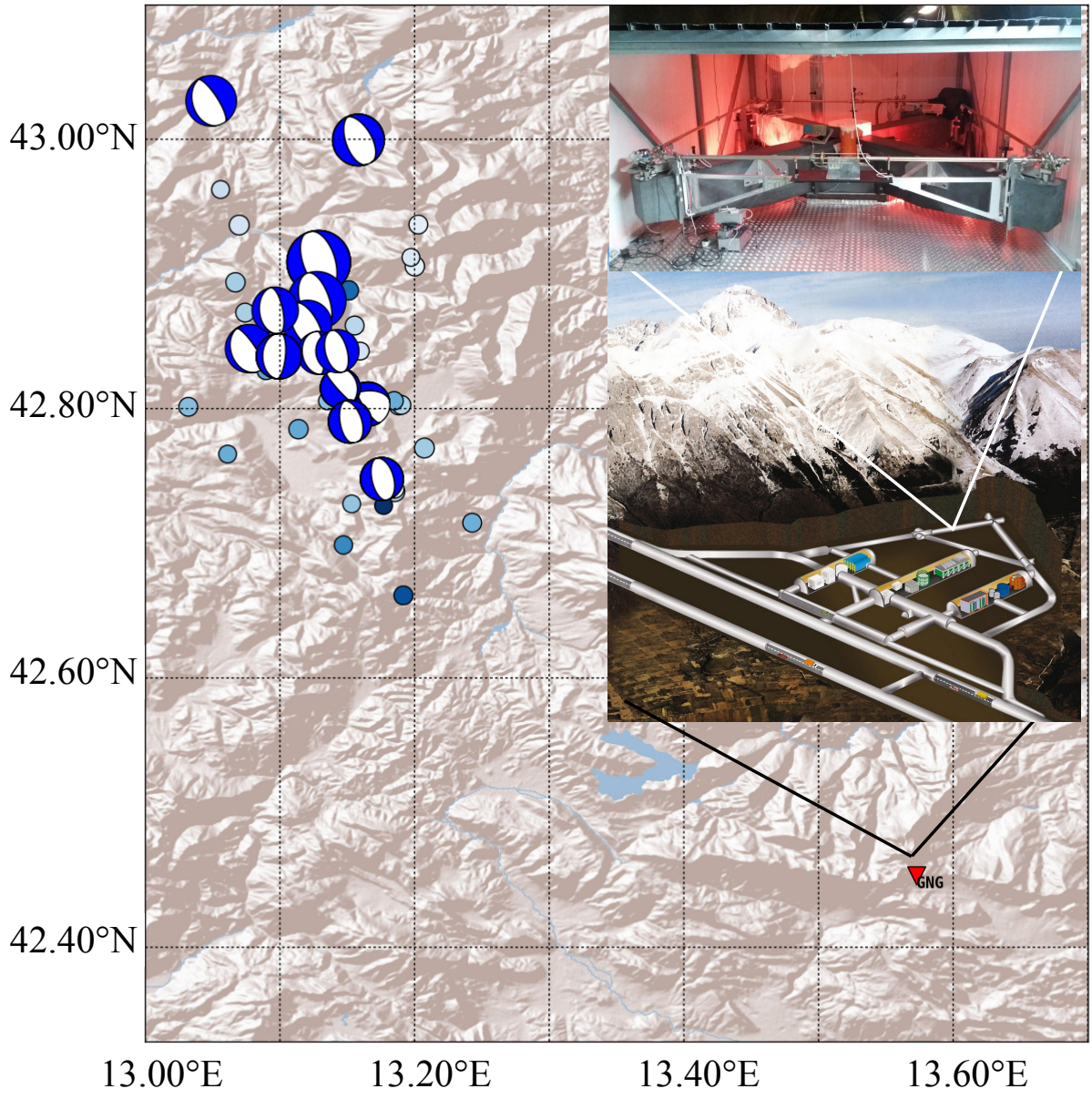

Figure 3.2: The map shows the epicenters locations and the focal mechanism of the 10 strongest events. Red triangle denotes the Gingerino seismic station. The top figure in the inset shows a map of the underground laboratories, while the bottom one shows the Gingerino RLG.

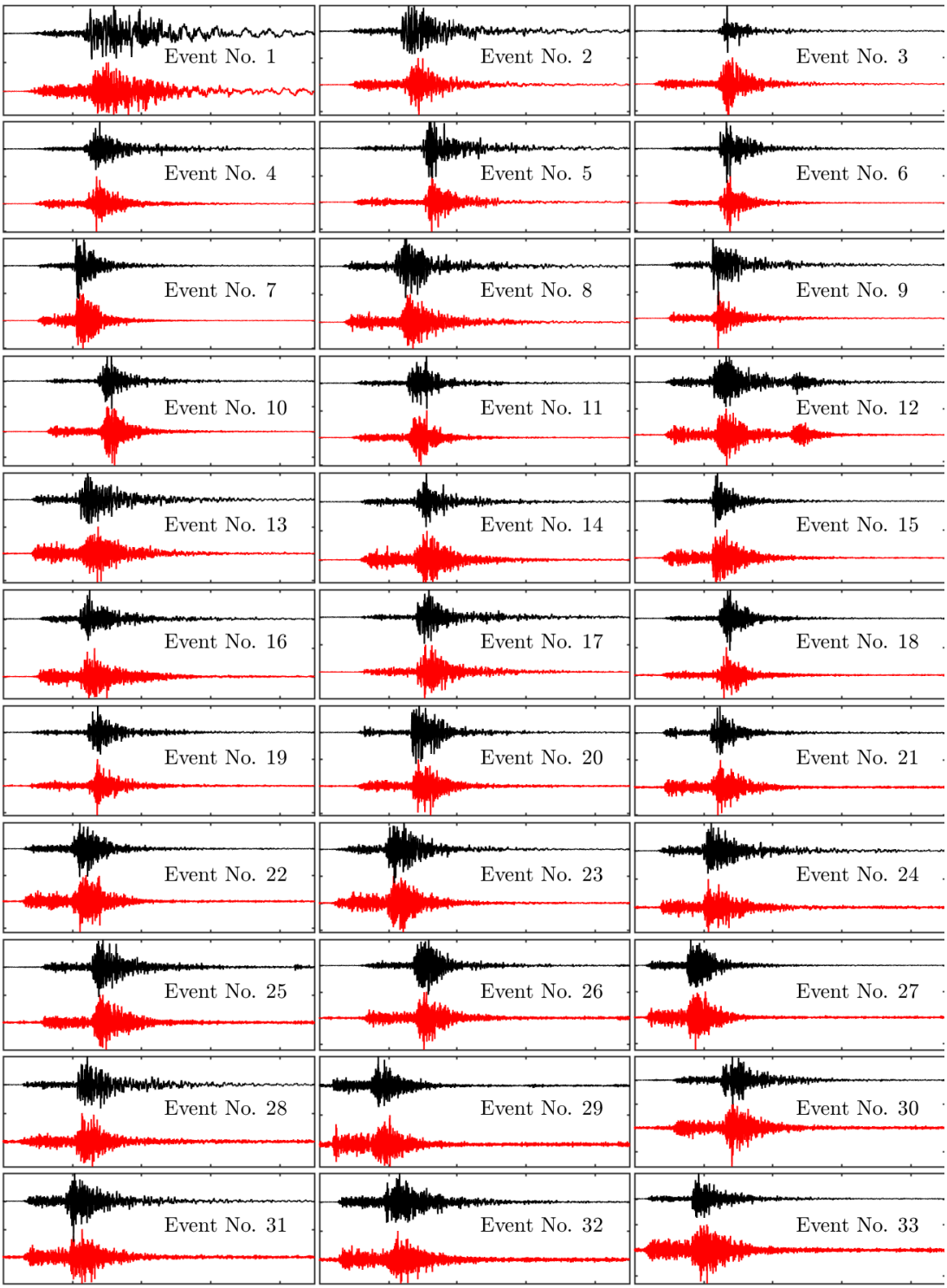

Figure 3.3: The recorded event waveforms, in red the vertical rotation rate, in black the transverse acceleration. The time window is 45-seconds long. Individual rotation and translation traces are normalized to their respective peak value.

For example, the displacement caused by a Love wave traveling as a plane wave along the $\hat{k}$-direction (see Fig. 3.1) can be expressed through the equation:

$$u_T = Ae^{i\omega(\frac{xk}{C_L}-t)} \tag{3.3}$$

Combining eq.3.3 with eq.3.2 we yelds:

$$\dot{\Omega}_z = \frac{-\ddot{u}_T}{2c_L} \tag{3.4}$$

which provides a direct estimation of the phase velocity c_L from a single-site measurement, as an amplitude ratio. Our data set, consisting in 33 events (see Table 4.1), permits us to extend the vertical rotation-rate/tranverse acceleration analysis to regional events whose epicentral distance and magnitude ranges from 30 km to 70 km and Ml 3.5 to Mw 5.9 respectively. First we try to provide a statistical estimation of the misfit between the theoretical back-azimuth (i.e the one derived from station and epicenter coordinates) and the estimated one. Then we calculate a frequency dependent phase velocity for different seismic phases in those frequency bands where we have high correlation between vertical rotation rate and transverse acceleration. Our analyses address three separate arguments which aim at verifying the ability of the 4D deployment to consistently retrieve magnitude and location of the the source, and the phase velocity of the incoming wavefield.

3.4.1 Source Magnitude

[Igel et al., 2007] considered the definition of the surface wave magnitude Ms and, using the relationship between displacement and rotation rate, they obtained an explicit relationship between the distance- and period-dependent rotation rate and Ms, for the domain of applicability of the surface wave magnitude scale (i.e. from 20° to 160° of epicentral

range). After measuring the peak rotation rate for Love waves from a dozen of tele-seismic events. [Igel et al., 2007] found that the magnitudes derived in that manner were in a fairly good agreement with those predicted on the base of the Ms scale (see Fig. 2 in [Igel et al., 2007]). Given the range of epicentral distances of our earthquakes a different magnitude scale should be adopted. We use then the definition of eq. 3.5.

$$M = log_{10}(A) + Blog_{10}(d) + C \tag{3.5}$$

where A is the peak ground displacement, d is the epicentral distance in km, and (B,C) are constants to be determined empirically. We fit the equation 3.5 to our rotational data expressed in angular displacement. The coefficients that best fit the eq. 3.5 in the least square sense are $B = (0.427 \pm 1.478)$ and $C = (1.829 \pm 2.565)$. The Peak angular displacement is represented versus distance in Fig. 3.4.

3.4.2 Back Azimuth estimation

The horizontal components of ground acceleration are rotated in steps $\delta\theta$ of one degree within the range [0,2π] and, for each trial backazimuth theta, we calculate the radial and transverse acceleration traces $\{\ddot{u}_R(\theta), \ddot{u}_T(\theta)\}$, where θ is the trial BAZ. Assuming that the hypothesis of plane-wave propagation and linear elasticity holds, we know that vertical rotation and transverse acceleration ([Aki and Richards, 2002], [Cochard et al., 2006a]) should show in the seismograms as the same waveform scaled by the frequency dependent phase velocity $C(f)$ (See eq. 4). We use the Wavelet coherence tool (WTC) [Grinsted et al., 2004] to obtain time-frequency maps of correlation between the vertical rotation rate Ω_z and the transverse accelerations set $\{\ddot{u}_T(\theta)\}$, obtained by the rotations described above. The result of this processing is an array of correlation values $C(\theta, t, f)$ that are functions of time and frequency and the trial backazimuth of the seismometer horizontal

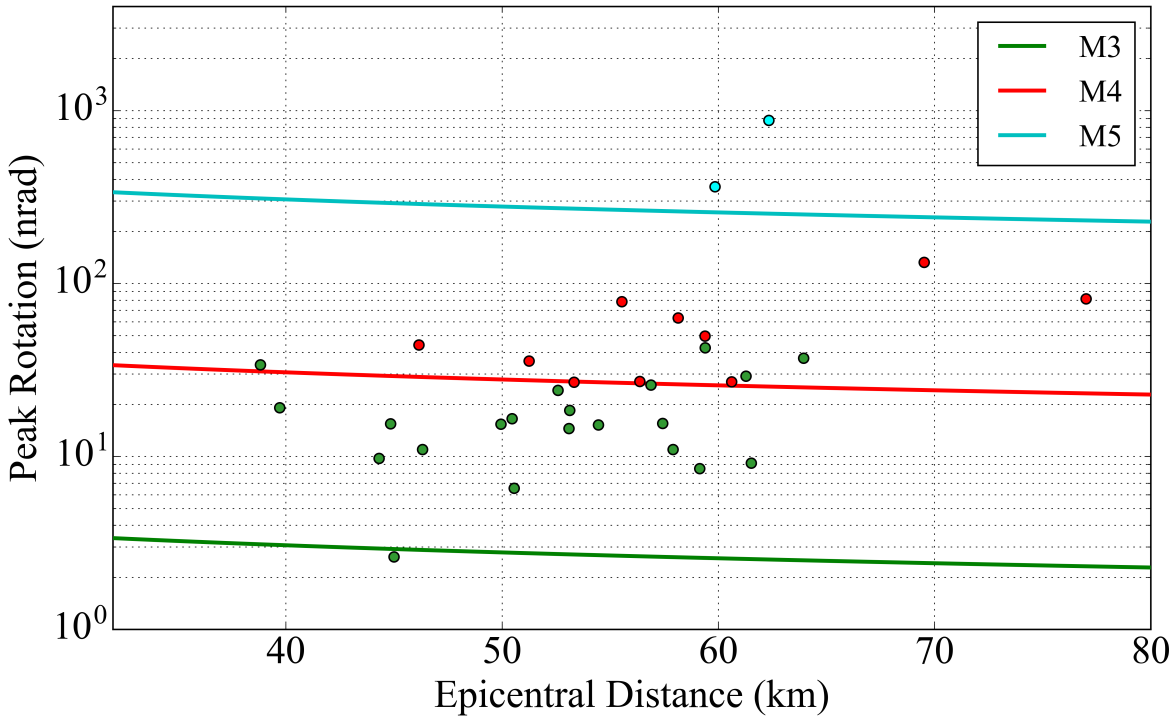

Figure 3.4: Peak angular displacement for the recorded events vs. epicentral distance, the continuous lines represents the local magnitude scale that we fit to the data

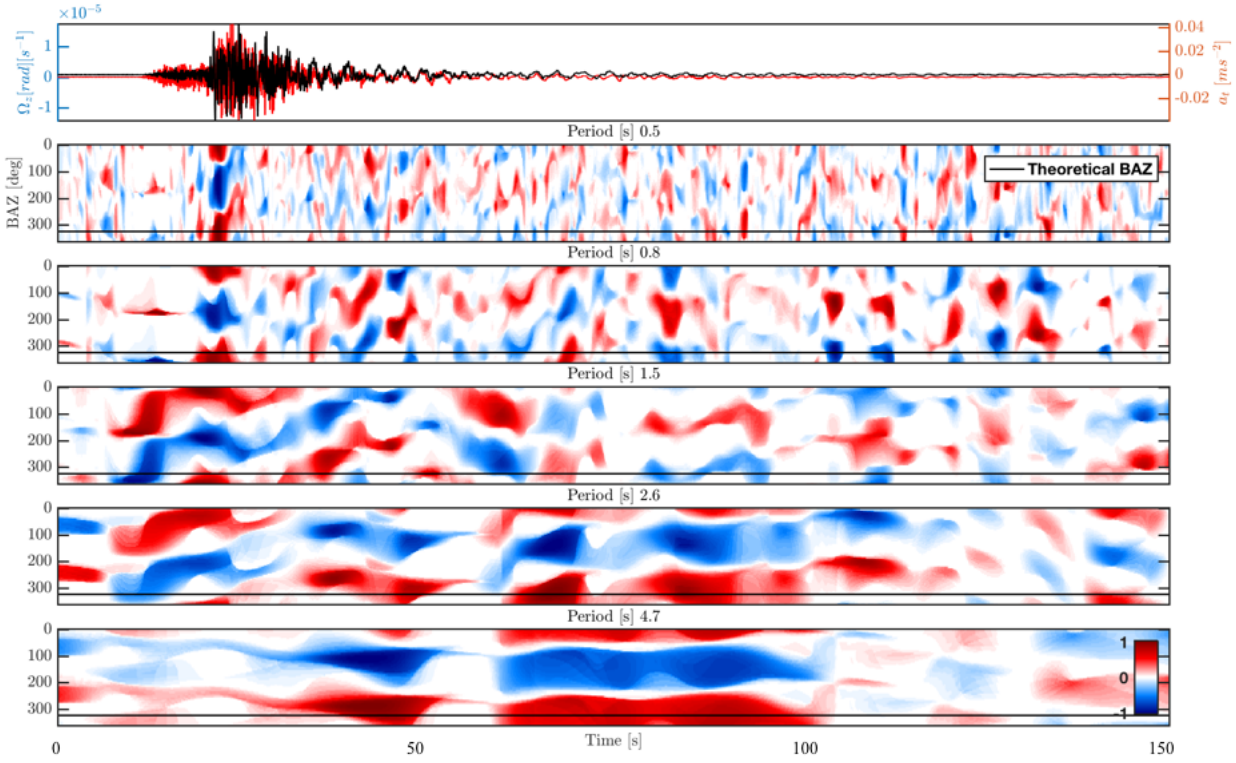

Figure 3.5: The back azimuth analysis in different frequency bands for the Visso M 5.9 mainshock, In this plot the red color denotes the correlation in red and anticorrelation in blue (see the colorbar). On top of the figure the superposition of rotation rate (red) and transverse acceleration (black).

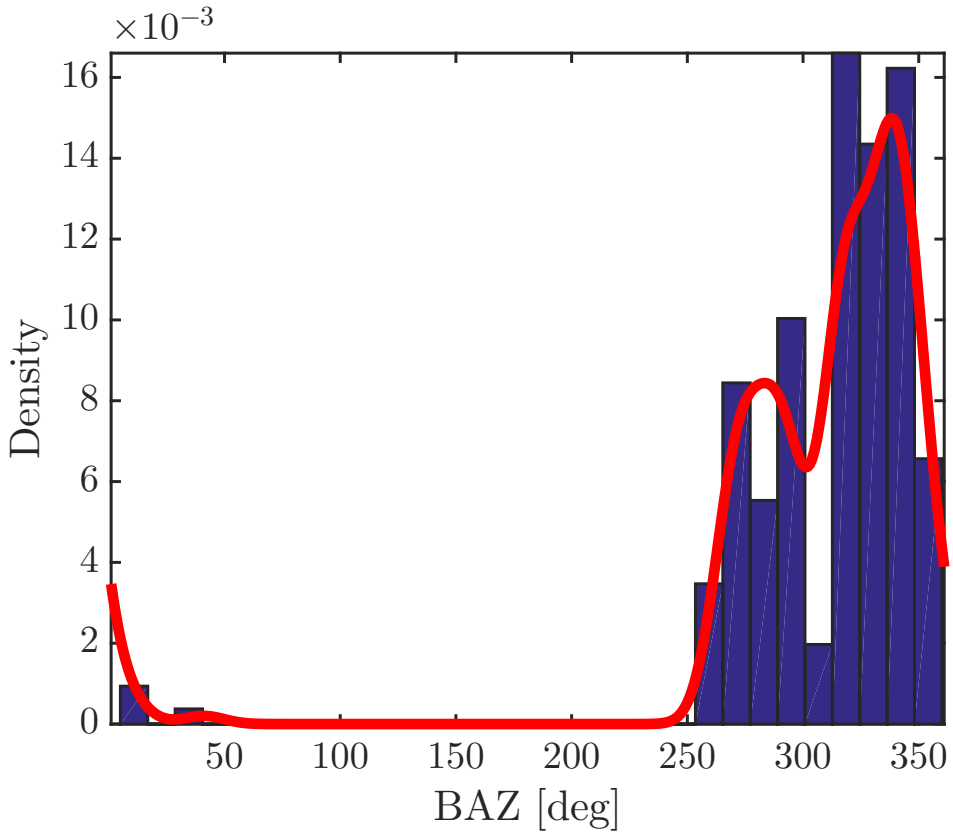

Figure 3.6: The Visso M 5.9 mainshock; histogram for the distribution of maximum correlation values in the Love waves time windows and in the 2 seconds to 5 seconds of period range. The solid red line represent the KDE estimation of the distribution. For this event the theoretical BAZ is 324°

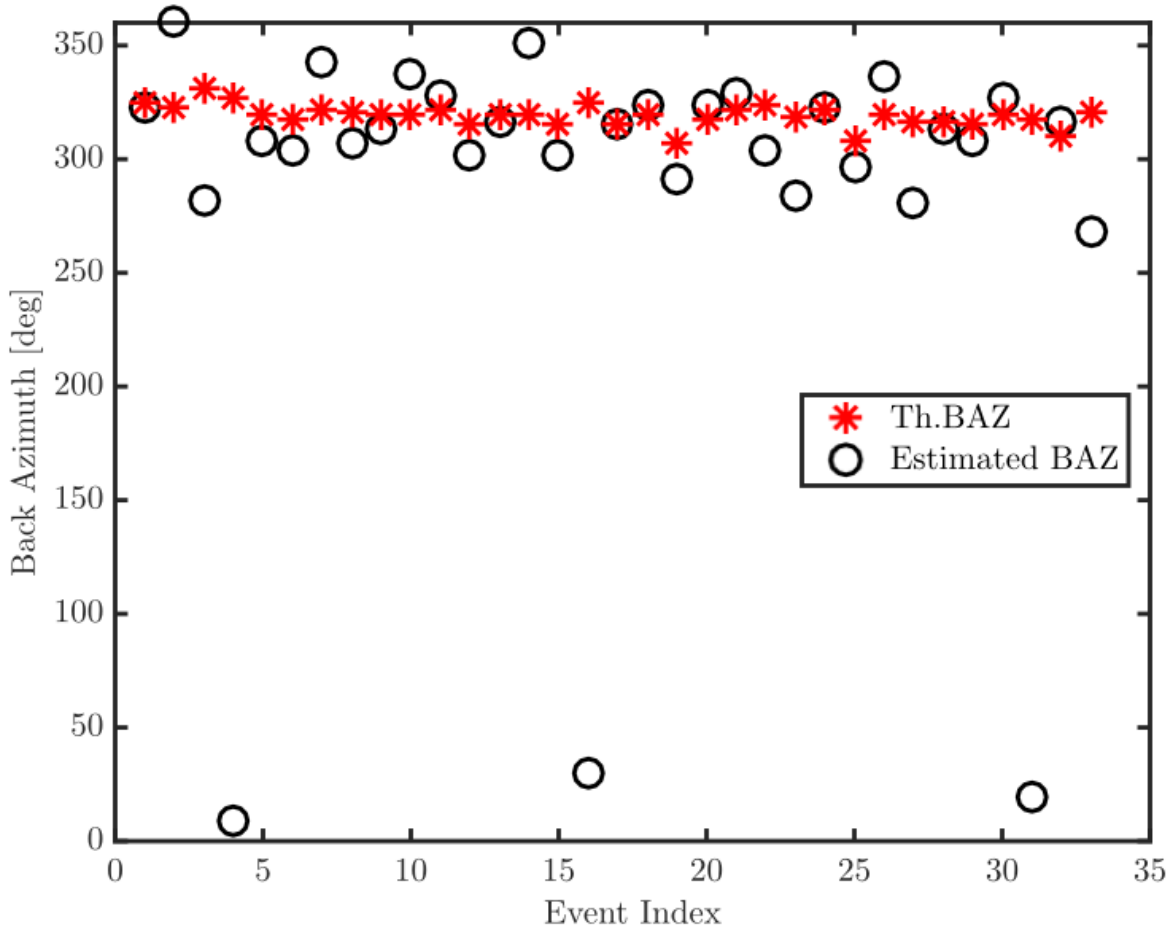

Figure 3.7: Theoretical and observed BAZ for all the events listed in Table 4.1

components. This representation allows us to obtain a time-frequency estimation of the back azimuth. This analysis is shown in Fig. 3.5 in the case of the the Visso MW 5.9 earthquake. The solid line in Fig. 3.5 represents the theoretical back azimuth. For this event the surface Love waves are very clear in both rotational and translational traces and, at periods longer than 3 seconds, the estimated BAZ is in good agreement with the theoretical one. In the frequency band around 2 Hz, a region of high coherence identifies the SH-wave arrival, whose BAZ corresponds to the theoretical one. A more quantitative and statistically consistent analysis of the back azimuth for the entire event database is described hereinafter. The $C(\theta, t, f)$ array is calculated for every event. We find the

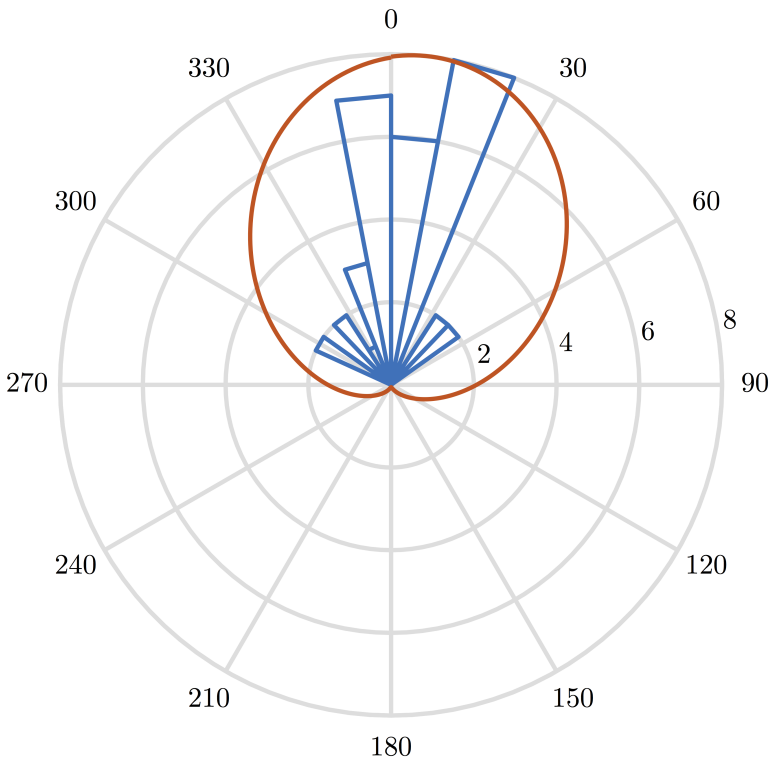

Figure 3.8: Misfit distribution and the relative gaussian KDE modeling in solid red line

maxima of correlation in a time window that goes from the beginning of the S-coda to the end of the surface waves phase. The obtained values are binned in histograms and the distribution is modeled with a gaussian function (KDE gaussian). In Fig. 3.6 we show the histogram and the gaussian KDE for the Visso earthquake. For this event, surface waves are well-defined, and the best agreement between predicted and observed BAZ is observed in concomitance of the Love-wave time-frequency window. We apply this processing to all the events and we resume the analysis by plotting the estimated backazimuth and the theoretical one for the entire set in Fig. 3.7. In Fig. 3.8 we represent the polar histogram of the misfits and the relative gaussian kernel modeling of the distribution. We outline that the theoretical BAZ is just an indication of the possible direction of the wave field. As a matter of fact, once accounting for lateral velocity variations, the complex topography and the underground setting of our instruments, the propagation direction of surface waves may

differ significantly from the expected one. From the analysis of teleseismic Love-wave at periods longer than 10s , [Simonelli et al., 2016] observed a misfit of about 5 degrees. From the analysis on this entire data set we can state that we observe a 10 degrees systematic misfit that can be compatible with the orientation error of the seismometer or caused by a structural effect. A future measure with a triaxial fiber optic gyroscope, used as a gyroscopic compass will allow us to orient our instrument and measure the previous orientation with a precision lower than 0.1 deg. We tried a cluster analysis in order to check if the misfit could be dependent on the events parameters reported in Table 4.1 and on the S/N ratio but the result does not show any clear dependence. In conclusion an average misfit of $\theta_{misf.} = 10^\circ \pm 18^\circ$ is observed.

3.4.3 Phase velocity estimation

The previous processing provided us the BAZ measurements, which allow us to orient the acceleration traces according to a ray parameter system RTZ oriented to the measured BAZ angles for each seismic event. For retrieving phase velocity data from our joint rotational-translational measurements, we use the frequency-domain formulation of eq. 4. In order to provide a seismic-phase dependent phase velocity dispersion measure we divide the seismograms to three time windows. The first one goes from the the P arrival to the SH arrival, describing then what we suppose to be the P to SH conversion in the P coda. The second window goes from the SH arrival, identified in the rotational trace, to end of the S-coda. The last window includes the regional Lg phase where surface waves should be observed. The visual inspection through all the events of the WTC between Ω_z and $\ddot{u}_T$ permitted us to select the spectral region where we have high correlation, this region ranges from [0.125 Hz to 4 Hz]. Our measurements are limited to time windows corresponding to different seismic phases and to a frequency window where the WTC shows and allow us to perform spectral ratios i.e WTC greater than 0.7. The amplitude spectral densities (ASD)

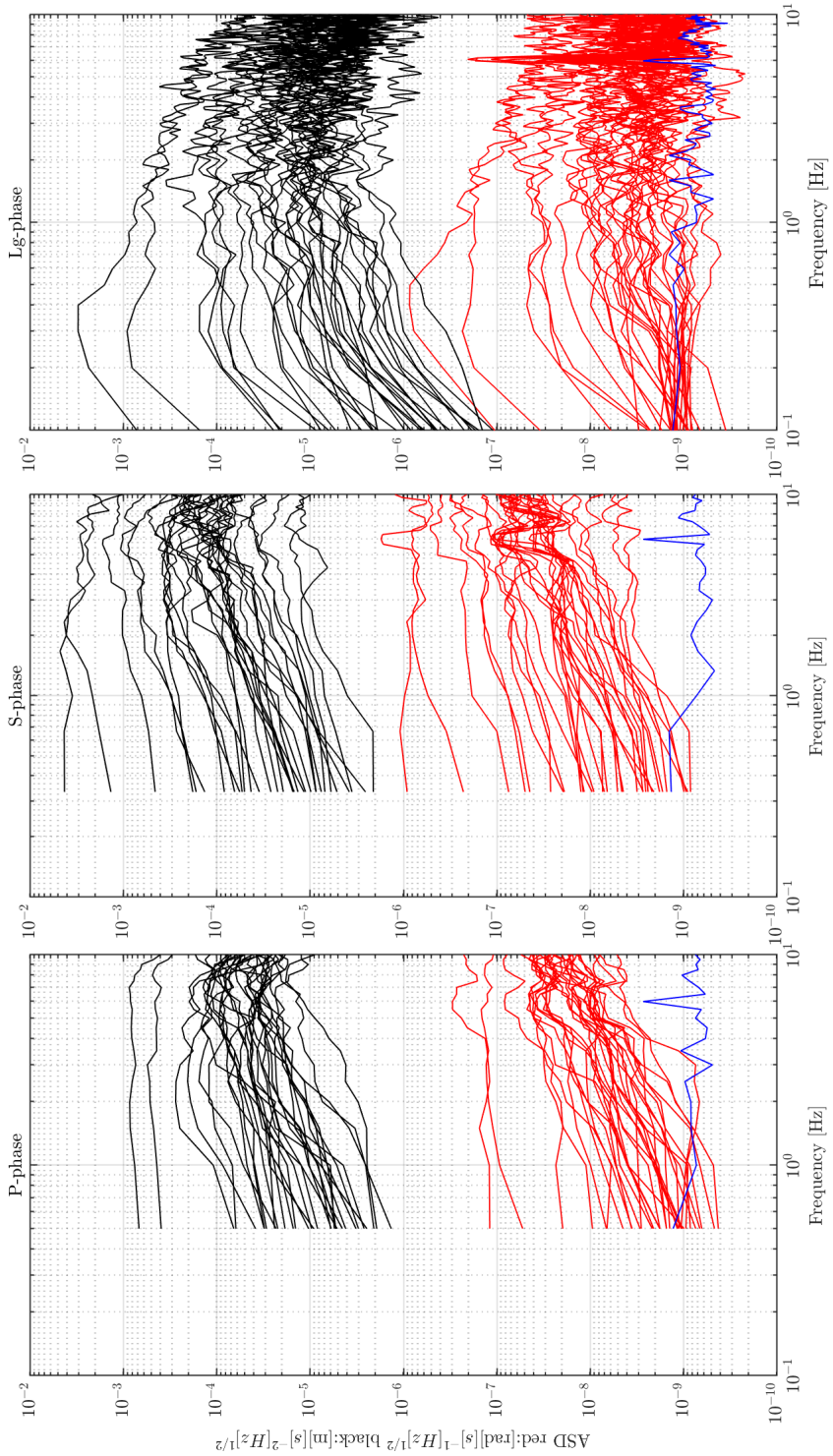

Figure 3.9: The amplitude spectral densities calculated with the multitaper method, in black the transverse acceleration and in red the vertical rotation rate. From left to right the three seismic phases that we analyzed, in blue the noise level of the RLG

of the signals are then calculated by using a multitaper method described by ([Thomson, 1982]) with a time/half-bandwith product of eight. For the three time windows we report the ASD values for the rotational (red) and translational (black) observables in Fig. 3.9. Eq.3.6 defines the dispersion curve for the j-th phase as the average of the single event derived dispersion curves. We omit from the calculation of the average those rotational ASD estimations at the generic frequency f_k for the events that are below a S/N ratio of 2.

$$C_j(f_k) = N^{-1} \sum_{i=1}^{N} c_j(f_k) = N^{-1} \sum_{i=1}^{N} \frac{a_T(f_k)}{2\Omega_z(f_k)} \tag{3.6}$$

The well known fact that the noise level of an instrument is frequency dependent justifies the choice of applying this selection criterium. The final result of the phase velocity analysis is shown in Fig.3.11. The error for the value of $C_j(f_k)$ at the discrete frequency f_k and for the phase j is quantified as the standard deviation of the estimates derived for individual events. For the Lg time window we observe a normal dispersion curve from 0.1 - 1 Hz, this is expected given the dispersive nature of surface Love waves. For the P-phase we see a general less dispersive behavior associated with a larger error. This is also quite evident if we focus on the relative amplitudes of the rotational/translational p-coda signals in Fig. 3.3. For the S-coda we find a pretty constant value of 2.8 km/s, in this case the error is in general smaller than the one for the P-coda. This estimates are compatible to the one reported by [Li et al., 2010], where a velocity profile crossing the Gran Sasso shows a similar shear waves velocity value. For the Visso mainshock we also provide the phase velocity analysis in the time domain (Fig. 3.10). This representation allows us to easily check the correlation between rotation and acceleration in band-pass filtered time windows by visual inspection. The phase velocity values in each line are estimated as the ratio of the peak values of the envelopes for that component. Each component is normalized for graphical reasons. The values obtained by this method are in agreement with the ones

obtained using the spectral ratios method described above.

3.5 Conclusions

This work presented the results from the operation of GINGERino, a Ring Laser Gyroscope co-located with a broad-band seismometer inside the INFN's Gran Sasso laboratories. Our data constitute some of the very first observations of earthquake-generated rotational motions by an intense seismic sequence at local distance. The observed events permitted us to fit a magnitude-distance relation for vertical rotation rates to the recorded peak values at local distance. We extended the application of roto-translational observations of ground motion to local events, thus exploring higher frequency ranges and larger rotation rate amplitudes. The Wavelet coherence (WTC) is used as a filter for identifying those regions of the time-period representation where the rotation rate and transverse acceleration signals exhibit significant coherence. The BAZ of the observed events has been estimated and compared to the predicted ones. This analysis confirms that also at regional distances we are able, by using 4C observations, to find the direction of the wave-field with an error that has been quantified as the standard deviation of the misfit distribution, in other words, supposing to perform an experiment with a station on a planet, without any seismic array present, still we can infer the direction of the wave field an possibly locate the epicenter of the event with only one station. This analysis shows a systematic mean value of 10 degrees of misfit that can be due to both a misalignment of the seismometer or to a structural effect. In a second step, after finding the set of BAZ angles, we oriented our seismometer components according to the ray parameters. We divided the seismograms in three different time windows that identifies the P-coda, S-coda and surface waves phases. For each time window and for all the events we calculated the amplitude spectral densities both for transverse acceleration and vertical rotation rate. The spectral ratio of transverse

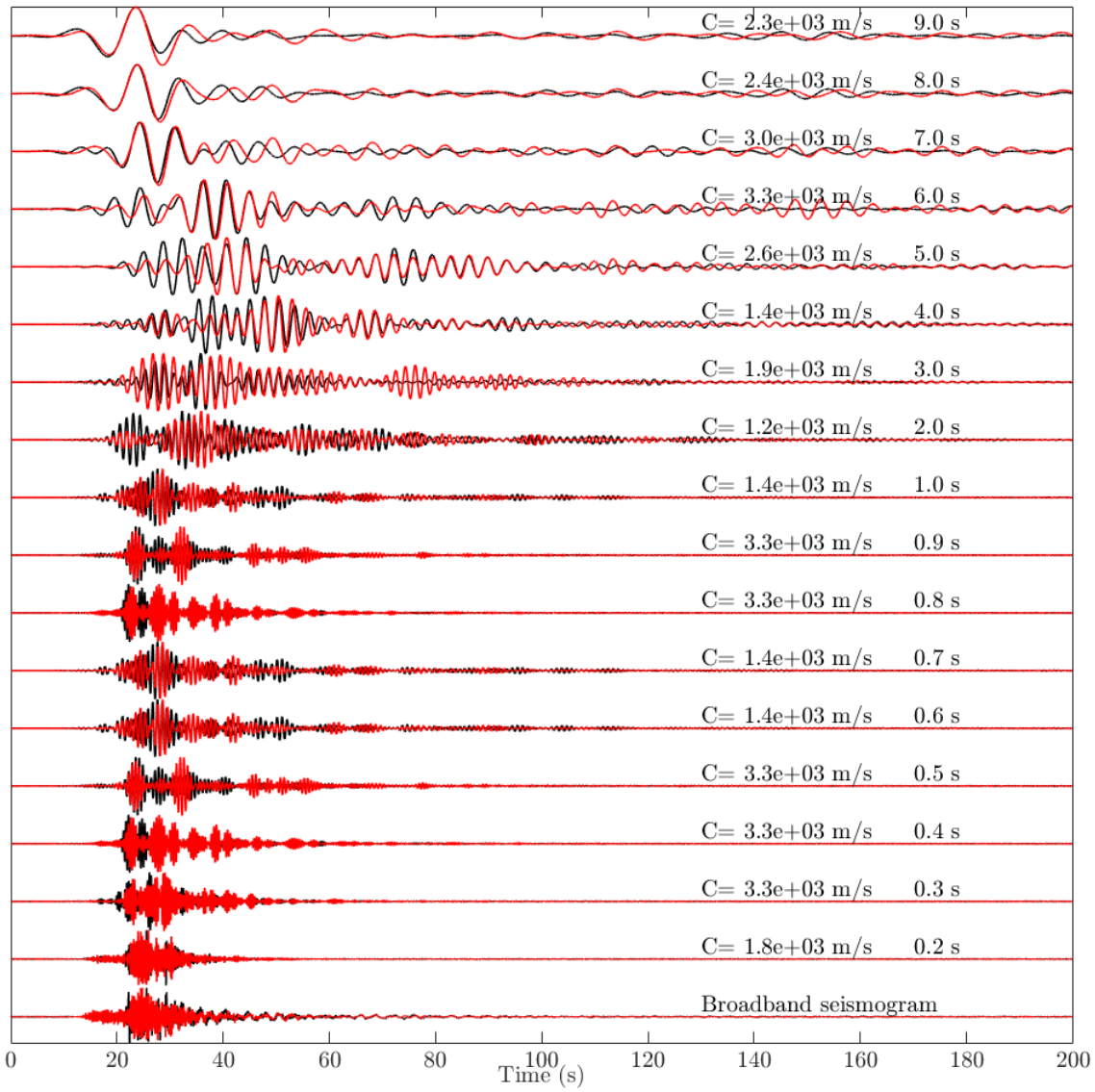

Figure 3.10: The Visso MW 5.9 mainshock. Superposition of vertical rotation rate (red) and transverse acceleration (black) and determination of phase velocities as a function of central frequency of the half octave bandpass filter. The phase velocity values are measured by taking the ratio of the envelopes of the band passed seismogram

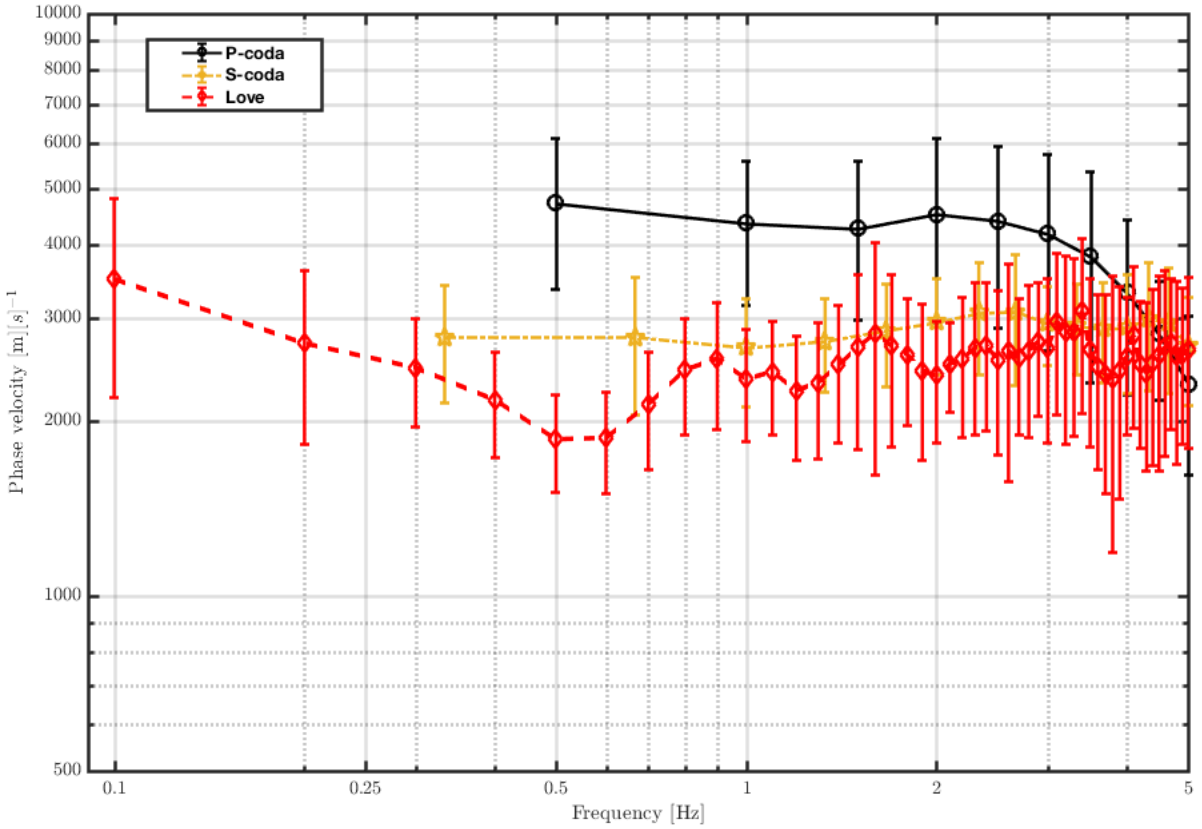

Figure 3.11: The result of the phase velocity estimation method applied to P-coda, S-coda and Love waves time windows

acceleration ad twice the rotation rate gives a measure of three dispersion curves. This allowed to retrieve estimates of phase velocities over the period range spanned by correlated arrivals. Coherency among ground rotation and translation is also observed throughout the coda of the P-wave arrival, an observation which is interpreted in terms of near-receiver P-SH converted energy due to 3D effects associated with the complex topography and anisotropy. Those particular coda waves, however, do exhibit a large variability in the rotation/acceleration ratio, as a likely consequence of differences in the wave-path and/or source mechanism. The future steps of this experiment are to increase the number and the span of observations both in therms of azimuthal coverage and distance. This will allow us to increase the robustness of phase velocity measurements. These are expected given the strong lateral heterogeneities in the lithospheric structure which are expected in a complex area such the central Apennines.

Chapter 4

6-Component Ground Motion Observations of Local Earthquakes: The 2016 Central Italy Sequence

Simonelli, A., Bernauer, F., Braun, T., Wassermann, J., and Igel, H. (2018). 6-component ground motion observations of local earthquakes: The 2016 central Italy sequence. In preparation.

The contributions as a first author to this paper consist in:

- *Installation of the seismic instrumentation during the field campaign*
- *Row data preparation and preprocessing*
- *Coding of the routines used for the analysis of the earthquakes*
- *Manuscript preparation*

Abstract

For many years the seismological community has looked for a reliable, sensitive, broadband three-component portable rotational sensor. In this preliminary study, we show the possibility of measuring and extracting relevant seismological information from local earthquakes. We employ portable three-component rotational sensors, insensitive to translations, which operate on optical interferometry principles (Sagnac effect). Multiple sensors recording redundantly add significance to the measurements. During the Central Italy seismic sequence in November 2016, we deployed two portable fiber-optic gyroscopes (BlueSeis3A from iXBlue and LCG demonstrator from Litef) and a broadband seismometer in Colfiorito, Italy. We present here the six-component observations, with analysis of rotational (three redundant components) and translational (three components) ground motions, generated by earthquakes at local distances. For each seismic event, we compare coherence between rotational sensors and estimate a back azimuth consistent with theoretical values. We also estimate phase velocities fro the Lg and Rg regional seismic phases in the 5 to 10 Hz frequency range.

4.1 Introduction

The rotational seismology is an emerging field of the Earth sciences that is devoted to understanding and exploitation of observations of rotational ground motions for improvement of a wide range of seismological applications . Several studies have already shown the high impact of a colocated broadband observation of the three linear components of translation and three components of rotation [Takeo and Ito, 1997, Cochard et al., 2006a, Ferreira and Igel, 2009, Bernauer et al., 2014, Donner et al., 2016]. [Igel et al., 2007] show that is possible to compare the component of vertical rotation measured at the G-Wettzell RLG to the transverse acceleration measured my a broadband seismometer. From this comparison

Lg waves dispersion curves are estimated. On the same instrument [Hadziioannou et al., 2012b] show the possibility to estimate the direction of the ocean generated noise. The importance of six component observations and the potential of this method in understanding the direction of the incoming wave-field and the local velocity structure is describer by [Wassermann et al., 2016]. This potential finds a natural field of application specially in the environments where it is hard to deploy arrays of seismometers like for example in planetary seismology or in ocean bottom seismic installations. [Lindner et al., 2016] demonstrate using the data collected in an OBS experiment the possibility of improving the performances of an OBS seismometer by correcting for the induced tilts, increasing thus his sensitivity. Rotational seismology as an experimental science is strongly connected with the advances in instrumentation. In fact, the need of observing the complete rotational ground motion vector was outlined by theoreticians [Aki and Richards, 2002]. Still, [Igel et al., 2014] the authors state that " Despite the success of ring laser-based observations, seismology still awaits an appropriate portable rotation sensor that is comparable in sensitivity with today high-quality broadband translation sensors". Today, this gap is closed and a rotational sensor that fulfills to the requirements for field measurements of the three components of ground rotation is finally available. The instrument called BlueSeis3C, is described in detail in [Bernauer et al., 2017].

In this paper, we report the first three components recording from two colocated fiber optic gyroscopes. The fiber optic gyroscope is a passive Sagnac interferometer, the measurement principle is described in the book from [Lefèvre, 2014] and offers the great advantage of being based on massless photons which ensures the complete decoupling from inertial forces. By principle it implies the insensitivity to translations and guarantees a pure rotation measure as an output. The setup of this experiment is shown in Fig. 4.1 and consists of two rotational and two translational sensors. The rotational sensors are respectively the BlueSeis3C, a new highly sensitive broadband, three component instrument by IxBlue,

Figure 4.1: The experimental setup: (top left) the BlueSeis3C; (top right) the seismometer Trillium 120c, (bottom left) the LCG-demonstrator; Bottom right the Guralp CMG-5

and an LCG-demonstrator from Litef. Ground translations were recorded by means of a seismometer from Nanometrics (Trillium compact 120s) and by an accelerometer from Guralp (CMG-5) installed in case of strong motions. The instruments were installed in an old uninhabited country house hosting located near Colfiorito-Italy (lat: 43°1′41.59″N, long: 12°52′40.50″E).

4.2 Geological framework

The central part of the Apennines chain in Italy is characterized by a quaternary NE-SW striking extensional regime, overstamping older compressional tectonics, composed by layers of Miocene Flysch deposits and Meso-Cenozoic carbonate rocks ([Martini et al., 2001], [Pucci et al., 2017]). High-resolution GPS measurements ([Hreinsdóttir and Bennett, 2009];[D'Agostino, 2014]) revealed an annual extension of 2-4 mm, which is primarily accommodated by an extensive system of high-angle SW dipping normal-faults. The particular sector of the Central Apennines struck by the 2016/17 seismic sequence is characterized by two major NNW-SSE trending extensional fault systems of adjacent, WSW dipping, active fault systems: developing in the western part along Gubbio-Colfiorito-Norcia - Lquila and aligning in the eastern part along Mount Vettore-Amatrice-Campotosto (Mount Gorzano fault) - Gran Sasso ridge ([Boncio et al., 2004];[Galadini and Galli, 2000];[Lavecchia et al., 2012];[Pucci et al., 2017]]. The main shocks of recent moderate damaging earthquakes in the Central Apennines (M5.8 - Norcia 1979, M6.0 Umbria-Marche 1997, M6.1 - Lquila 2009) occurred mainly on this western fault system and bear witness of the seismogenic activity, whereas the Mount Vettore and Gran Sasso faults seem to have been silent since historical times [Boncio et al., 2004]. However, the only important seismic event raising suspicion to indicate seismic activity on the eastern fault system is the Me6.2 earthquake of 7 October 1639 (I = IX-X MCS, M= 6.2, CPTI15) on the northern portion

Table 4.1: The recorded events

	Event 1	Event 2
Date	12 Nov	12 Nov
Time	12:34:11	12:59:18
Lat.	42.996	42.997
Long.	13.140	13.138
Mag.	3.8 ML	3.7 ML
Dist [km]	20.8	20.5
Depth [km]	9.0	9.0
BAZ [deg]	101.5	102
Peak Z rot. rate [rad]$[s]^{-1}$	7.46e-5	7.39e-5
Peak N rot. rate [rad]$[s]^{-1}$	6.96e-5	5.55e-5
Peak E rot. rate [rad]$[s]^{-1}$	7.03e-5	4.85e-5
Peak Z acc. [m]$[s]^{-1}$	6.65e-3	6.60e-3
Peak N acc. [m]$[s]^{-1}$	1.45e-2	1.4e-2
Peak E acc. [m]$[s]^{-1}$	1.30e-2	1.3e-2

of the Gorzano fault, while the southern segment was struck also recently by the L'Aquila 2009 sequence [Lavecchia et al., 2012]; [Chiaraluce, 2012].

4.3 Observations and processing

This test campaign lasted a couple of days, in this time interval we record two earthquakes, the principal properties of this events are summarized in Tab. 4.1. The data contain three components of rotation rate from each sensor (BlueSeis3A and LCG) and three components of ground velocity. In Fig. 4.3 and Fig. 4.2 we show in red the three components of rotation rate measured with the BlueSeis3A instrument and in black the three components of ground acceleration from Trillium 120 for the two analyzed events, respectively.

We analyzed the data in these stepsThe processing of the data and the relative analysis develops in three steps: 1) The coherence check between the two rotational sensors signals 2) The Back azimuth estimation in different frequency bands 3) The phase velocity estimation both for Lg and Rg phases.

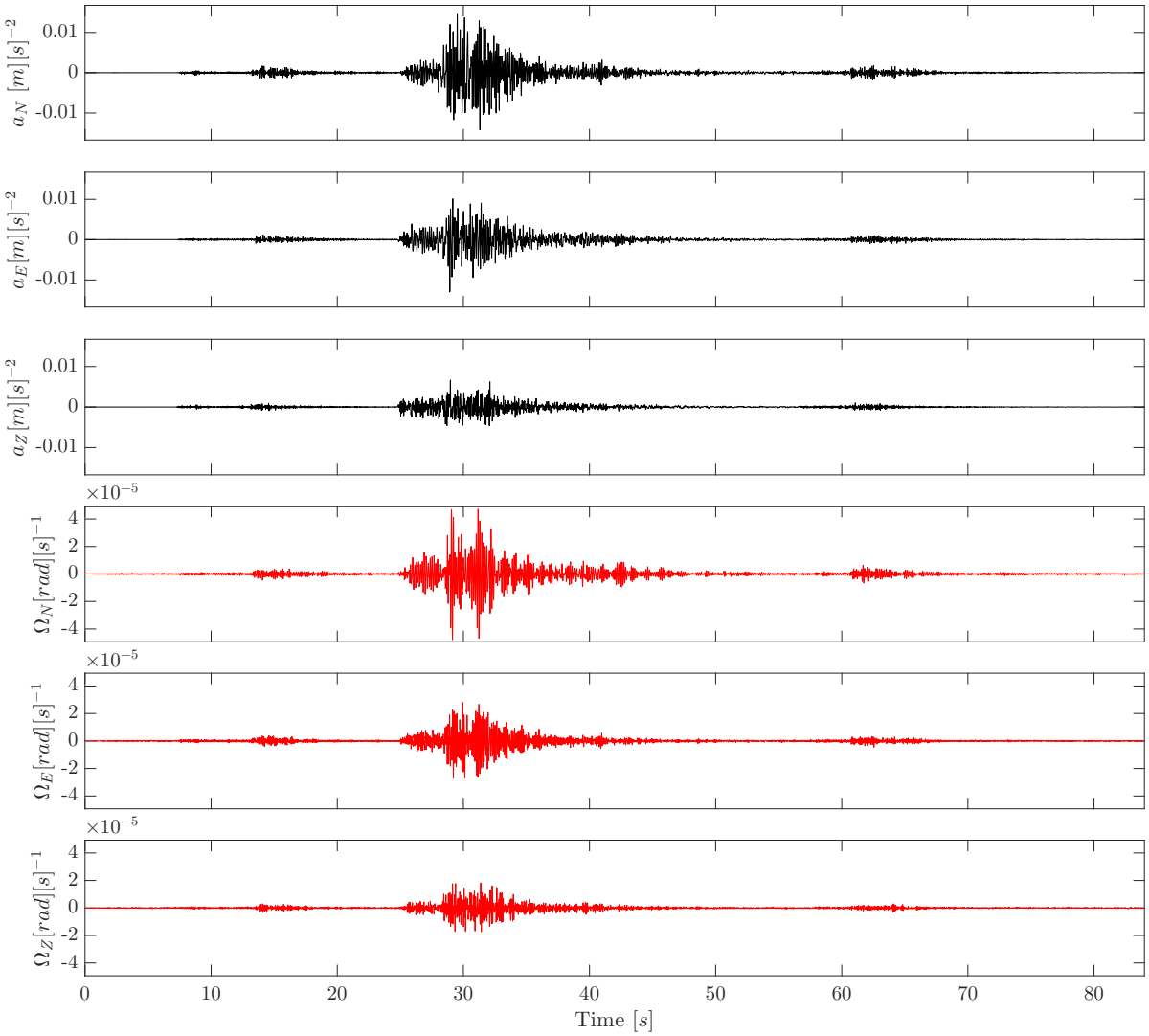

Figure 4.2: Event 1. Broadband ground acceleration after numerical instrumental response correction and numerical differentiation in black; rotation rate (red) measured of the ML 3.8 earthquake of the 12 Nov 2016 at 12:34:11

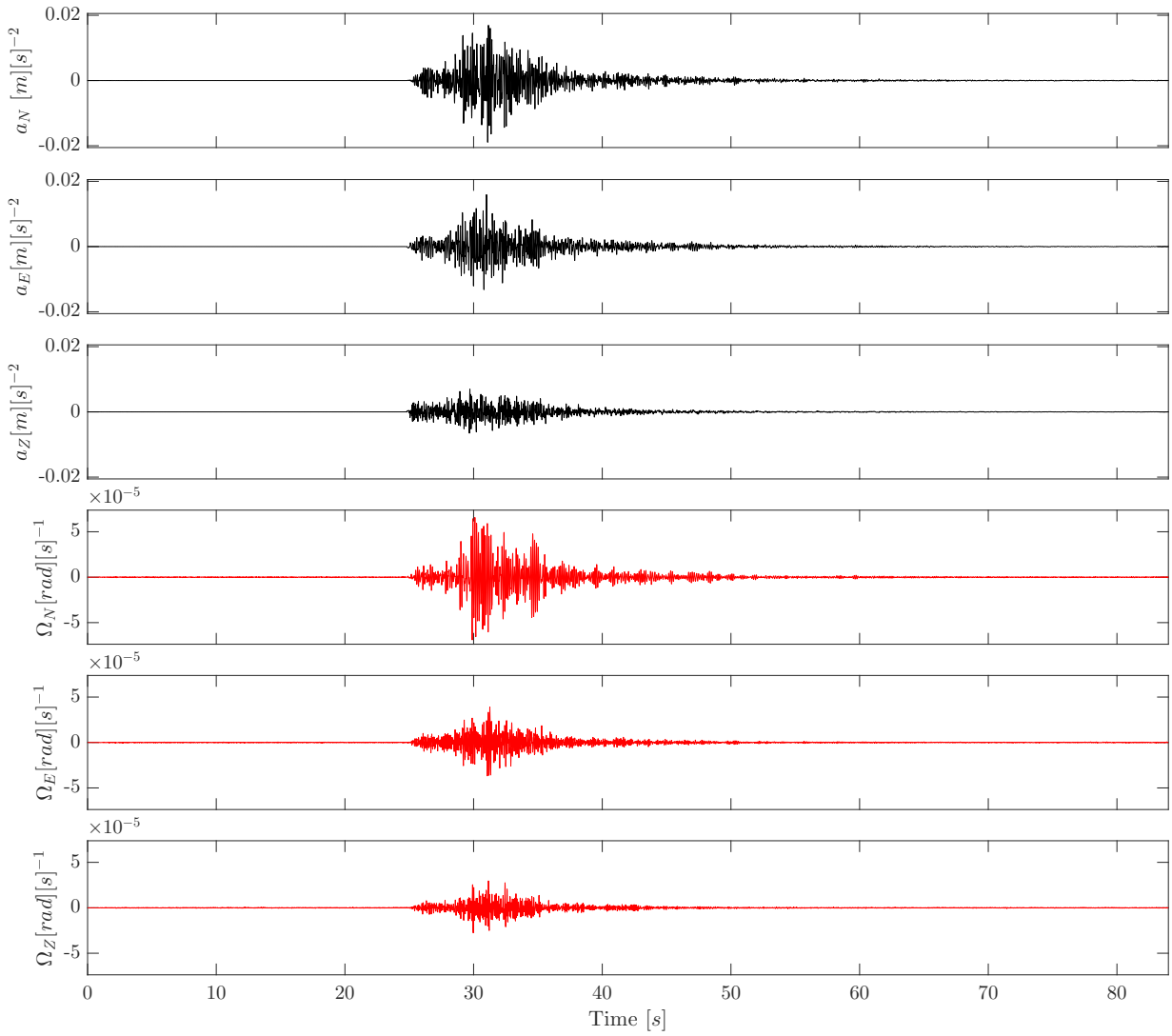

Figure 4.3: Event 2. Broadband ground acceleration after numerical instrumental response correction and numerical differentiation in black; rotation rate (red) measured after the ML 3.7 earthquake of the 12 Nov 2016 at 12:59:18

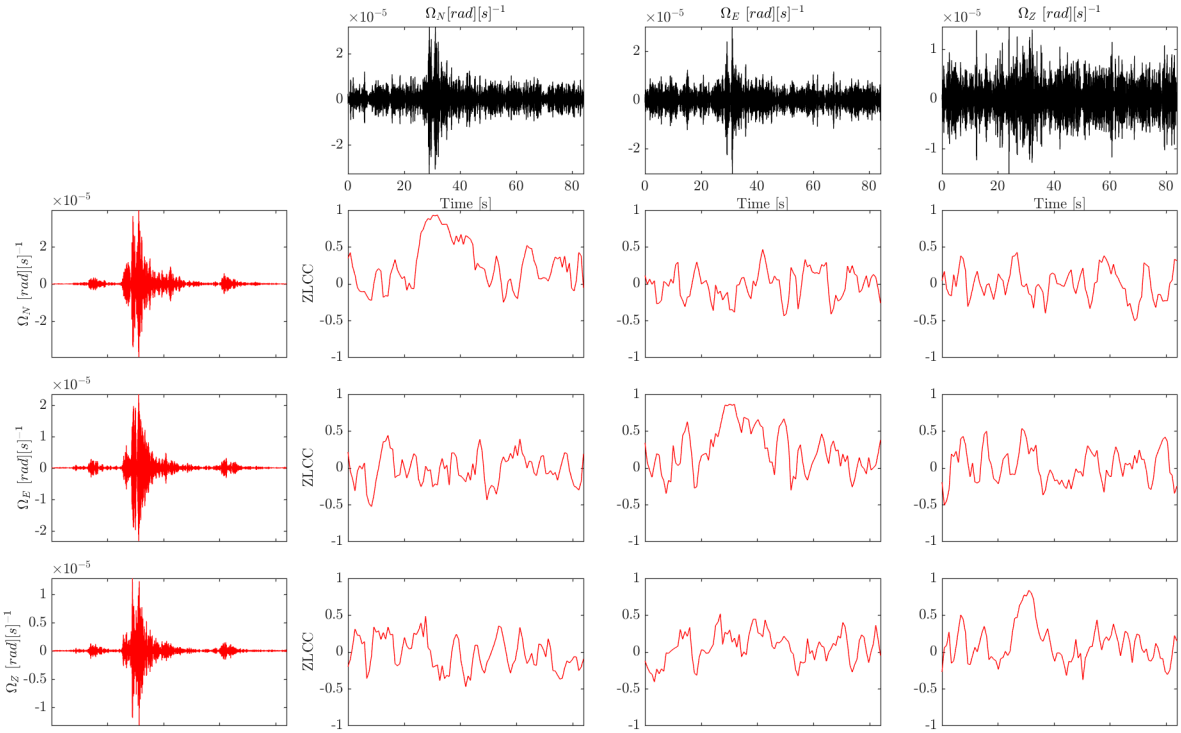

Figure 4.4: The ZLCC check between the rotational components recorded by LCG demonstrator in black and BlueSeis3A for the event number one of Tab. 4.1, the data are band-pass filtered in the interval [5-10] Hz

4.3.1 Zero lag correlation check on the rotational data

We name the rotational data measured with the BlueSeis3A sensor as $\{\Omega_{Z,N,E}\}$ and the data measured with Litef as $\{\omega_{Z,N,E}\}$ where the subscripts indicates the orientation of each component. The traces are bandpass filtered in the (5-20 Hz) range. The choice of this frequency interval is given after visual inspection of the events magnitude spectra, see Fig 4.6. The LCG sensor in fact was showing signal only in that frequency band. In order to check the coherence between the two sensors we calculate the Zero lag correlation coefficient functions (ZLCC) for every combination of $\{\Omega_i, \omega_j\}$ and for both events. The window length used for this estimation is one second and the overlap is 50 %.

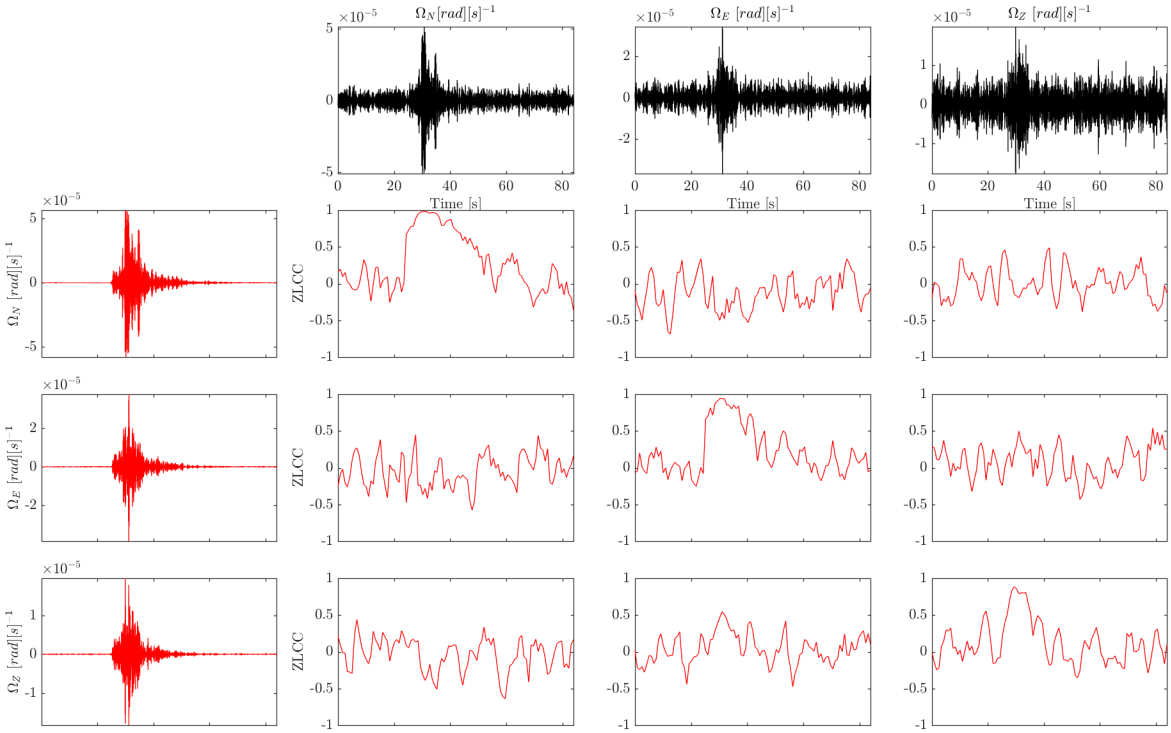

Figure 4.5: The ZLCC check between the rotational components recorded by LCG demonstrator in black and BlueSeis3A for the event number two of Tab. 4.1

As expected the correlation is very high and positive for the components that shares the same orientation as we can see from Fig. 4.4 and 4.5. From the figures the difference in the signal-to-noise ratio between the two sensors is also evident. For the LCG the onset of s-waves is barely visible. Especially the z-component of the event number one as seen by the LCG (Fig. 4.4) is buried in the noise but still the comparison with the same component recorded by the Blueseis3C gives a clear correlation higher than 0.8. In the time regions out of the s-phase the correlation is low since the instrumental noises of the two instrument are independent. This test of inherent coherence between different sensors based on the same robust optical detection principle is a very important cross check for our recordings. It is also important to note that the peak values of the rotation rates for the two events are compatible.

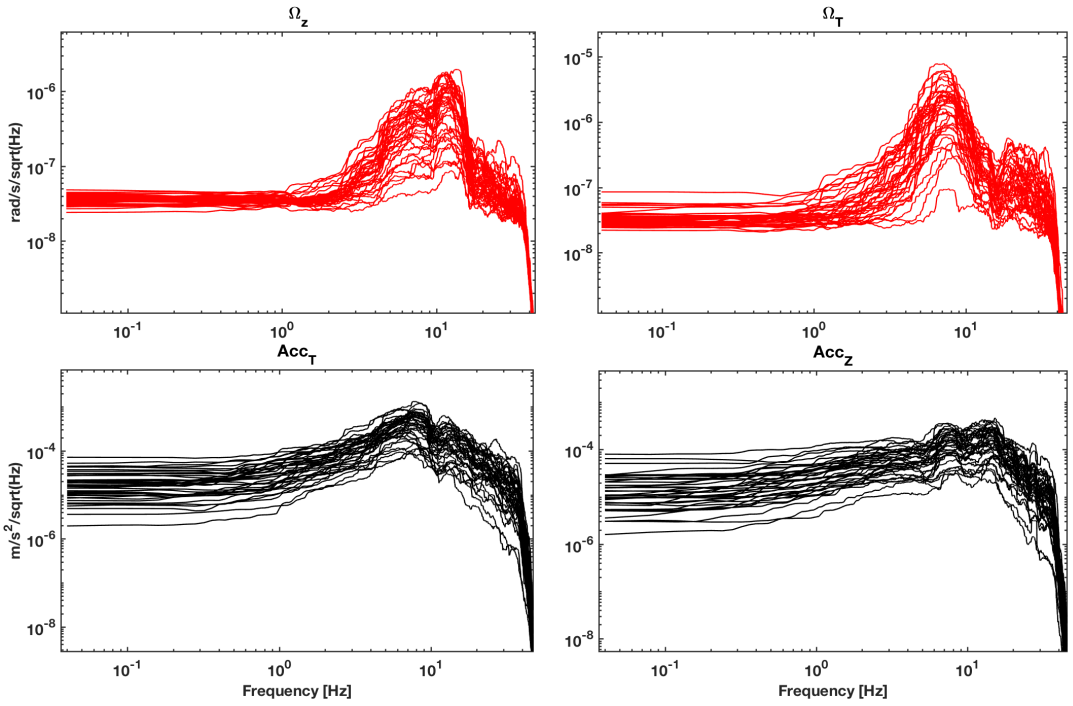

Figure 4.6: Amplitude spectra calculated for the S phase window of the recoded events.

4.3.2 BAZ determination

- The velocity data are corrected for the instrumental response of the seismometer and differentiated respect to time in order to get the ground acceleration

- The horizontal components of ground acceleration are rotated clockwise from Nord in steps $\delta\theta$ of one degree from 0° to 360°, we get then a set of horizontal components $\{R_i, T_i\}$ where R and T are the radial and transverse components of ground acceleration at the BAZ angle θ_i.

- For every couple of observables $\{\Omega_Z, T_i\}$ we calculate the wavelet coherence (WCT) in order to identify the time-frequency regions where the two signals exhibits a cor-

relation that is higher than 0.7. The result of this processing consists is an array $WCT(t, f, \theta)$. This step of processing permits to identify the direction of the incoming wave-field for different seismic phases at different wavelengths.

- We determine the maximum values of WTC in seven frequency bands and in a time windows starting at the P onset and lasting until the end of the Lg phase
- We bin the BAZ values obtained in the previous step in histograms in order to identify the most probable direction for every frequency band. The result of this analysis is shown in Fig. 4.7 and Fig. 4.8 for event one and two respectively.

A completely symmetric approach of the processing described above permits to estimate the direction of the wave-field using Rg waves. We rotate this time the horizontal rotation rates (tilts) an we let the vertical acceleration fixed. The processing is identical the only difference is the sign of the correlation that , as predicted by theory is opposite. In most of the frequency bands where the BAZ has been estimated, the peak of the distribution of maxima of correlation coincides with the theoretical Back azimuth. There are by the way some spectral regions where the BAZ estimated with our method differs from the theoretical one. In particular for Rg waves, the estimation of BAZ is in agreement with the theoretical BAZ only for frequencies below 1 Hz. Further studies on a larger data set may resolve this issue

4.3.3 Phase velocity measurements

The availability of 6C observations permits to estimate the phase velocity both for Lg and Rg waves. We rotate our components according to ray-parameters assuming the BAZ estimated in the previous step. The couple of observables that we use for the purpose are $\{\Omega_Z, a_T\}$ and $\{\Omega_T, a_Z\}$ where the first set is the transverse acceleration and the vertical rotation rate and the second one is the vertical acceleration and the transverse rotation

rate i.e the rotation rate measured around the axis that is transverse to the direction of propagation of the seismic wave. It's well known from literature that with the first couple of observables it is possible to obtain Love waves phase velocity measurements [Igel et al., 2005] by using the formula $c_L = -a_T/2\Omega_T$ and for Ryleigh waves $c_R = a_Z/\Omega_T$ see. [Suryanto, 2006]. We rewrite the equations above and we get

$$a_Z = c_R\Omega_T, \tag{4.1a}$$

$$a_T = -2c_L\Omega_Z, \tag{4.1b}$$

Assuming plane wave propagation the equations are solved by orthogonal linear regression (ODR), see [Wassermann et al., 2016]. Those data points in the rotational data that has a signal-to-noise ratio close to one are excluded from the fit together with the associated acceleration data, the aim of this step is to exclude noise from the fit . The goodness of the ODR is estimated as the sum of the orthogonal distances.

The results of this analysis is shown in Tab.4.2. We can see clearly both from Fig.4.11 and from the data reported in Tab.4.2 that for Lg waves the single event derived estimations are consistent each other, they differ only by 6%. Also the mean value between the two estimations is in accordance with the expected phase velocity for Lg waves in the [5-10 Hz] span [Eslick et al., 2008].

For Rg waves only the event number one gives a result that is acceptable, we get a value that is 13% slower than the relative Lg waves estimation; this is in accordance with theory. For the event number two the slope of the experimental data scatter plot is not in accord with equation 4.1 b. We have to note from Tab. 4.2 that in general the value of Zero lag correlation of the observables $\{\Omega_Z, a_T\}$ is higher than $\{\Omega_T, a_Z\}$, this of course reflects also on the error on the ODR fit that, in the case of Rg waves estimation is two orders of magnitude larger.

Table 4.2: The results of the ODR on the events band pass filtered in the [5-10] Hz interval; we report the estimated phase velocity for Lg and Rg waves, the Error on the linear fit of equations 4.1 as the sum of orthogonal distances and the maximum values of zero lag correlation coefficient estimated my means of sliding one second long window

Event	Lg [m][s]$^{-1}$	Fit error	Max ZLCC	Rg [m][s]$^{-1}$	Fit error	Max ZLCC
1	784	4.1e-9	0.92	350	1.7e-7	0.62
2	739	8.7e-9	0.94	644	3.7e-7	0.66

4.4 Discussion and conclusions

In this paper we presented the first 6C broadband observations from two local earthquakes during the 2016 Central Italy seismic sequence. After validating the rotational observations by comparing via ZLCC the recordings of the two 3C rotational sensors we proceeded with the analysis of vertical rotation rate versus transverse acceleration in order to identify the back-azimuth of the incoming wave-field for Lg and SH arrivals. This analysis confirms the goodness of this method in the 4 to 8 Hz band where the peaks of the BAZ values distributions coincides with the theoretical Back azimuth. In the spectral region where the couples of observables are coherent $\{\Omega_Z, a_T\}$ and $\{\Omega_T, a_R\}$ we could estimate the phase velocity values both for Lg and Rg waves. This work shows that 6C earthquakes observations at local distances can provide a correct estimation of the event BAZ, the phase velocities that we measure are in good agreement with the theoretical relations that we expect for Lg waves. A future deployment of a similar setup on a longer time window will permit to give to our promising first observations a statistically consistent meaning.

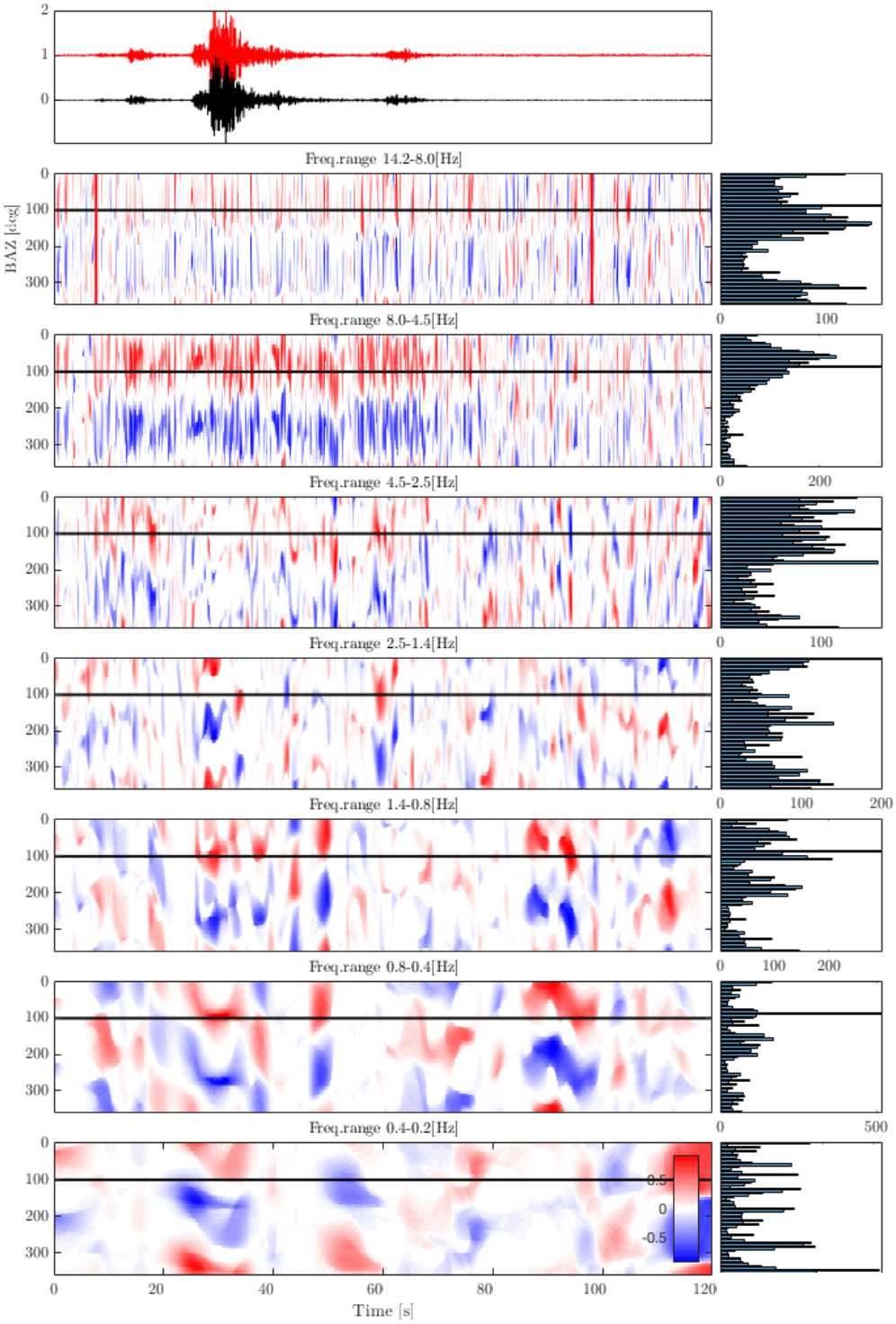

Figure 4.7: The BAZ estimation and the distribution of the maximum vales of WTC vs angle for event 1 estimated after step-rotation of horizontal seismometer traces and correlation with vertical rotation rate (Lg waves). The red trace represents the vertical rotation rate and the black trace the transverse acceleration. The black continuous line is the theoretical BAZ: 101.5°

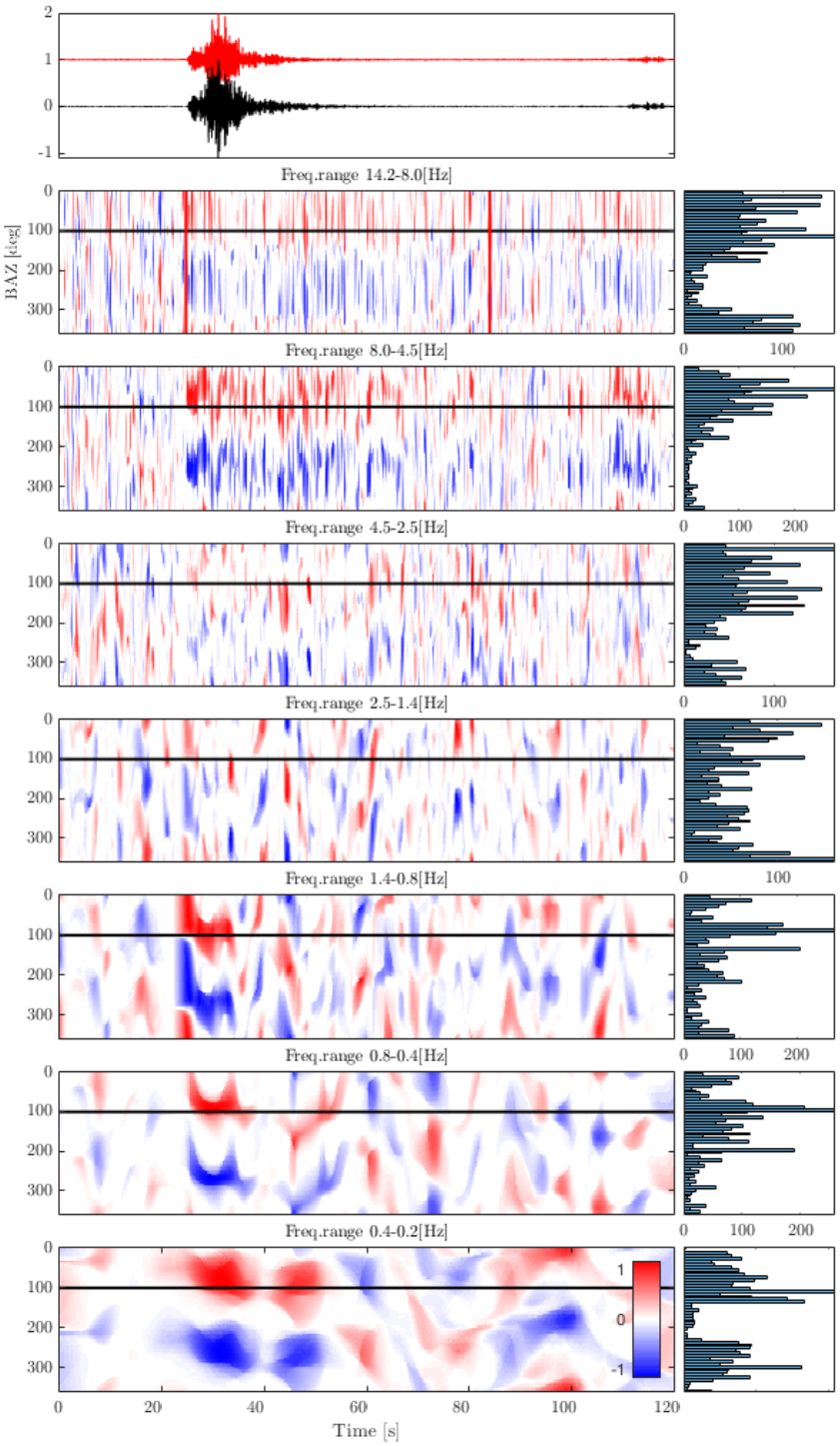

Figure 4.8: The BAZ estimation and the distribution of the maximum vales of WTC vs angle for event 2 estimated after step-rotation of horizontal seismometer traces and correlation with vertical rotation rate (Lg). The red trace represents the vertical rotation rate and the black trace the transverse acceleration. The black continuous line is the theoretical BAZ: 102°

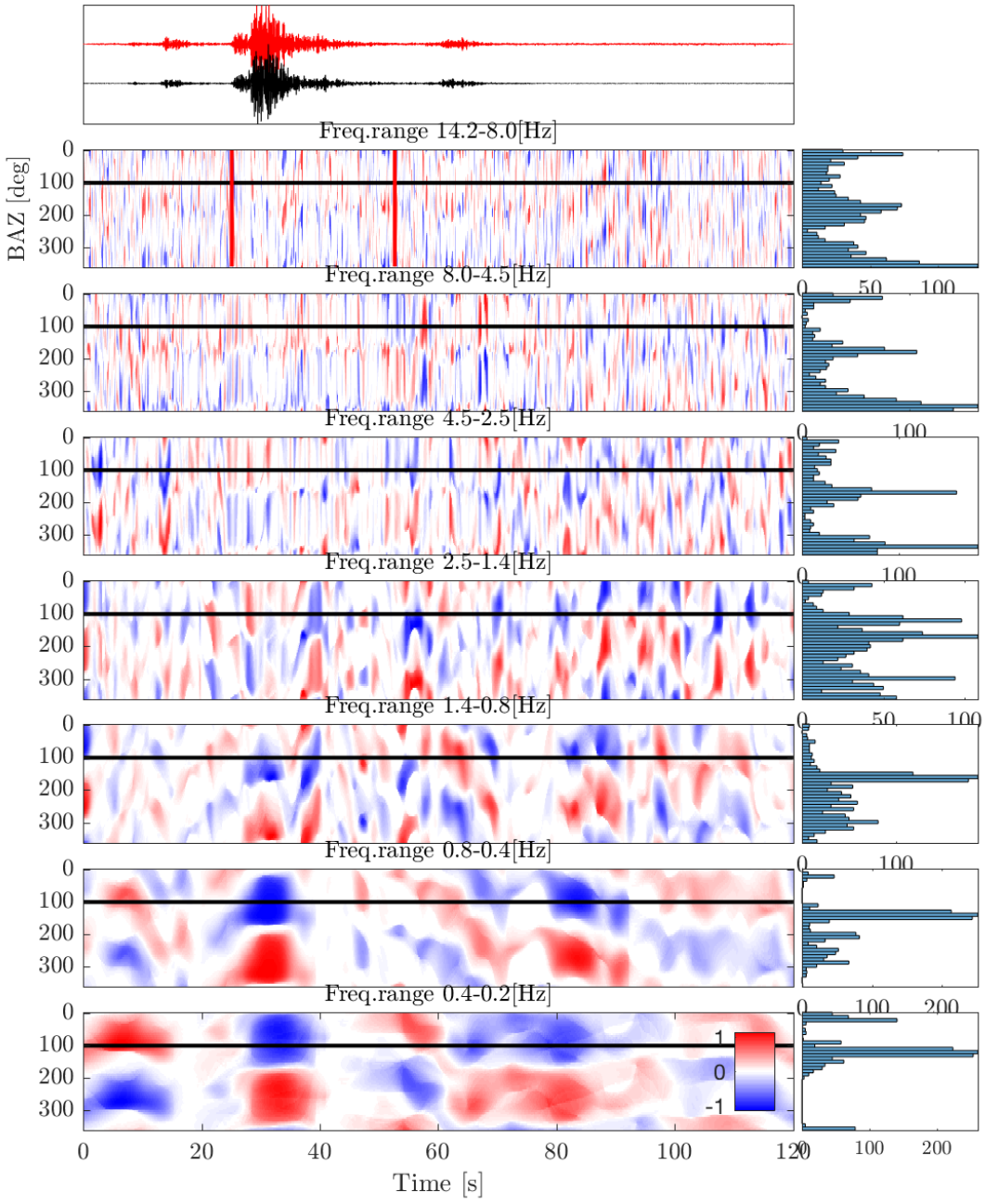

Figure 4.9: The BAZ estimation and the distribution of the maximum vales of WTC vs angle for event 1 estimated after step-rotation of horizontal rotation rate traces and correlation with vertical acceleration (Rg waves). The red trace represents the transverse rotation rate and the black trace the vertical acceleration. The black continuous line is the theoretical BAZ: 101.5°

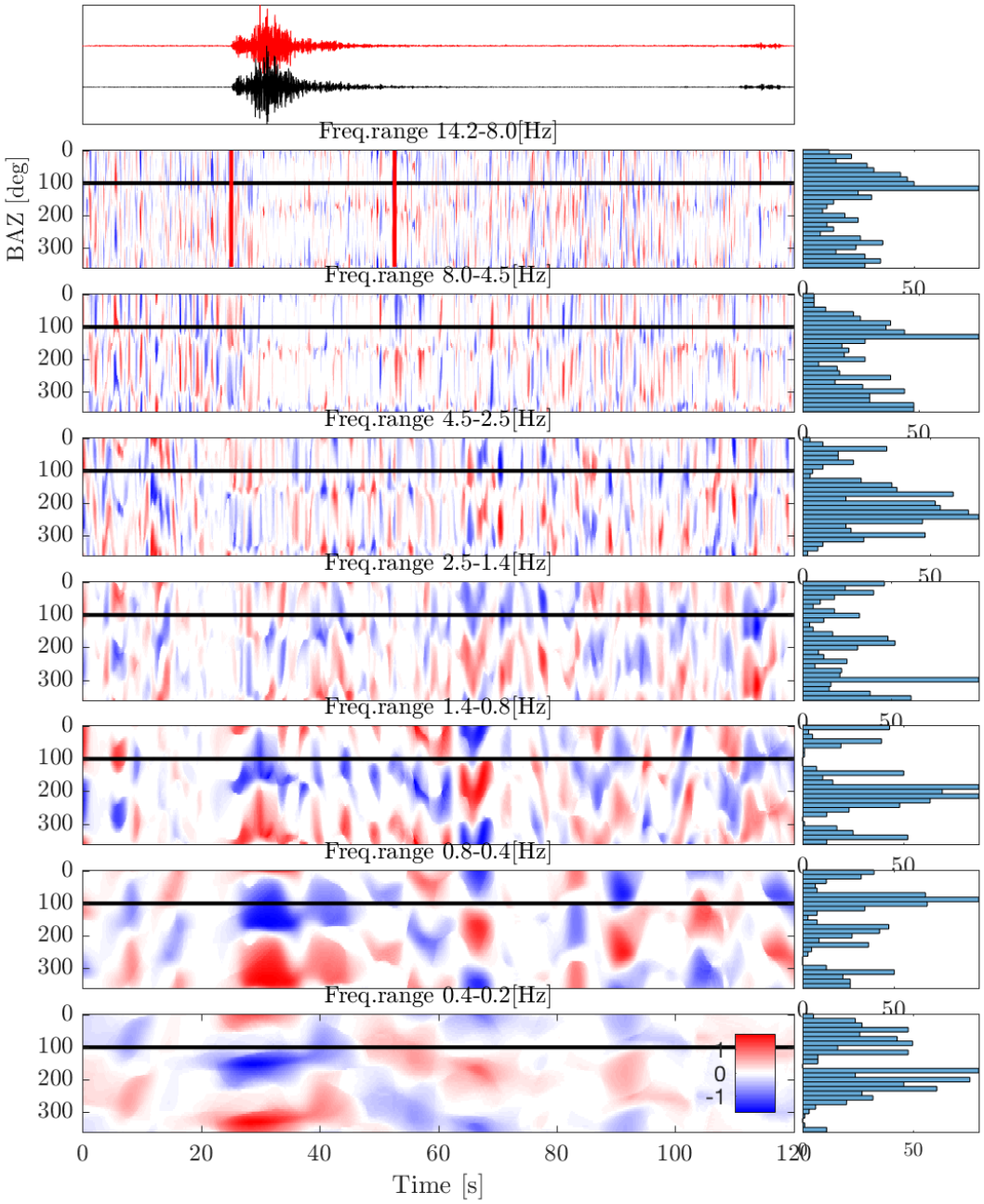

Figure 4.10: The BAZ estimation and the distribution of the maximum vales of WTC vs angle for event 2 estimated after step-rotation of horizontal rotation rate traces and correlation with vertical acceleration (Rg waves). The red trace represents the transverse rotation rate and the black trace the vertical acceleration. The black continuous line is the theoretical BAZ: 102°

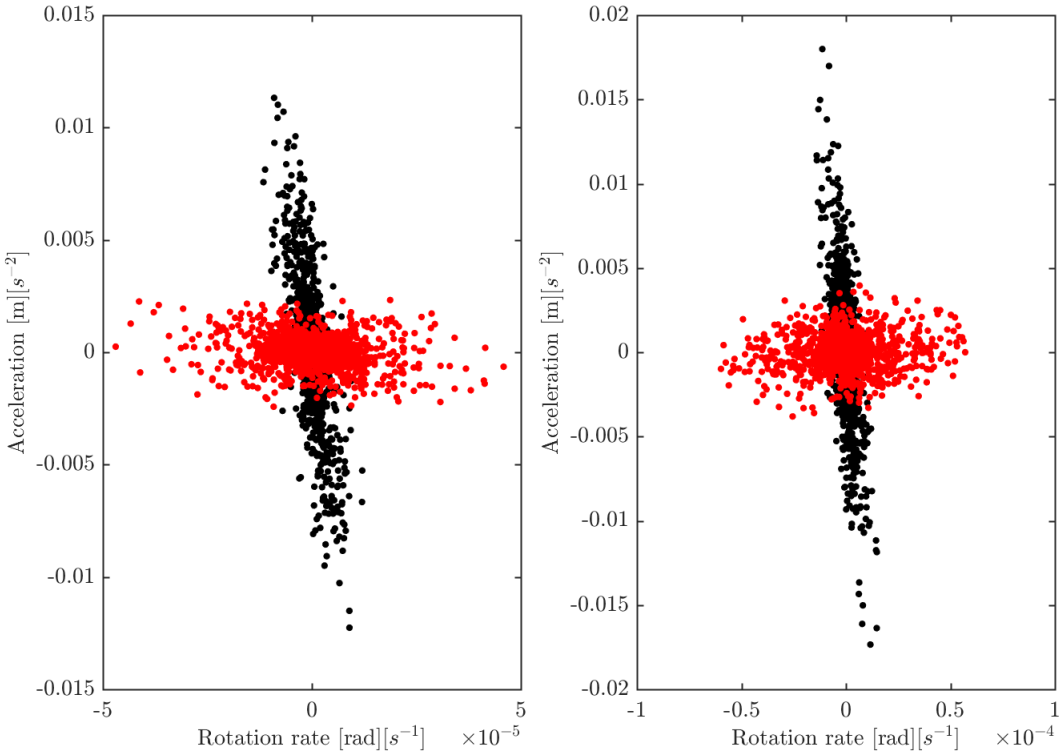

Figure 4.11: Scatter plot of the couple of sets $\{\Omega_Z, a_T\}$ in Black (Lg waves) and $\{\Omega_T, a_Z\}$ in Red (Rg waves); on the left panel the event number one, on the right panel the event number two.

Conclusions

The interest on measuring rotational motions of the ground dates back to at least two centuries ago. The existence of this type of ground motions was predicted in the theory of linear elasticity. Monuments and obelisks rotated after the occurrence of strong seismic events are reported in historical documents and suggested as an evidence the existence of the ground rotations. However those effect we know today that they could be caused by only simple linear accelerations. This was suggesting probably much larger amplitude for rotations induced by earthquakes. Several experiments aimed at measuring this type of ground motion failed due to the unsufficient sensitivity of the first mechanical instruments. After the fifties, the first active laser gyroscopes were developed for navigation purposes and after a few years they were able to "see the Earth's rotation". The first measurements of rotational motions induced by earthquakes by the way date back only to 1995. The first complete characterization and quantitative connection with the translational motions was given only after the first measurements made with the G-Wettzell RLG. These measurements demonstrated the possibility of estimating the direction of the wave field of an earthquake with a single station and the possibility to measure the phase velocity of surface waves or shear waves. At the beginning of this Ph.D. project only the G-wettzell measurements supported with real data the power of the methods derived from rotational seismology. It was necessary to confirm and verify this results in others geological and structural contexts. It was necessary to expand the study to local and regional events, to measure large events near the source. To check the behavior of the rotational motions with the depth. Moreover, given the experimental nature of seismology, if was desirable to test the power of a portable six components station in a field experiment. This is expected to replace the logistical complexity of an array of seismometers, with a simpler single station configuration . Hereinafter we recap the steps of this work before moving on to the future perspectives for this research field. In the introduction we provided the mathematical expressions for the expected rotation rates under linear elasticity and plane wave assump-

tion. The basic principles that permits to measure precisely and accurately the rotational motions are described starting from the Sagnac principle to its implementation in RLG and FOG. An historical review of earthquake-induced rotations guided the reader up to nowadays performing a parallel comparison of the state of the instruments development and of the techniques of data processing. The open questions present at the beginning of this thesis work are described. The following chapters are structured as stand alone papers, sorted in chronological sense. Here we just briefly recall the conclusions present at the end of every chapter.

- After G-Wettzell another large ring laser, with an area larger than $10m^2$ was built in Gran Sasso underground laboratory, it has a sensitivity of the order of 10^{-10} rad/s, in the frequency band of interest for seismology. Together with the colocated seismometer it constitutes an underground rotational observatory. This enlarge the possibility to observe earthquakes from tele seismic distance to very local, given the geographical location of the instrument. This permits also to compare the rotational observations of large distant events with the newborn ROMY system of ring lasers and the above mentioned G-Wettzell, opening thus a new season for multi station observations.

- Underground rotations has been observed after the first unsuccessful attempt of the G-Pisa ring laser, a first observation of a teleseismic event is reported in chapter 2 and its relative analysis. This confirms in another structural context the possibility of BAZ estimation for tele seismic events. The phase velocity analysis for Love waves show a normal dispersion in agreement with the PREM model of the Earth for periods longer than 10 seconds

- After the first light other events were recorded and characterized; a study on the seismometers noise indicate that the site is good in the microseism region but a high

noise at long period is present; we show that this noise is probably due to the forced air convection since it seems directed as the tunnel orientation where the air flows.

- A large dataset of local and regional events occurred during the 2016 seismic sequence of central Italy is recorded. The quantity of data collected permitted a statistical study on the BAZ estimation at shorter distances and in different frequency bands. The phase velocity for different seismic phases is estimated my mean of spectral ratios far all the events and the results are stacked in order to obtain a dispersion curve for three time intervals: the P-coda, S-coda and Lg phase.

- A first campaign is performed using the state of the art of portable 3C rotational sensors in Colfiorito. The "BlueSeis3A" and the "LCG-demostrator" recorded simultaneously the seismic activity following the Mw 6.5 main shock of Norcia. Both sensors show coherent data for what concern the measured rotations. For the first time the six components observations of earthquakes at local distances are reported. The data are processed in order to estimate the BAZ of the incoming wave field using the Love waves and for the first time (given the availability of the horizontal rotation rates) using Rayleigh waves. An estimation of the local phase velocity is given in the 5-10 Hz range for Love and Rayleigh waves.

The 2017 has been a turning point for what concerns the seismic instrumentation dedicated to the detection of rotational ground motions. For the first time a large ring laser system called ROMY is able to reconstruct with unprecedented sensitivity the ground rotation vector. With this new experiment the number of rotational observatories grows up to three. We have since years consistent observations from the G-ring in Wetzell, Germany and, since 2015 stable observations from Gingerino in Gran-Sasso, Italy. At the same time a commercially available three component portable sensor is available (Blueseis3A by IxBlue). It common practice since decades to observe translational ground motions

generated by earthquakes in a global scale by means of broadband seismometers networks but global multi-site observations of the rotational component of tele-seismic events is still missing. In this work for the first time we compare and analyze the rotational ground motion generated by the same earthquakes (Mexico Mw 8.0, Kamchatka Mw 7.6, Iraq Mw 7.2) occurred in 2017, as detected by different Instruments at different sites. This will permit for example to highlight the role of the local crustal structure causing the P-SH near-receiver conversion. This causes the observed rotational signals in the P-wave coda. On the other hand, the availability of six components observations from the ROMY ring laser and from the BlueSeis3A will permit to completely characterize the seismic wave field in terms of wave type, direction of propagation and polarization on real data. As a general conclusion the waveforms are gaining more and more importance in seismology not only for ground translations but also for all the possible degrees of freedom of the ground motion.

Appendices

The wavelet decomposition method for phase velocity estimation

In this appendix we describe more in detail the mathematics that underlies to the wavelet analysis performed in the last two chapters of this thesis. Let suppose to have the couple of sets of observables defined as: $\{\omega_Z,a_T\}$ and $\{\omega_T,a_z\}$.

As we know from theory these two couples of observables should show themself in the respective seismograms as the same waveform scaled respectively by the phase velocity for Love and Rayleigh waves. In the following we consider for example the set $\{\omega_Z,a_T\}$. In order to check the coherence of the the two couples of seismic signals we define the zero lag wavelet coherence (ZLWC) following the next steps. We define the wavelet cross spectrum for our couple of observables e.g. the transverse acceleration and vertical rotation rate as:

$$C_{\omega_Z,a_T} = S(C^*_{\omega_Z}(a,b)Ca_T(a,b)) \tag{2}$$

here the $W_{\omega_Z} = C^*_{\omega_Z}(a,b)$ and $W_{a_T} = C_{a_T}(a,b)$ are the continuos wavelet transforms of $\{\omega_Z,a_T\}$ and S is a smoothing function we can calculate then the wavelet coherence between the two signals as

$$WCT(a,b) = \frac{|S(C_{\omega_Z,a_T})|^2}{|S(W_{\omega_Z})|^2|S(W_{a_T})|^2} \tag{3}$$

we multiply eq. 3 by

$$\Phi(a,b) = \begin{cases} 1 & \text{if } \angle C_{\omega_Z,a_T} \text{ is 0 or } 2\pi \\ 0 & \text{elsewhere} \end{cases} \tag{4}$$

where $\angle C_{\omega_Z,a_T}$ in the angle of the wavelet cross spectrum, thus accounting for the signal phase relationships.

$$F(a,b) = WCT(a,b)S(\Phi(a,b)) \tag{5}$$

We know that the phase velocity for Love waves can be calculated as a simple amplitude

ratio $C_L = -a_T(t)/(2\omega_T(t))$ we express this equation in the wavelet domain as follow:

$$C_L(a,b) = \frac{W_{\omega_Z}(a,b)}{2W_{a_T}(a,b)} \tag{6}$$

We then select the regions of the scale/translation plane where we are allowed to consider the values of $C_L(a,b)$ as reliable by multiplying the obtained estimation by the veto function 5 i.e.

$$C_L^{Cohere}(a,b) = \frac{W_{\omega_Z}(a,b)}{2W_{a_T}(a,b)} F(a,b) \tag{7}$$

A similar processing applies to the couple of observables ω_T,a_z for Rayleigh waves, where eq. 7 assumes in this case the form

$$C_R^{Cohere}(a,b) = \frac{W_{\omega_T}(a,b)}{W_{a_Z}(a,b)} F(a,b) \tag{8}$$

We report two examples of the method described applied to the MW9.0 Tohoku-Oki earthquake. In Fig. 12 we report the BAZ estimation in different period ranges, is easy to notice how in the microseism period range the BAZ flips from the expect direction of the ocean noise at the WET station to the event BAZ at about 37 deg. In Fig. 13 we report the analysis that permits to estimate the phase velocity in the time-period domain as described by eq. 7.

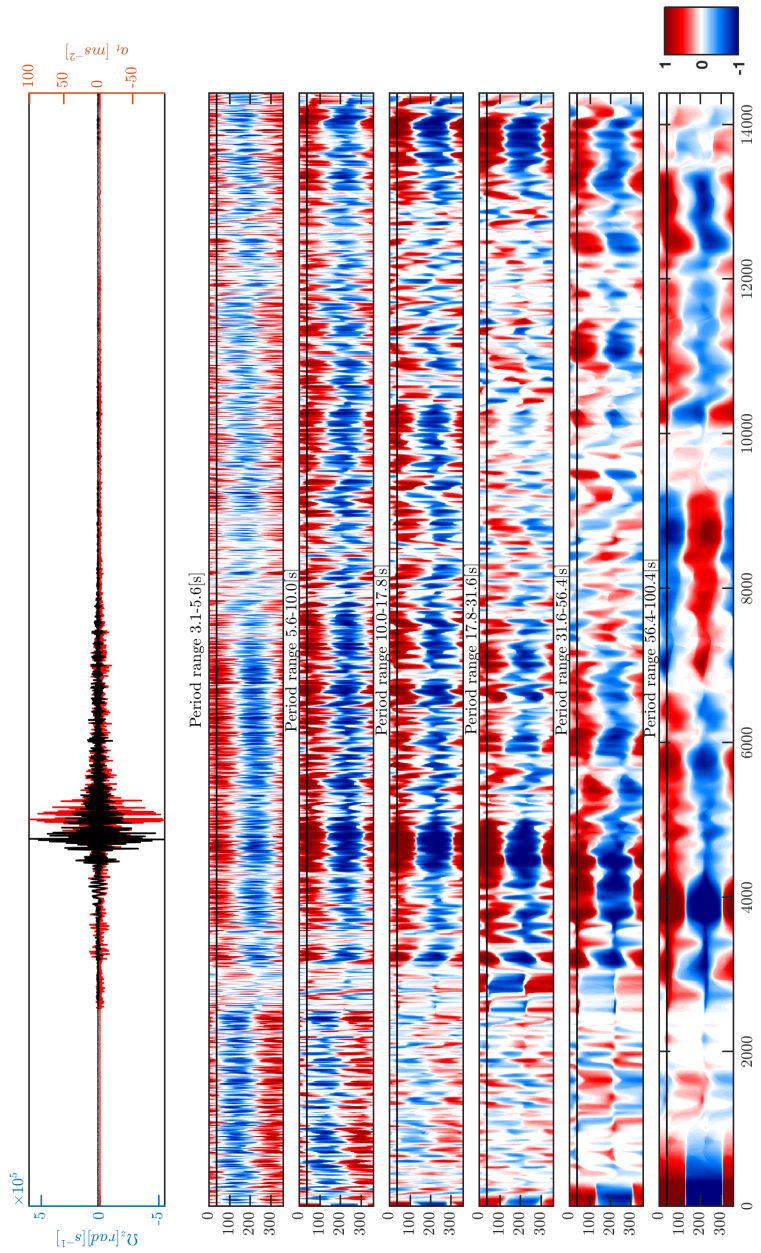

Figure 12: Wavelet decomposition BAZ analysis fot the MW9.0 Tohoku-Oki earthquake recorded at the Wettzell station

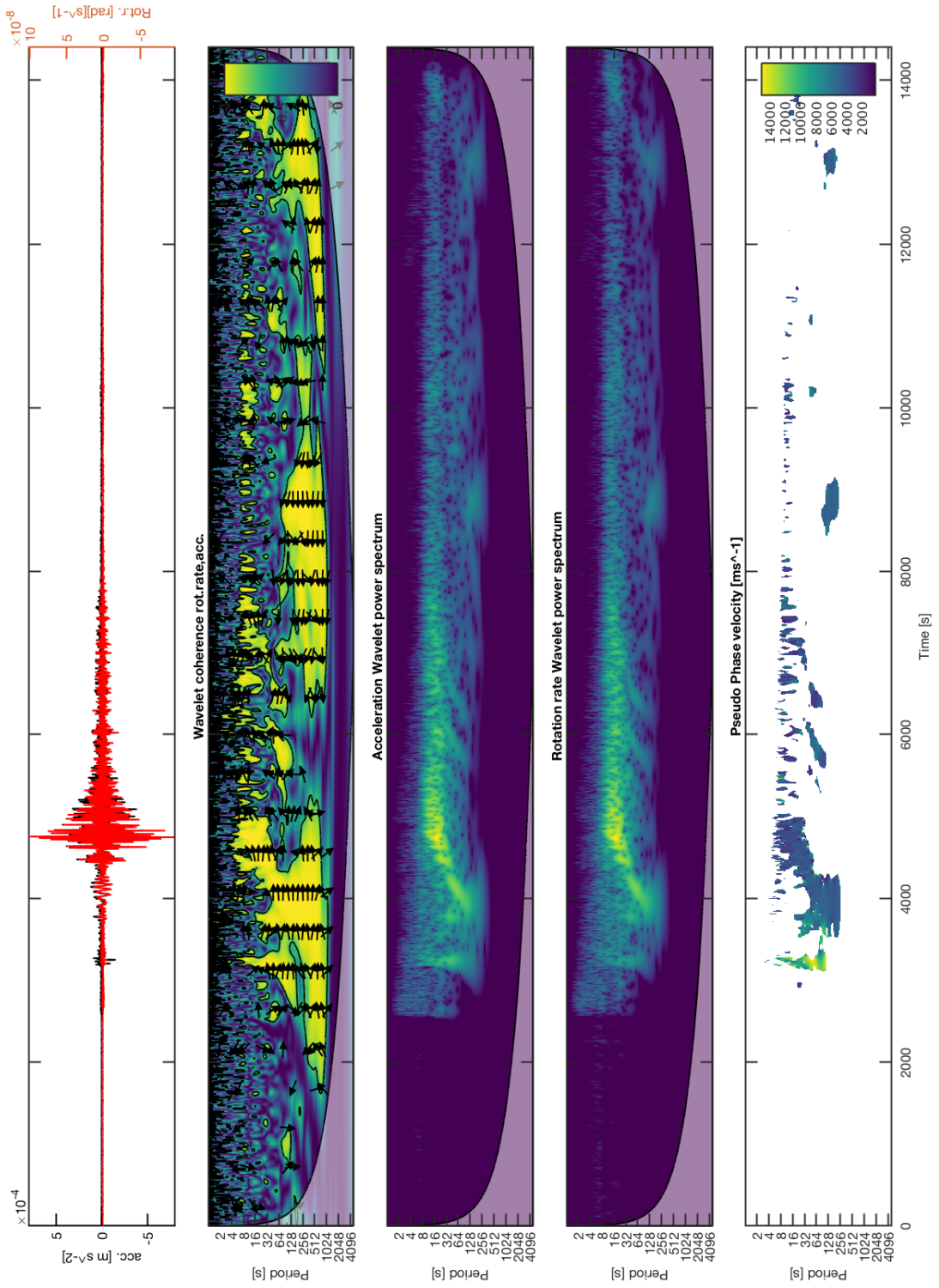

Figure 13: The phase velocity estimation method applied to to Tohoku-Oki earthquake as recorded by the Wettzell station, in this case we measure the Love waves phase velocity and SH

Bibliography

[sit, a] Canterbury Ring Laser Group, `http://www.phys.canterbury.ac.nz/ringlaser/cashmere_cavern_laboratory.shtml`

[sit, b] The ROMY project, `https://www.geophysik.uni-muenchen.de/romy/`

[Phy, 2016] (2016). Observation of gravitational waves from a binary black hole merger. *Phys. Rev. Lett.*, 116:061102.

[Aki and Richards, 1980] Aki, K. and Richards, P. G. (1980). *Quantitative Seismology, Vol. 1: Theory and Methods*. W H Freeman & Co (Sd).

[Aki and Richards, 2002] Aki, K. and Richards, P. G. (2002). *Quantitative seismology*.

[Beauduin et al., 1996] Beauduin, R., Lognonn P., Montagner, J. P., Cacho, S., Karczewski, J. F., and Morand, M. (1996). The effects of the atmospheric pressure changes on seismic signals or how to improve the quality of a station. *Bulletin of the Seismological Society of America*, 86:1760–1769.

[Beghi et al., 2012] Beghi, A., Belfi, J., Beverini, N., Bouhadef, B., Cuccato, D., Virgilio, A. D., and Ortolan, A. (2012). Compensation of the laser parameter fluctuations in large ring-laser gyros: a Kalman filter approach. *Appl. Opt.*, 51(31):7518–7528.

[Belfi et al., 2016] Belfi, J., Beverini, N., Bosi, F., Carelli, G., Cuccato, D., De Luca, G., Di Virgilio, A., Gebauer, A., Maccioni, E., Ortolan, A., Porzio, A., Santagata, R., Simonelli,

A., and Terreni, G. (2016). First Results of GINGERino, a deep underground ringlaser. *ArXiv e-prints,* `http://arxiv.org/abs/1601.02874`.

[Belfi et al., 2017] Belfi, J., Beverini, N., Bosi, F., Carelli, G., Cuccato, D., Luca, G. D., Virgilio, A. D., Gebauer, A., Maccioni, E., Ortolan, A., Porzio, A., Saccorotti, G., Simonelli, A., and Terreni, G. (2017). Deep underground rotation measurements: Gingerino ring laser gyroscope in gran sasso. *Review of Scientific Instruments*, 88(3):034502.

[Belfi et al., 2012a] Belfi, J., Beverini, N., Bosi, F., Carelli, G., Di Virgilio, A., Kolker, D., Maccioni, E., Ortolan, A., Passaquieti, R., and Stefani, F. (2012a). Performance of "G-pisa" ring laser gyro at the VIRGO site. *Journal of Seismology*, 16(4):757–766.

[Belfi et al., 2012b] Belfi, J., Beverini, N., Bosi, F., Carelli, G., Di Virgilio, A., Maccioni, E., Ortolan, A., and Stefani, F. (2012b). A 1.82 m 2 ring laser gyroscope for nano-rotational motion sensing. *Applied Physics B: Lasers and Optics*, 106(2):271–281.

[Belfi et al., 2012c] Belfi, J., Beverini, N., Carelli, G., Di Virgilio, A., Maccioni, E., Saccorotti, G., Stefani, F., and Velikoseltsev, A. (2012c). Horizontal rotation signals detected by "g-pisa" ring laser for the mw=9.0, march 2011, Japan earthquake. *Journal of Seismology*, 16(4):767–776.

[Bernauer et al., 2017] Bernauer, F., Wassermann, J., Guattari, F., Frenois, A., Bigueur, A., Gaillot, A., de Toldi, E., Ponceau, D., Schreiber, U., and Igel, H. (2017). Blueseis3a - full characterization of a 3c broadband rotational seismometer. *SRL.* submitted.

[Bernauer et al., 2012] Bernauer, M., Fichtner, A., and Igel, H. (2012). Measurements of translation, rotation and strain: new approaches to seismic processing and inversion. *Journal of Seismology*, 16(4):669–681.

[Bernauer et al., 2014] Bernauer, M., Fichtner, A., and Igel, H. (2014). Reducing nonuniqueness in finite source inversion using rotational ground motions. *Journal of Geophysical Research: Solid Earth*, 119(6):4860–4875.

[Bird and Carafa, 2016] Bird, P. and Carafa, M. M. C. (2016). Improving deformation models by discounting transient signals in geodetic data: 1. concept and synthetic examples. *Journal of Geophysical Research: Solid Earth*, 121(7):5538–5556. 2016JB013056.

[Boncio et al., 2004] Boncio, P., Lavecchia, G., Milana, G., and Rozzi, B. (2004). Seismogenesis in central apennines, italy: an integrated analysis of minor earthquake sequences and structural data in the amatrice-campotosto area. *Annals of Geophysics*, 47(6).

[Bosi et al., 2011] Bosi, F., Cella, G., Di Virgilio, A., Ortolan, A., Porzio, A., Solimeno, S., Cerdonio, M., Zendri, J., Allegrini, M., Belfi, J., et al. (2011). Measuring gravitomagnetic effects by a multi-ring-laser gyroscope. *Physical Review D*, 84(12):122002.

[Brokešová and Málek, 2010] Brokešová, J. and Málek, J. (2010). New portable sensor system for rotational seismic motion measurements. *Review of Scientific Instruments*, 81(8):084501.

[Butler et al., 2006] Butler, R. W., Tavarnelli, E., and Grasso, M. (2006). Structural inheritance in mountain belts: An alpine,ÄöÑapennine perspective. *Journal of Structural Geology*, 28(11):1893 – 1908. Tectonic inversion and structural inheritance in mountain belts.

[Chiaraluce, 2012] Chiaraluce, L. (2012). Unravelling the complexity of apenninic extensional fault systems: a review of the 2009 l'aquila earthquake (central apennines, italy). *Journal of Structural Geology*, 42:2–18.

[Chiaraluce et al., 2017] Chiaraluce, L., Di Stefano, R., Tinti, E., Scognamiglio, L., Michele, M., Casarotti, E., Cattaneo, M., De Gori, P., Chiarabba, C., Monachesi, G.,

Lombardi, A., Valoroso, L., Latorre, D., and Marzorati, S. (2017). The 2016 central italy seismic sequence: A first look at the mainshocks, aftershocks, and source models. *Seismological Research Letters*.

[Cochard et al., 2006a] Cochard, A., Igel, H., Schuberth, B., Suryanto, W., Velikoseltsev, A., Schreiber, U., Wassermann, J., Scherbaum, F., and Vollmer, D. (2006a). Rotational motions in seismology: Theory, observation, simulation. In Teisseyre, R., Majewski, E., and Takeo, M., editors, *Earthquake Source Asymmetry, Structural Media and Rotation Effects*, pages 391–411. Springer, New York.

[Cochard et al., 2006b] Cochard, A., Igel, H., Schuberth, B., Suryanto, W., Velikoseltsev, A., Schreiber, U., Wassermann, J., Scherbaum, F., and Vollmer, D. (2006b). Rotational motions in seismology: theory, observations, simulation. In et al., T., editor, *Earthquake source asymmetry, structural media and rotation effects*. Springer Verlag.

[Cuccato et al., 2014] Cuccato, D., Beghi, A., Belfi, J., Beverini, N., Ortolan, A., and Di Virgilio, A. (2014). Controlling the non-linear intracavity dynamics of large he–ne laser gyroscopes. *Metrologia*, 51(1):97.

[D'Agostino, 2014] D'Agostino, N. (2014). Complete seismic release of tectonic strain and earthquake recurrence in the apennines (italy). *Geophysical Research Letters*, 41(4):1155–1162.

[Di Domenica et al., 2014] Di Domenica, A., Bonini, L., Calamita, F., Toscani, G., Galuppo, C., and Seno, S. (2014). Analogue modeling of positive inversion tectonics along differently oriented pre-thrusting normal faults: An application to the central-northern apennines of italy. *GSA Bulletin*, 126(7-8):943.

[Di Virgilio et al., 2014] Di Virgilio, A., Allegrini, M., Beghi, A., Belfi, J., Beverini, N., Bosi, F., Bouhadef, B., Calamai, M., Carelli, G., Cuccato, D., et al. (2014). A ring lasers array for fundamental physics. *Comptes Rendus Physique*, 15(10):866–874.

[Donner et al., 2016] Donner, S., Bernauer, M., and Igel, H. (2016). Inversion for seismic moment tensors combining translational and rotational ground motions. *Geophysical Journal International*, 207:562 – 570.

[Donner et al., 2017] Donner, S., Lin, C.-J., Hadziioannou, C., Gebauer, A., Vernon, F., Agnew, D. C., Igel, H., Schreiber, U., and Wassermann, J. (2017). Comparing direct observation of strain, rotation, and displacement with array estimates at piñon flat observatory, california. *Seismological Research Letters*.

[Dunn and Hosman, 2014] Dunn, R. W. and Hosman, A. R. (2014). Detection of volcanic infrasound with a ring laser interferometer. *Journal of Applied Physics*, 116(17).

[Dziewonski and Anderson, 1981] Dziewonski, A. M. and Anderson, D. L. (1981). Preliminary reference earth model. *Physics of the Earth and Planetary Interiors*, 25(4):297 – 356.

[Eslick et al., 2008] Eslick, R., Tsoflias, G., and Steeples, D. (2008). Field investigation of love waves in near-surface seismology. *GEOPHYSICS*, 73(3):G1–G6.

[Ferrari, 2006] Ferrari, G. (2006). *Note on the Historical Rotation Seismographs*, pages 367–376. Springer Berlin Heidelberg, Berlin, Heidelberg.

[Ferreira and Igel, 2009] Ferreira, A. M. G. and Igel, H. (2009). Rotational motions of seismic surface waves in a laterally heterogeneous earth. *Bulletin of the Seismological Society of America*, 99(2B):1429–1436.

[Galadini and Galli, 2000] Galadini, F. and Galli, P. (2000). Active tectonics in the central apennines (italy)–input data for seismic hazard assessment. *Natural Hazards*, 22(3):225–268.

[Grinsted et al., 2004] Grinsted, A., Moore, J. C., and Jevrejeva, S. (2004). Application of the cross wavelet transform and wavelet coherence to geophysical time series. *Nonlinear Processes in Geophysics*, 11(5/6):561–566.

[Hadziioannou et al., 2012a] Hadziioannou, C., Gaebler, P., Schreiber, U., Wassermann, J., and Igel, H. (2012a). Examining ambient noise using colocated measurements of rotational and translational motion. *Journal of Seismology*, 16(4):787–796.

[Hadziioannou et al., 2012b] Hadziioannou, C., Gaebler, P., Schreiber, U., Wassermann, J., and Igel, H. (2012b). Examining ambient noise using colocated measurements of rotational and translational motion. *Journal of Seismology*, 16(4):787–796.

[Haskell, 1953] Haskell, N. A. (1953). The dispersion of surface waves on multilayered media*. *Bulletin of the Seismological Society of America*, 43(1):17.

[Hreinsdóttir and Bennett, 2009] Hreinsdóttir, S. and Bennett, R. A. (2009). Active aseismic creep on the alto tiberina low-angle normal fault, italy. *Geology*, 37(8):683–686.

[Hurst et al., 2014] Hurst, R. B., Rabeendran, N., Schreiber, K. U., and Wells, J.-P. R. (2014). Correction of backscatter-induced systematic errors in ring laser gyroscopes. *Applied optics*, 53(31):7610–7618.

[Igel et al., 2014] Igel, H., Bernauer, M., Wassermann, J., and Schreiber, K. U. (2014). Seismology, rotational, complexity. In Meyers, R. A., editor, *Encyclopedia of Complexity and Systems Science*, pages 1–26. Springer, New York.

[Igel et al., 2007] Igel, H., Cochard, A., Wassermann, J., Flaws, A., Schreiber, U., Velikoseltsev, A., and Pham Dinh, N. (2007). Broad-band observations of earthquake-induced rotational ground motions. *Geophysical Journal International*, 168(1):182.

[Igel et al., 2005] Igel, H., Schreiber, U., Flaws, A., Schuberth, B., Velikoseltsev, A., and Cochard, A. (2005). Rotational motions induced by the M8.1 Tokachi-oki earthquake, September 25, 2003. *Geophys. Res. Lett.*, 32:L08309.

[Kaláb et al., 2013] Kaláb, Z., Knejzlík, J., and Lednická, M. (2013). Application of newly developed rotational sensor for monitoring of mining induced seismic events in the Karvina region. *Acta Geodyn Geomater*, 10(2):170.

[Lavecchia et al., 2012] Lavecchia, G., Ferrarini, F., Brozzetti, F., De Nardis, R., Boncio, P., and Chiaraluce, L. (2012). From surface geology to aftershock analysis: Constraints on the geometry of the l'aquila 2009 seismogenic fault system. *Italian Journal of Geosciences*, 131(3):330–347.

[Lay and Wallace, 1995] Lay, T. and Wallace, T. C. (1995). *Modern global seismology*, volume 58. Academic press.

[Lee et al., 2011] Lee, W., Evans, J. R., and Huang, B.-S. (2011). Measuring rotational ground motions in seismological practice.

[Lee et al., 2009] Lee, W. H. K., Igel, H., and Trifunac, M. D. (2009). Recent advances in rotational seismology. *Seismological Research Letters*, 80(3):479.

[Lefèvre, 2014] Lefèvre, H. C. (2014). *The fiber-optic gyroscope*. Artech House, London, 2 edition.

[Li et al., 2010] Li, H., Bernardi, F., and Michelini, A. (2010). Love wave tomography in italy from seismic ambient noise. *Earthquake Science*, 23(5):487–495.

[Lindner et al., 2016] Lindner, F., Wassermann, J., Schmidt-Aursch, M. C., Schreiber, K. U., and Igel, H. (2016). Seafloor ground rotation observations: Potential for improving signal-to-noise ratio on horizontal obs components. *Seismological Research Letters*, 88(1):32–38.

[Malinverno and Ryan, 1986] Malinverno, A. and Ryan, W. B. F. (1986). Extension in the tyrrhenian sea and shortening in the apennines as result of arc migration driven by sinking of the lithosphere. *Tectonics*, 5(2):227–245.

[Marano and Fah, 2014] Marano, S. and Fah, D. (2014). Processing of translational and rotational motions of surface waves: performance analysis and applications to single sensor and to array measurements. *Geophysical Journal International*, 196(1):317–339.

[Martini et al., 2001] Martini, I. P., Sagri, M., and Colella, A. (2001). Neogene—quaternary basins of the inner apennines and calabrian arc. In *Anatomy of an Orogen: the Apennines and adjacent Mediterranean basins*, pages 375–399. Springer.

[McLeod et al., 1998] McLeod, D., Stedman, G., Webb, T., and Schreiber, U. (1998). Comparison of standard and ring laser rotational seismograms. *Bulletin of the Seismological Society of America*, 88(6):1495–1503.

[Michele et al., 2016] Michele, M., Stefano, R. D., Chiaraluce, L., Cattaneo, M., Gori, P. D., Monachesi, G., Latorre, D., Marzorati, S., Valoroso, L., Ladina, C., Chiarabba, C., Lauciani, V., and Fares, M. (2016). The amatrice 2016 seismic sequence: a preliminary look at the mainshock and aftershocks distribution. *Annals of Geophysics*, 59(0).

[Nader et al., 2012] Nader, M. F., Igel, H., Ferreira, A. M. G., Kurrle, D., Wassermann, J., and Schreiber, K. U. (2012). Toroidal free oscillations of the earth observed by a ring laser system: a comparative study. *Journal of Seismology*, 16(4):745–755.

[Nilsson et al., 2012] Nilsson, T., Böhm, J., Schuh, H., Schreiber, U., Gebauer, A., and Klügel, T. (2012). Combining vlbi and ring laser observations for determination of high frequency earth rotation variation. *Journal of Geodynamics*, 62:69–73.

[Pancha et al., 2000] Pancha, A., Webb, T., Stedman, G., McLeod, D., and Schreiber, K. (2000). Ring laser detection of rotations from teleseismic waves. *Geophysical Research Letters*, 27(21):3553–3556.

[Peterson et al., 1993] Peterson, J. et al. (1993). Observations and modeling of seismic background noise.

[Pucci et al., 2017] Pucci, S., De Martini, P., Civico, R., Villani, F., Nappi, R., Ricci, T., Azzaro, R., Brunori, C., Caciagli, M., Cinti, F., et al. (2017). Coseismic ruptures of the 24 august 2016, mw 6.0 amatrice earthquake (central italy). *Geophysical Research Letters*, 44(5):2138–2147.

[Pujol, 2009] Pujol, J. (2009). Tutorial on rotations in the theories of finite deformation and micropolar (cosserat) elasticitytutorial on rotations in the theories of finite deformation and micropolar (cosserat) elasticity. *Bulletin of the Seismological Society of America*, 99(2B):1011.

[Richter, 1958] Richter, C. F. (1958). *Elementary Seismology (Books in Geology)*. W H Freeman & Co (Sd).

[Sagnac, 1913] Sagnac, G. ((1913)). Lther lumineux dmontr par lffet du vent relatif dther dans un interfromtre en rotation uniforme. *Comptes rendus hebdomadaires de lcadmie des sciences de Paris*, 157:70810.

[Santagata et al., 2015] Santagata, R., Beghi, A., Belfi, J., Beverini, N., Cuccato, D., Di Virgilio, A., Ortolan, A., Porzio, A., and Solimeno, S. (2015). Optimization of the

geometrical stability in square ring laser gyroscopes. *Classical and Quantum Gravity*, 32(5):055013.

[Schlueter, 1903] Schlueter, W. (1903). Schwingungsart und weg der erdbebenwellen. *Beitrge zur Geophysik*, 5:314–359.

[Schreiber et al., 2011] Schreiber, K., Klügel, T., Wells, J.-P., Hurst, R., and Gebauer, A. (2011). How to detect the chandler and the annual wobble of the earth with a large ring laser gyroscope. *Physical Review Letters*, 107(17):173904.

[Schreiber et al., 2004] Schreiber, K., Velikoseltsev, A., Rothacher, M., Klügel, T., Stedman, G., and Wiltshire, D. (2004). Direct measurement of diurnal polar motion by ring laser gyroscopes. *Journal of Geophysical Research: Solid Earth (1978–2012)*, 109(B6).

[Schreiber et al., 2009] Schreiber, K. U., Klügel, T., Velikoseltsev, A., Schlüter, W., Stedman, G. E., and Wells, J.-P. R. (2009). The large ring laser G for continuous earth rotation monitoring. *Pure and Applied Geophysics*, 166(8):1485–1498.

[Schreiber et al., 2006a] Schreiber, K. U., Stedman, G. E., Igel, H., and Flaws, A. (2006a). Ring laser gyroscopes as rotation sensors for seismic wave studies. In *Earthquake Source Asymmetry, Structural Media and Rotation Effects*, pages 377–390. Springer.

[Schreiber and Wells, 2013a] Schreiber, K. U. and Wells, J.-P. R. (2013a). Invited review article: Large ring lasers for rotation sensing. *Review of Scientific Instruments*, 84(4):041101.

[Schreiber and Wells, 2013b] Schreiber, K. U. and Wells, J.-P. R. (2013b). Invited review article: Large ring lasers for rotation sensing. *Review of Scientific Instruments*, 84(4):041101.

[Schreiber et al., 2006b] Schreiber, U., Igel, H., Cochard, A., Velikoseltsev, A., Flaws, A., Schuberth, B., Drewitz, W., and Müller, F. (2006b). The GEOsensor project: rotations, a new observable for seismology. In *Observation of the Earth System from Space*, pages 427–443. Springer.

[Scisciani and Calamita, 2009] Scisciani, V. and Calamita, F. (2009). Active intraplate deformation within adria: Examples from the adriatic region. *Tectonophysics*, 476(1):57 – 72. Ten years after the Umbria-Marche earthquake, Central Italy.

[Simonelli et al., 2017a] Simonelli, A., , Bernauer, F., Braun, T., Wassermann, J., and Igel, H. (2017a). 6-component ground motion observations of local earthquakes: The 2016 central italy sequence. *In preparation*.

[Simonelli, 2014] Simonelli, A. (2014). Il giroscopio laser come sensore di rotazioni: simulazioni e attivit† sperimentale. Master's thesis, University of Pisa, `https://etd.adm.unipi.it/theses/available/etd-06202014-163524/`.

[Simonelli et al., 2016] Simonelli, A., Belfi, J., Beverini, N., Carelli, G., Virgilio, A. D., Maccioni, E., Luca, G. D., and Saccorotti, G. (2016). First deep underground observation of rotational signals from an earthquake at teleseismic distance using a large ring laser gyroscope. *Annals of Geophysics*, 59(0).

[Simonelli et al., 2017b] Simonelli, A., Igel, H., Wassermann, J., Belfi, J., Virgilio, A., Beverini, N., E.Maccioni, Luca, G. D., and Saccorotti, G. (2017b). Rotational motions from the 2016, central italy seismic sequence, as observed by an underground ring laser gyroscope. *GJI.* submitted.

[Stedman et al., 1995] Stedman, G., Li, Z., and Bilger, H. (1995). Sideband analysis and seismic detection in a large ring laser. *Applied optics*, 34(24):5375–5385.

[Suryanto, 2006] Suryanto, W. (2006). Rotational motions in seismology.

[Takeo and Ito, 1997] Takeo, M. and Ito, H. M. (1997). What can be learned from rotational motions excited by earthquakes? *Geophysical Journal International*, 129(2):319.

[Tavarnelli, 1996] Tavarnelli, E. (1996). The effects of pre-existing normal faults on thrust ramp development: An example from the northern apennines, italy. *Geologische Rundschau*, 85(2):363–371.

[Teisseyre, 2012] Teisseyre, R. (2012). Rotation and strain seismology. *Journal of seismology*, 16(4):683–694.

[Thomson, 1982] Thomson, D. J. (1982). Spectrum estimation and harmonic analysis. *Proceedings of the IEEE*, 70(9):1055–1096.

[van Driel et al., 2015] van Driel, M., Wassermann, J., Pelties, C., Schiemenz, A., and Igel, H. (2015). Tilt effects on moment tensor inversion in the near field of active volcanoes. *Geophysical Journal International*, 202(3):1711–1721.

[Wassermann et al., 2016] Wassermann, J., Wietek, A., Hadziioannou, C., and Igel, H. (2016). Toward a single-station approach for microzonation: Using vertical rotation rate to estimate love-wave dispersion curves and direction finding. *Bulletin of the Seismological Society of America*, 106(3):1316–1330.